

PAPER • OPEN ACCESS

Foundations and interpretations of the pulsed-Townsend experiment

To cite this article: M J E Casey *et al* 2021 *Plasma Sources Sci. Technol.* **30** 035017

View the [article online](#) for updates and enhancements.

You may also like

- [Review of laser-driven ion sources and their applications](#)
Hiroyuki Daido, Mamiko Nishiuchi and Alexander S Pirozhkov
- [Divergence of fast ions generated by interaction of intense ultra-high contrast laser pulses with thin foils](#)
A Andreev, T Ceccotti, A Levy et al.
- [Carbon ion beam focusing using laser irradiated, heated diamond hemispherical shells](#)
D T Offermann, K A Flippo, S A Gaillard et al.

Foundations and interpretations of the pulsed-Townsend experiment

M J E Casey¹ , P W Stokes¹ , D G Cocks² , D Bošnjaković³ ,
I Simonović³ , M J Brunger^{4,5} , S Dujko³ , Z Lj Petrović^{6,7} ,
R E Robson^{1,8}  and R D White^{1,*} 

¹ College of Science and Engineering, James Cook University, Townsville, QLD, Australia

² Research School of Physics, The Australian National University, Canberra, ACT, Australia

³ Institute of Physics, University of Belgrade, Zemun, Belgrade, Serbia

⁴ College of Science and Engineering, Flinders University, Adelaide, SA, Australia

⁵ Department of Actuarial Science and Applied Statistics, Faculty of Business and Information Science, UCSI University, Kuala Lumpur, Malaysia

⁶ School of Engineering, Ulster University, Newtownabbey, Antrim, Northern Ireland, United Kingdom

⁷ Serbian Academy of Sciences and Arts, Belgrade, Serbia

⁸ Centre for Quantum Dynamics, Griffith University, Nathan, QLD, Australia

E-mail: ronald.white@jcu.edu.au

Received 22 November 2020, revised 1 February 2021

Accepted for publication 17 February 2021

Published 25 March 2021



Abstract

The pulsed-Townsend (PT) experiment is a well known swarm technique used to measure transport properties from a current in an external circuit, the analysis of which is based on the governing equation of continuity. In this paper, the Brambring representation (1964 *Z. Phys.* **179** 532) of the equation of continuity often used to analyse the PT experiment, is shown to be fundamentally flawed when non-conservative processes are operative. The Brambring representation of the continuity equation is not derivable from Boltzmann's equation and consequently transport properties defined within the framework are not clearly representable in terms of the phase-space distribution function. We present a re-analysis of the PT experiment in terms of the standard diffusion equation which has firm kinetic theory foundations, furnishing an expression for the current measured by the PT experiment in terms of the universal bulk transport coefficients (net ionisation rate, bulk drift velocity and bulk longitudinal diffusion coefficient). Furthermore, a relationship between the transport properties previously extracted from the PT experiment using the Brambring representation, and the universal bulk transport coefficients is presented. The validity of the relationship is tested for two gases Ar and SF₆, highlighting also estimates of the differences.

Keywords: pulsed townsend experiment, transport coefficient definition, pulsed townsend governing equation, kinetic theory, Brambring's equation


(Some figures may appear in colour only in the online journal)

1. Introduction

The use of accurate electron swarm transport coefficients in simulations has wide ranging implications for modelling

physics, from atmospheric processes through to medical imaging and therapies [2–21]. For the well established swarm experimental techniques, the various experimental parameters (such as temperature, sample purity, uniformity of the applied field, ...) are assumed to be highly accurate (within the reported error bars), and the techniques for extracting the measured quantities are generally considered to be well understood. Within the swarm community itself, consensus on the

* Author to whom any correspondence should be addressed.

 Original content from this work may be used under the terms of the [Creative Commons Attribution 4.0 licence](https://creativecommons.org/licenses/by/4.0/). Any further distribution of this work must maintain attribution to the author(s) and the title of the work, journal citation and DOI.

extraction of transport parameters/coefficients is essential as this explicitly impacts upon the accuracy of swarm-derived cross-sections [22–43] that may be subsequently used directly for modelling of gas and liquid-phase transport [12, 13], or the direct application of electron swarm transport coefficients in fluid modelling of plasmas [3, 44]. As such, high accuracy is required in both the measurement and definition of the transport coefficients to ensure applications in technology and medicine can be made with confidence.

Transport coefficient definition/measurement was an active area of debate in the 1960–1990s [45–54], and misunderstandings still exist [30]. For example, it is important to understand that different swarm experiments operate in different regimes—time of flight (TOF) and pulsed-Townsend (PT) for example in the hydrodynamic regime, where the space-time dependence of all quantities can be projected onto the number density, $n(\mathbf{r}, t)$ [55], while the steady state Townsend (SST) approach operates in the non-hydrodynamic regime, where one has to treat the space (\mathbf{r}) and time (t) dependence more generally [47, 56].

In the hydrodynamic regime, there are two fundamental types of transport coefficients, which we call flux and bulk¹⁰. The flux coefficients are defined through well-known flux-gradient relationships, such as Fick's law. The bulk coefficients, however, are defined through the diffusion equation, which applies, for example, to the analysis of the various measured currents in both the TOF and PT experiments. Thus we can say quite generally, without reference to the specific form of the solution of the diffusion equation, for any experiment amenable to a hydrodynamic description, that it is the bulk quantities which are extracted and therefore it is these which are tabulated in the literature. On the other hand, the SST experiment is inherently non-hydrodynamic, and measures the microscopic Townsend ionisation coefficient, α , through the particle density relation $n \sim \exp(\alpha z)$. The SST experiment cannot be analysed through the diffusion equation [57], and therefore does not measure any of the hydrodynamic transport coefficients.

In spite of much discussion over the past 30–60 years [45–54], there does, however, remain some residual confusion about what transport coefficients/properties are extracted from the PT experiment, and how they relate to the standard flux and bulk transport coefficients¹¹. Currently, the PT experiment is one of the swarm methods in active use, with key groups in Switzerland [58, 63] and México [32, 68], as well as the scanning drift tube experiment in Hungary [69–71] and the double-shutter drift tube experiment in Japan [72], which provide much of the present-day electron swarm data. Consequently, it is essential that the transport properties extracted from the PT

experiments are identified correctly. This represents the focus of the current study.

We begin this paper with a brief review of fundamental swarm transport theory and definitions in section 2, in order to revisit the vexed issue of transport coefficient definition in relation to the PT experiment and their relation to transport coefficients which are derivable from the Boltzmann equation. We demonstrate that the Brambring form of the continuity/diffusion equation [1] generally used to analyse the PT experiment is fundamentally flawed when non-conservative processes are operative. A general solution of the full diffusion equation has long been available in the literature [73, 74], and in section 3 we specifically show how it can be adapted to the PT experiment to extract the standard definitions of the transport coefficients with firm foundations in kinetic theory. With our focus on the PT experiment, in section 3 we demonstrate that the existing transport property measurements extracted from PT experiments using the fundamentally flawed Brambring equation for the current in the external circuit [1], can be transformed to the standard bulk transport coefficient definitions. Transformation of existing measured PT transport properties, for the particular examples of Ar and SF₆, are presented in section 4 and compared with the bulk transport coefficients extracted from TOF experiments and calculated using a multi-term solution of Boltzmann's equation. Thereafter, some concluding remarks are drawn in section 5.

2. Theory

2.1. The exact continuity equation, the hydrodynamic regime and the diffusion equation

The exact continuity equation can be derived either from first principles, or from Boltzmann's equation:

$$\frac{\partial f}{\partial t} + \mathbf{v} \cdot \nabla f + \mathbf{a} \cdot \frac{\partial f}{\partial \mathbf{v}} = -J(f), \quad (1)$$

for the phase-space distribution function, $f(z, \mathbf{v}, t)$, a function of velocity \mathbf{v} and time t , with spatial gradients taken along the z axis, and acceleration \mathbf{a} due to external forces, with collisional processes represented by Boltzmann's collision integral J . Integrating equation (1) over velocity space yields the continuity equation (here, in one dimension):

$$\frac{\partial n}{\partial t} + \frac{\partial \Gamma}{\partial z} = S(z, t), \quad (2)$$

where $n(z, t)$ is the charged-particle density, $\Gamma(z, t) = \int v_z f(z, \mathbf{v}, t) d\mathbf{v}$ is the charged-particle flux in the external field direction and the right-hand side is the rate of production of particles, given by $S(z, t) = \int J_{\text{NC}}(f) d\mathbf{v}$, the integral of the non-conservative collision operator, J_{NC} , for processes such as attachment and ionisation.

Swarm experiments are traditionally designed to operate in the hydrodynamic regime [2, 44, 75]. In this regime, the space-time dependence of $f(z, \mathbf{v}, t)$ is a function of the number density (n), and can be expressed in terms of a density gradient expansion:

¹⁰ While some associate them with particular experiments, such nomenclature hides their fundamental nature [50].

¹¹ With regard to the extracted coefficients, we note that while some PT analyses report α_T/n_0 (the macroscopic form of Townsend's first ionisation coefficient), the quantity R_{net} has been extracted directly by Franck and co-workers [58–64] and Ridenti *et al* [65], reported for the PT measurements of Aschwanden [66] (along with α_T/n_0) when analysis of the current transients was hindered by the strong electron attachment, and in Phelps and Pitchford [67] measurements were transformed to R_{net} , to illustrate a few examples.

$$f(z, v, t) = n(z, t)f^{(0)}(v) - f^{(1)}(v)\frac{\partial n(z, t)}{\partial z} + f^{(2)}(v)\frac{\partial^2 n(z, t)}{\partial z^2} + \dots, \quad (3)$$

while normalisation requires $\int f^{(j)}(v)dv = \delta_{j0}$. Hence, the flux and source terms in the continuity equation (2) can be identified with:

$$\Gamma(z, t) = nW - D_L \frac{\partial n}{\partial z} + \zeta_L \frac{\partial^2 n}{\partial z^2} + \dots, \quad (4)$$

$$S(z, t) = nR_{\text{net}} - S^{(1)} \frac{\partial n}{\partial z} + S^{(2)} \frac{\partial^2 n}{\partial z^2} + \dots, \quad (5)$$

where ζ_L is the longitudinal component of the third-order transport coefficient tensor (the skewness tensor) [76]. Equation (4) is familiar as a generalisation of Fick's law. The flux drift velocity and the flux longitudinal diffusion coefficient are designated W and D_L respectively, with the net (or effective) production rate given by $R_{\text{net}} = R_{\text{ionis}} - R_{\text{att}}$. The flux transport properties in (4) and non-conservative source terms in (5) can be written in terms of the appropriate integrals of the $f^{(j)}$ appearing in equation (3), or otherwise [51, 56, 77, 78].

Substitution of equations (4) and (5) into equation (2), and grouping coefficients of gradients in the number density, yields the standard diffusion equation, when higher order terms in the hydrodynamic expansion are neglected:

$$\frac{\partial n}{\partial t} + W_B \frac{\partial n}{\partial z} - D_{B,L} \frac{\partial^2 n}{\partial z^2} = nR_{\text{net}}, \quad (6)$$

where we define the bulk (B) transport coefficients in terms of the flux coefficients and the corrections due to the non-conservative source terms:

$$W_B = W + S^{(1)}, \quad (7)$$

$$D_{B,L} = D_L + S^{(2)}. \quad (8)$$

In a drift tube experiment, $S^{(1)}$ and $S^{(2)}$ can be interpreted as modifications to the position of the centre of mass and spread about the centre of mass, respectively, arising from non-conservative processes. In general,

$$S^{(1)} = \int J_{\text{NC}}(f^{(1)})dv, \quad (9)$$

$$S^{(2)} = \int J_{\text{NC}}(f^{(2)})dv. \quad (10)$$

Swarm experiments operating in the hydrodynamic regime may be analysed on the basis of the diffusion equation and hence generally sample the bulk transport coefficients. The solution of the diffusion equation for various experimental arrangements, e.g., for sources distributed in space and/or emitting for finite times, can be found by appropriate integration of this fundamental solution over space and/or time respectively, as we highlight below.

2.2. Townsend's first ionisation coefficient(s) and the fundamentally flawed Brambling equation of continuity

The Townsend ionisation coefficient is generally defined under steady state conditions. Confusion over the definition of the Townsend coefficient has however existed for an extended period, with the article by Crompton [45] representing a great overview and attempt to address this issue. In short, there are two definitions of the Townsend ionisation coefficient. The macroscopic version of Townsend's first (net) ionisation coefficient, α_T , (which is the difference of the ionisation and attachment (often referred to as η) coefficients), is defined by the relation to the particle flux (or current):

$$\Gamma \sim \exp(\alpha_T z). \quad (11)$$

The microscopic version of the Townsend (net) ionisation coefficient, α , is defined by the relation to the density:

$$n(z) \sim \exp(\alpha z). \quad (12)$$

The two definitions are quite different, as are their relationships to the other transport coefficients and to each other, as we explore below.

The PT experiment [58, 79–82] may be analysed using the diffusion equation (6). On the other hand, the continuity equation proposed by Brambling [1] is:

$$\frac{\partial n}{\partial t} + \frac{\partial \Gamma}{\partial z} = \alpha_T \Gamma, \quad (13)$$

that is equation (2) with a source term:

$$S = \alpha_T \Gamma. \quad (14)$$

It is unclear from the Brambling paper [1] which form of the Townsend ionisation coefficient was proposed in their continuity equation, and perhaps their equation defines its own form of the Townsend ionisation coefficient. We do highlight, however, that the steady-state solution of equation (13) for the flux is consistent with the macroscopic form of the Townsend coefficient (11) and hence we use that form in the Brambling representation of the equation of continuity. This is a notational issue, however, which does not impact the following arguments.

Most importantly, the Brambling form of the continuity equation (13) is not derivable from the Boltzmann equation (1), except in the trivial case of no ionisation or attachment, where $S = 0$. To illustrate issues associated with the Brambling representation of the equation of continuity (13), let us consider a very simple benchmark system: elastic scattering with an attachment process with a collision frequency, ν_{att} , that is independent of energy. From the Boltzmann equation, the attachment collision operator has the form: $J_{\text{att}}(f) = \nu_{\text{att}} f$. The source term in the exact continuity equation (2) in the hydrodynamic regime takes the form:

$$\begin{aligned} S(z, t) &\equiv \int [J_{\text{elast}}(f) + J_{\text{att}}(f)] dv \\ &= 0 + \nu_{\text{att}} \int \left[n f^{(0)}(v) - f^{(1)}(v) \frac{\partial n}{\partial z} \right] dv \end{aligned}$$

$$\begin{aligned}
 & + f^{(2)}(v) \frac{\partial^2 n}{\partial z^2} + \dots \Big] dv \\
 & = n\nu_{\text{att}} \int f^{(0)}(v) dv - \nu_{\text{att}} \int f^{(1)}(v) dv \frac{\partial n}{\partial z} \\
 & + \nu_{\text{att}} \int f^{(2)}(v) dv \frac{\partial^2 n}{\partial z^2} + \dots \\
 & = n\nu_{\text{att}} + 0 + 0 + \dots,
 \end{aligned} \tag{15}$$

where the last line follows by virtue of the normalisation condition on the $f^{(j)}$, and J_{elast} denotes the elastic collision operator. In this case, $S(z, t)$ is proportional to the density with no contributions arising from the derivatives of the density. This is inconsistent with the Brambring form for the source term (14), which would have additional first and second order density spatial derivative contributions which are independent of the energy dependence of the non-conservative processes, viz substituting the expression for the flux Γ into equation (14). Physically, if the attachment collision frequency is independent of energy then it cannot modify the position of the centre of mass (first moment of the density) nor the rate of spread/diffusion (second moment of the density) of the pulse. In contrast, the Brambring equation has explicit modifications to both of these moments of the pulse, whenever there are non-conservative processes operative, irrespective of the energy dependence of the non-conservative collision frequency.

While the Brambring representation of the equation of continuity is thus fundamentally flawed from a physical viewpoint, in the following sections, we highlight how to relate the transport properties extracted from the PT experiment via an analysis using the Brambring representation of the continuity equation (and related equation for the measurable current in the external circuit), with the standard definition of the transport coefficients from a Boltzmann equation/kinetic theory perspective. This will have importance for the application of PT transport properties in fluid/moment models of plasmas for example, as well as for the extraction of cross-sections through the swarm inversion process.

3. Interpreting transport coefficients from the measured current in the pulsed-Townsend experiment

3.1. Solution of the standard diffusion equation

Firstly, consider an idealised TOF experiment in a finite geometry $0 \leq z \leq L$, in which a sharp pulse of n_0 charge carriers is released from a source plane $z = z_0$ at time $t = t_0$, i.e.,

$$n(z, t_0) = n_0 \delta(z - z_0). \tag{16}$$

The solution of the diffusion equation (6) for $z_0 = 0$, $t_0 = 0$ and infinite geometry ($L \rightarrow \infty$) is the well known travelling pulse [2, 53]:

$$n(z, t) = \frac{n_0 \exp(R_{\text{net}} t)}{\sqrt{4\pi D_{B,L} t}} \exp\left[-\frac{(z - W_B t)^2}{4D_{B,L} t}\right]. \tag{17}$$

In finite geometry, assuming perfectly absorbing boundaries, and

$$n(0, t) = 0 = n(L, t), \tag{18}$$

the solution of the diffusion equation may be obtained using the Poisson summation theorem [73, 74] as,

$$\begin{aligned}
 n(z, t; z_0, t_0) &= \frac{n_0}{\sqrt{4\pi D_{B,L}(t - t_0)}} \exp \\
 &\times \left\{ R_{\text{net}} t + \frac{W_B}{2D_{B,L}} \left[z - z_0 - \frac{1}{2} W_B (t - t_0) \right] \right\} \\
 &\times \sum_{j=-\infty}^{\infty} \left\{ \exp\left[-\frac{(z - z_0 - 2jL)^2}{4D_{B,L}(t - t_0)}\right] \right. \\
 &\left. - \exp\left[-\frac{(z + z_0 - 2jL)^2}{4D_{B,L}(t - t_0)}\right] \right\}.
 \end{aligned} \tag{19}$$

One can consider more elaborate boundary conditions, however for the current study the simplified boundary conditions (18) are sufficient.

It is convenient for the purposes of the following discussion to consider the situation where the left hand boundary recedes to $-\infty$. This may be achieved mathematically by an appropriate transformation of coordinates, in which L now denotes the distance of the right hand boundary from the source, which is now located at the origin of coordinates. Equation (19) then becomes, with $t_0 = 0$,

$$\begin{aligned}
 n(z, t; L) &= \frac{n_0 \exp\left(R_{\text{net}} t + \frac{W_B}{2D_{B,L}} \left(z - \frac{1}{2} W_B t\right)\right)}{\sqrt{4\pi D_{B,L} t}} \\
 &\times \left\{ \exp\left[-\frac{z^2}{4D_{B,L} t}\right] - \exp\left[-\frac{(z - 2L)^2}{4D_{B,L} t}\right] \right\},
 \end{aligned} \tag{20}$$

describing the spatio-temporal variation of $n(z, t)$ in a TOF drift tube.

3.2. Extracting bulk transport coefficients from the pulsed-Townsend experiment

Consider now the PT experiment—a plane parallel swarm system where all spatial variation is confined to the z direction, normal to the electrodes. Under typical measurement conditions, the transit time of the electrons is much less than the RC time constant of the circuit [2] and the current in the external circuit is given by:

$$I = \frac{q}{L} \int_0^L \Gamma(z', t) dz'. \tag{21}$$

Using Fick's law (4), this can be written in terms of the transport coefficients and is given by:

$$I(t) = \frac{qW}{L} \int_0^L n(z, t) dz, \tag{22}$$

where the diffusive contribution has been eliminated due to the relation:

$$\int_0^L D_L \frac{\partial n}{\partial z} dz = D_L n(L) - D_L n(0) = 0, \quad (23)$$

for perfectly absorbing boundary conditions. It follows from (22) that the measurable current in the external circuit is given by:

$$I(t) = \frac{n_0 q W}{2L} \exp(R_{\text{net}} t) \left\{ \left[1 - \phi \left(\frac{W_B t - L}{\sqrt{4D_{B,L} t}} \right) \right] + \exp \left(\left[\frac{W_B}{D_{B,L}} \right] L \right) \left[\phi \left(\frac{W_B t + L}{\sqrt{4D_{B,L} t}} \right) - 1 \right] \right\}, \quad (24)$$

where ϕ represents the error function. Hence, full current transients for the current in the external circuit of the PT experiment fitted to equation (24) can yield the bulk transport coefficients: the net ionisation rate coefficient $R_{\text{net}} = R_{\text{ionis}} - R_{\text{att}}$, the bulk drift velocity W_B , and the bulk diffusion coefficient $D_{B,L}$. Even though the current scales with the flux drift velocity, W , the time-dependence of the measured current is determined by the bulk transport coefficients— R_{net} , W_B and $D_{B,L}$ via (24). This is consistent with the conclusions of Blevin and Fletcher [50] and Robson [53]. If the initial number of electrons is known, then we can also simultaneously extract the flux drift velocity from an analysis of the current in the external circuit. This provides an additional transport coefficient that can be used for cross-section fitting/extraction from swarm experiments.

4. Relating existing PT transport properties to the standard transport coefficient definitions

Given the wealth of experimental work and associated extraction of transport properties and fitting of cross-sections to the PT data, the obvious question remaining is how do we relate the PT experimental transport properties to the transport coefficients which are grounded in the Boltzmann equation/kinetic theory.

Here, we return to the Brambring representation of the equation of continuity (13) and find the equivalent expression for the current in an external circuit¹². If we substitute Fick's law expression (4) into the Brambring equation (13) (retaining

only first order terms in the density gradient expansion¹³), on re-arranging we obtain the diffusion-type equation:

$$\frac{\partial n}{\partial t} + [\tilde{W} + \tilde{\alpha}_T \tilde{D}_L] \frac{\partial n}{\partial z} - \tilde{D}_L \frac{\partial^2 n}{\partial z^2} = n \tilde{\alpha}_T \tilde{W}. \quad (25)$$

The tildes here denote transport properties arising from the Brambring representation of the diffusion equation. Since the Brambring representation of the equation of continuity (13) is not derivable from Boltzmann's equation/kinetic theory, the terms drift velocity, diffusion coefficient and alpha as defined by the Brambring representation do not have a standard kinetic theory definition (i.e. are not representable in terms of an integral of the phase-space distribution function and hence cannot be found directly in terms of a solution of Boltzmann's equation or Monte Carlo simulation) when non-conservative processes are operative and hence may not have the standard meaning of drift velocity, diffusion, etc, under such conditions.

Following the same procedure as above, but using the Brambring representation of the diffusion equation (25) instead of the conventional diffusion equation (6), it follows that the functional form of the current in the external circuit is given by:

$$I(t) = \frac{n_0 q W}{2L} \exp(\tilde{\alpha}_T \tilde{W} t) \times \left\{ \left[1 - \phi \left(\frac{(\tilde{W} + \tilde{\alpha}_T \tilde{D}_L)t - L}{\sqrt{4\tilde{D}_L t}} \right) \right] + \exp \left(\left[\frac{\tilde{W} + \tilde{\alpha}_T \tilde{D}_L}{\tilde{D}_L} \right] L \right) \times \left[\phi \left(\frac{(\tilde{W} + \tilde{\alpha}_T \tilde{D}_L)t + L}{\sqrt{4\tilde{D}_L t}} \right) - 1 \right] \right\}. \quad (26)$$

This is the same expression as that from the original Brambring paper (see equation (12) of reference [1]) and used by the experimental groups [58, 79, 83, 84], expressed using the PT transport properties. It is important to note that the W appearing in the first factor on the rhs of equation (26) is the flux drift velocity W , not the bulk drift velocity W_B or the PT transport property \tilde{W} .

The key to relating the PT transport properties to the standard transport coefficients is to understand how they are extracted from the fitting of the current in the external circuit in a typical analysis of the PT experiment. The expression for the current in the external circuit, whether it be the expression

¹² While the functional form of the current in the external circuit and its relation to the transport coefficients can be a source of uncertainty, these are distinct from the uncertainties that can typically be obtained from approximate analysis of the current in the external circuit. Indeed, some analyses have used quite simplified approaches to extract the various transport properties from the current in the external circuit [58, 65, 79, 83–85], which may lead to further issues.

For example, extracting \tilde{W} , through dividing L by the measured electron transit time, T_e , where the transit time is defined as the difference in times between the measured current's rise and fall to the respective half values. This is a measure of a drift velocity, but not one that is consistent with the flux or bulk drift velocities, or equation (24). Using that \tilde{W} to then determine any further parameters (e.g. $\tilde{\alpha}_T$ or \tilde{D}_L) will further propagate uncertainties in the other derived coefficients/parameters. Non-linear curve fitting to the full equation (24) should in fact be performed (as in, for example, reference [81]) in all cases.

In addition, extracting $\tilde{\alpha}_T$ from the rising component of the measured current [58] (and \tilde{W} from the earlier step) fails to capture the diffusion contributions to the current in the external circuit.

Using these simplified processes to establish initial estimates of the parameters, to start the non-linear curve fitting of the measured current (as in reference [81], for example) is, however, good practice.

¹³ This representation of the current in the external circuit fails to capture the second order contributions to the source term and hence the equation cannot be an accurate representation of the experimentally measured current in the external circuit when the product $\alpha_T \zeta_L$ becomes appreciable relative to D_L . While measurement of the skewness term has not been performed to date, many transient and stationary effects may skew the profile and require consideration [76, 86, 87].

arising from the diffusion equation (24) or the expression arising from the unphysical Brambring equation (26), takes the same general form, i.e. is mathematically equivalent:

$$I(t) = a \exp(bt) \left\{ \left[1 - \phi \left(\frac{ct - L}{\sqrt{4dt}} \right) \right] + \exp \left(\left[\frac{c}{d} \right] L \right) \left[\phi \left(\frac{ct + L}{\sqrt{4dt}} \right) - 1 \right] \right\}, \quad (27)$$

where a , b , c and d can be found from the non-linear curve fitting procedure and are related to the standard bulk transport coefficients/PT transport properties through comparisons with equations (24)/(26), or equivalently through comparison of equations (6)/(25). If in the previous analyses of PT experiments expression (26) has been fitted to the current in the external circuit, it then follows that the PT transport properties ($\tilde{\alpha}_T$, \tilde{W} , \tilde{D}_L) can be related to the bulk transport coefficients (R_{net} , W_B , $D_{B,L}$) via¹⁴:

$$R_{\text{net}} = \tilde{\alpha}_T \tilde{W} = b, \quad (30)$$

$$W_B = \tilde{W} + \tilde{\alpha}_T \tilde{D}_L = c, \quad (31)$$

$$D_{B,L} = \tilde{D}_L = d. \quad (32)$$

If the initial number of electrons n_0 is measured accurately, the fitting parameter a can provide a technique to measure the flux drift velocity, W —the first experiment able to do so!

We now consider some examples, transforming the PT transport properties extracted from existing PT measurements, through implementation of the theoretical relationships (30)–(32), in order to compare with the bulk transport coefficients which have firm foundations in kinetic theory/Boltzmann's equation. TOF measurements are included as measurements of bulk coefficients since they are analysed according the diffusion equation (6). It is important to note:

- The relationships (e.g. $W_B = \tilde{W} + \tilde{\alpha}_T \tilde{D}_L$) are presented only when all transport properties from the PT experiment (\tilde{W} , $\tilde{\alpha}_T$, \tilde{D}_L) are available from a single study to do the transformation.
- The intent of this section is purely to highlight the validity of the relationship between the PT transport properties and the bulk transport coefficients. Hence,
 - We do not preference any particular measurement technique over the other, but rather focus on the presentation of coefficients with firm theoretical foundations. Assessment of the quality of any experimental measurements is beyond the scope of the present work.

¹⁴ It is important to make the distinction that the relationship (30), $R_{\text{net}} = \tilde{\alpha}_T \tilde{W}$, is valid for the PT transport properties $\tilde{\alpha}_T$ and \tilde{W} . The relationship between R_{net} , the SST α_T and the bulk transport coefficients, however, is given by [53, 56].

$$R_{\text{net}} = \alpha_T W_B - \alpha_T^2 D_{B,L} + \dots \quad (28)$$

which, in the limit of small diffusion, may be approximated by

$$R_{\text{net}} \approx \alpha_T W_B. \quad (29)$$

- Transport coefficient calculations are obviously dependent on the cross-section set used. The calculations presented here are for comparison with the transformed PT results and should not be interpreted as the reference for quality of the experimental results or analysis.
- The error propagation associated with the application of the theoretical relationships (30)–(32) on existing PT transport properties results in large error bars. Ideally, reanalysis of the PT experiment current transients according to equation (24) would be preferred, if available, for appropriate determination of experimental error.

In the following subsections we present the results for Ar and SF₆. Ar is considered somewhat of a benchmark gas known for high accuracy measurements and well known cross-sections [33], while SF₆ provides a good example of when the differences are quite important due to its strong electron attachment and ionisation.

The numerical methods employed in the solution of Boltzmann's equation (1) for the calculated coefficients have been described in detail previously, and the reader is referred to references [88, 89].

4.1. Argon

Figures 1 and 2 present some of the available experimentally measured bulk drift velocities, W_B , and ionisation rate coefficients, R_{ionis} , for electron swarms in Ar. In the upper panel of figure 1, the W_B transformed via the theoretical relationship (31) from the \tilde{W} extracted from the PT experiment of de Urquijo *et al* [90] and Hernández-Ávila *et al* [91, 92] are shown with the W_B measured from the TOF apparatus of Küçükarpaci and Lucas [93, 94] and Nakamura and Kurachi [37], and the W_B from the scanning drift tube measurements of Korolov *et al* [69]. Measurements of W_B are sparse in the E/n_0 region where the transformation is most pronounced, although the trend of the de Urquijo *et al* W_B lies somewhat above the highest W_B datum of Nakamura and Kurachi [37] at 50 Td, the Küçükarpaci and Lucas [93, 94] W_B at around 150 Td, and the measurements of Korolov *et al* [69]. In contrast, both the \tilde{W} and W_B measurements of Hernández-Ávila *et al* [91, 92] tend to lie below the 50 Td Nakamura and Kurachi [37] value and the measurements of Korolov *et al* [69], with the highest E/n_0 measurement of Küçükarpaci and Lucas [93, 94] in good agreement with the transformed W_B . For Ar, the \tilde{W} and W_B differ by up to 4.2% for the de Urquijo *et al* [90] measurements and up to 8.2% for the Hernández-Ávila *et al* [91, 92] measurements, due to the relative magnitudes of the $D_{B,L}$ and $\tilde{\alpha}$ (as shown in figure 11 of de Urquijo *et al* [90]), the difference increasing with E/n_0 . These results highlight the accuracy of the PT measurements and associated analysis in reference [90].

The bulk and flux drift velocity calculated using the cross-section set extracted from Magboltz [95] are also displayed in figure 1 for comparison. While these calculations are dependent on the cross-section set utilised, good agreement is observed between the calculated W_B and the W_B transformed from the PT measurements of de Urquijo *et al* [90].

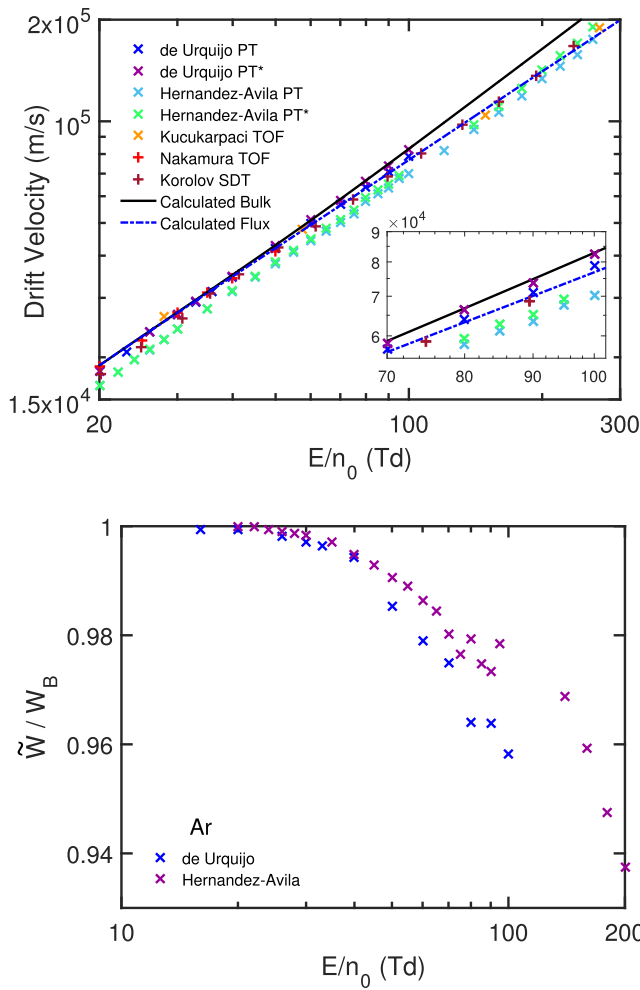


Figure 1. The drift velocity for electron swarms in gaseous argon. For the PT measurements, the bulk drift velocity W_B has been transformed from the PT measurements of \tilde{W} through the theoretical relationship (31), and is denoted by the asterisk (*). (Upper) The W_B transformed from the PT measurements of de Urquijo *et al* [90] (transformed using the $D_{B,L}$ first reported in reference [97] although recorded with the \tilde{W} and $\tilde{\alpha}_T$ reported in reference [90]) and Hernández-Ávila *et al* [91, 92] are compared with the W_B TOF measurements of Küçükarpaci and Lucas [93, 94] and Nakamura and Kurachi [37], and the W_B from the scanning drift tube (SDT) apparatus of Korolov *et al* [69]. (Lower) The ratio of the PT-measured to bulk drift velocities, \tilde{W}/W_B , for the measurements of de Urquijo *et al* [90] and Hernández-Ávila *et al* [91, 92]. ‘Calculated’ represents the flux and bulk drift velocities calculated from a solution of the Boltzmann equation using the cross-sections extracted from Magboltz [95].

The lower panel of figure 1 displays the ratio of the PT drift measurement to the bulk drift velocity, \tilde{W}/W_B . The ratio illustrates the difference between the drift velocities, which increases with increasing E/n_0 , as expected from the increasing magnitude of the $\tilde{\alpha}_T \tilde{D}_L$ term.

Figure 2 shows a comparison of R_{ionis} in Ar which is, to our knowledge, limited to the transformed PT measurements of de Urquijo *et al* [90] and Hernández-Ávila *et al* [91, 92], through the theoretical relationship (30), and the R_{ionis} extracted directly from the PT measurements of Dahl *et al* [58] and Haefliger and Franck [63, 96]. At the lower E/n_0 of the

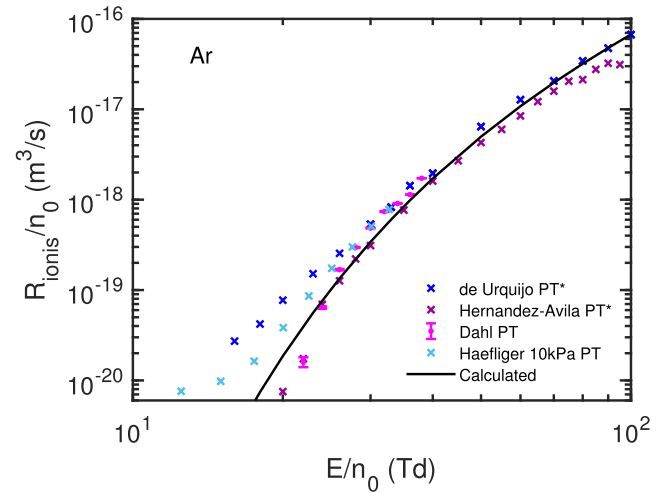


Figure 2. The ionisation rate coefficient for electron swarms in gaseous argon. The R_{ionis} transformed from the PT measurements of de Urquijo *et al* [90] and Hernández-Ávila *et al* [91, 92], through the theoretical relationship (30) and denoted by the asterisk (*), are compared with the (positive) R_{ionis} values reported in Dahl *et al* [58] and Haefliger and Franck [63, 96] (the representative measurement at 10 kPa has been used). ‘Calculated’ represents the R_{ionis} calculated from a solution of the Boltzmann equation using the cross-sections extracted from Magboltz [95].

de Urquijo *et al* measurements, good agreement is observed with the majority of the Haefliger and Franck coefficients (measured over a range of pressures, although only the 10 kPa measurement is displayed in figure 2), and over intermediate E/n_0 with the Dahl *et al* measurements. Over the full E/n_0 range of the (positive) Dahl *et al* measurements, very good consistency with the transformed Hernández-Ávila *et al* [91, 92] R_{net} is observed.

4.2. SF₆

Figures 3 and 4 present the bulk drift velocity, W_B , and net rate coefficient, R_{net} , from some of the available PT and TOF measurements for electron swarms in SF₆. The upper panel of figure 3 includes W_B transformed from the \tilde{W} measurements of Aschwanden [66] and Xiao *et al* [98], via the theoretical relationship (31), and the W_B TOF measurements of Nakamura [99] and Naidu and Prasad [100]. The transformation to W_B from the measured \tilde{W} of both Aschwanden and Xiao *et al* results in a *decrease* in magnitude below 361 Td, a consequence of the attachment-dominated $\tilde{\alpha}$, and *increase* in magnitude above this E/n_0 as ionising collisions dominate the $\tilde{\alpha}$ (and similarly, R_{net} in the lower panel of figure 3). The transformation of the Aschwanden [66] drift velocity results in a decrease of up to 4.7% in the attachment-dominated region, and an increase of up to 9.2% in the ionisation-dominated region, at the highest E/n_0 , while the transformation of the Xiao *et al* [98] measurements results in a decrease of up to 5.2% in the attachment-dominated region, and an increase of up to 2.3% in the ionisation-dominated region. The results shown in the upper panel of figure 3 highlight, in particular, the accuracy of the PT measurements and associated analysis in the work of Aschwanden [66].

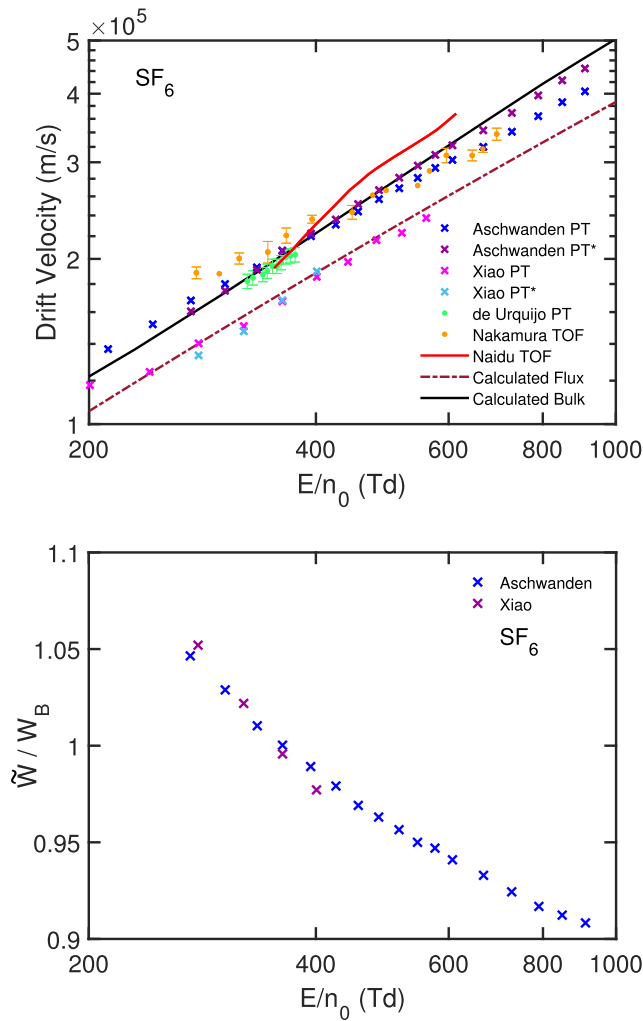


Figure 3. The drift velocity for electron swarms in gaseous SF_6 . For the PT measurements, the bulk drift velocity W_B has been transformed from the PT measurements of \tilde{W} through the theoretical relationship (31), and is denoted by the asterisk (*). (Upper) The W_B transformed from the PT measurements of Aschwanden [66] (with the necessary PT transport properties available for $E/n_0 \geq 273$ Td) and Xiao *et al* [98] (with the necessary properties available for $E/n_0 = 279\text{--}401$ Td), are shown alongside the \tilde{W} measured by the PT apparatus of de Urquijo *et al* [103] (where, in the absence of $D_{B,L}$, W_B could not be determined). Also displayed are the W_B TOF measurements of Nakamura [99] and Naidu and Prasad [100] (digitised from Christophorou and Olthoff [102]). (Lower) The ratio of the PT-measured to bulk drift velocities, \tilde{W}/W_B , for the PT measurements of de Urquijo *et al* [103], Xiao *et al* [98] and Xiao *et al* [104]. ‘Calculated’ represents the flux and bulk drift velocities calculated from a solution of the Boltzmann equation using the cross-section data of Biagi [101] from the LXCat database.

Compared to the other W_B measurements (from the TOF apparatus), the transformation of the Aschwanden data increases the differences when compared to the measurements of Nakamura over all E/n_0 , but decreases the differences from the Naidu and Prasad W_B . Similarly, for the four data points of the Xiao *et al* measurements, where all PT transport properties were reported (279–401 Td), the transformation to W_B increases the differences from the other experimental measurements.

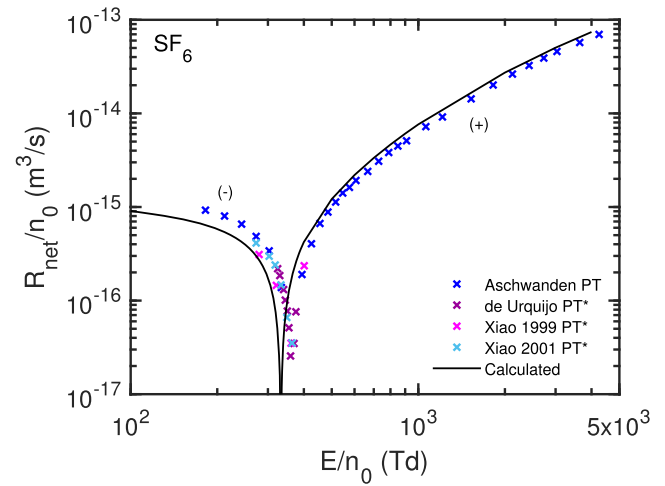


Figure 4. The ionisation coefficient for electron swarms in gaseous SF_6 . The absolute value of the R_{net} reported from the PT measurements of Aschwanden [66] are compared with the R_{net} transformed through the theoretical relationship (30) and denoted by the asterisk (*), from the PT measurements of de Urquijo *et al* [103], Xiao *et al* [98] and Xiao *et al* [104]. ‘Calculated’ represents the R_{net} calculated from a solution of the Boltzmann equation using the cross-section data of Biagi [101] from the LXCat database.

We are thus unable to reconcile the PT measurements of \tilde{W} from Xiao *et al*.

The flux and bulk drift velocity and R_{net} values calculated using the cross-section data of Biagi [101] from the LXCat database, are also shown in figures 3 and 4. These representative calculations are dependent on the cross-section set used, and are included only to indicate the magnitudes of the transport coefficients, in particular highlighting the effect of the non-conservative processes on the calculated W_B compared to the flux drift velocity, W ¹⁵. In both the attachment and ionisation-dominated regions, the transformation of the Aschwanden \tilde{W} changes in the direction consistent with the representative calculations. As a result, the transformed experimental results of Aschwanden are in good agreement with our representative calculations.

The lower panel of figure 3 displays the ratio of the PT drift measurement to the bulk drift velocity, \tilde{W}/W_B . The ratio illustrates the contribution of the $\tilde{\alpha}_T \tilde{D}_L$ term in relationship (30), to the transformation to W_B . The change in sign of R_{net} results in a decrease to W_B relative to the measured \tilde{W} for the lower E/n_0 , followed by an increase of W_B relative to \tilde{W} . The magnitude of the difference increases further from the breakdown E/n_0 value, consistent with the magnitude of R_{net} .

In the absence of any other R_{net} measurements in SF_6 , to our knowledge¹⁶, figure 4 only displays the rate coefficient of Aschwanden [66], reported directly in that thesis,

¹⁵ We make no comment on the validity of that cross-section set here, only to highlight that we are unable to predict accurately the breakdown reduced field as shown in figure 4.

¹⁶ We note that many values of the attachment rate coefficient have been reported for SF_6 in various buffer gases (see the review of Christophorou and Olthoff [102]), but in the absence of any mean energy values for the PT measurements, the comparison of R_{att} at a common mean energy cannot be made.

and the rate coefficients of de Urquijo *et al* [103] and Xiao *et al* [98, 104], transformed through the relationship (30), with good agreement observed between all.

5. Concluding remarks

In this study we have addressed, from a fundamental viewpoint, the issue of the analysis and interpretation of the PT experiment. We have shown that the governing equation traditionally used to analyse the PT experiment—the Brambring representation of the equation of continuity—is fundamentally flawed, and transport properties subsequently defined through that equation do not have a clear representation in terms of the distribution function. We have presented an expression for the current in the external circuit of the PT experiment in terms of the standard diffusion equation and the universal transport coefficients defined through it—the bulk transport coefficients. In addition, we have developed a relationship between the transport properties extracted from the PT experiment using the Brambring representation of the equation of continuity and the bulk transport coefficients, and highlighted the validity of the relationship for various gases. Given the errors that are necessarily propagated through this process, we suggest that all previous transport properties extracted from PT experimental data where non-conservative processes are operative be re-analysed according to the diffusion equation based current expression to enable measurement of standard bulk transport coefficients prior to any subsequent application (e.g. evaluating complete and accurate sets of scattering cross-sections, and further utilisation in modelling of plasmas and ionised gases [3, 12, 13, 44, 105]).

A consequence of the present analysis is the necessary reconciliation between experimental and theoretical studies involving PT measurements.

As a minimum for any swarm study, the *exact* definition of any transport property/coefficient measured or used for further analyses must be identified. Further, the definition of any transport property/coefficient must be consistent with those defined through kinetic theory and representable in terms of the phase-space distribution function.

In addition, the following are recommended for clear identification in experimental studies:

- Primary reference to the exact source equation used for analysis, and any assumptions entailed.
- A description of the method of the analysis of all measurements.
- A detailed estimate of the error associated with the statistical analysis (including systematic errors, reproducibility, etc), alongside the reported experimental uncertainty.
- The applicability of the hydrodynamic or non-hydrodynamic regime, and the methods used to ensure sampling under appropriate conditions. This point is generally well accomplished in the literature.
- Clear uncertainty estimates of all elements (e.g. pressure, mixture ratio, etc) and how they propagate through to the final result [106–109].

Prior to the use of any swarm transport measurements in theoretical models (low temperature plasma models), the effect of non-conservative collisions must be identified, since it is when flux and bulk values start to differ significantly that one needs to pay attention to the nature of the transport data required in their models. A detailed prescription has been presented previously [110].

Using ‘wrong’ theory yields results that may be up to a factor of 10 different under some circumstances, though often effects are of the order of 10%–30%. However, if one uses a similar theory to implement the cross-sections obtained from incorrectly interpreted data one returns to the original experimental data. Plasma modelling is sufficiently robust that small changes in the transport data are easily compensated by small self consistent adjustments of the local field. Problems occur when one uses more exact models to describe plasmas. PIC codes with a properly implemented and tested Monte Carlo simulation will provide correct calculation of fluxes and thus the effect of the cross-sections obtained from the incorrectly interpreted data may become large, as stated above. Even more so, as the plasma field is calculated self consistently small changes in the local E/n_0 as compared to the properly determined values would originate. Some processes with a high threshold, such as dissociation and ionization, are very strongly affected by the local normalised electric field, even by orders of magnitude (see reference [111], for example).

In this vein, it is recommended that theoretical studies clearly identify the definition of any utilised experimental measurements and any further analysis of those measurements (e.g. transformation from one transport coefficient to another via approximate relationships with associated errors propagated).

In addition to these recommendations to aid reconciliation within the literature, the present work also seeds further investigation, specifically into the analysis and interpretation of the PT experiment. For example, the impact of the boundary conditions, on the electron density at the electrodes, on the expression for the current in the external circuit, and the ability to extract higher order transport coefficients (e.g. skewness) from the current measured from the PT experiment should also be studied.











Acknowledgments

The authors would like to thank the Australian Research Council through its Discovery Programme (DP180101655) for financial support. S Dujko, D Bošnjaković and I Simonović are supported by the Ministry of Education, Science and Technological Development of the Republic of Serbia and the Institute of Physics (Belgrade), while Z Lj Petrović is grateful to the SASA F155 project and Ulster University for support.

Data availability statement

The data that support the findings of this study are available upon reasonable request from the authors.

ORCID iDs

M J E Casey  <https://orcid.org/0000-0003-0193-211X>
 P W Stokes  <https://orcid.org/0000-0002-0956-5927>
 D G Cocks  <https://orcid.org/0000-0002-9943-7100>
 D Bošnjaković  <https://orcid.org/0000-0002-2725-5287>
 I Simonović  <https://orcid.org/0000-0001-6704-9042>
 M J Brunger  <https://orcid.org/0000-0002-7743-2990>
 S Dujko  <https://orcid.org/0000-0002-4544-9106>
 Z Lj Petrović  <https://orcid.org/0000-0001-6569-9447>
 R E Robson  <https://orcid.org/0000-0003-2613-4229>
 R D White  <https://orcid.org/0000-0001-5353-7440>

References

- [1] Brambring J R 1964 *Z. Phys.* **179** 532
- [2] Huxley L G H and Crompton R W 1974 *The Diffusion and Drift of Electrons in Gases* (New York: Wiley)
- [3] Adamovich I et al 2017 *J. Phys. D: Appl. Phys.* **50** 323001
- [4] Brunger M J 2017 *Int. Rev. Phys. Chem.* **36** 333
- [5] Campbell L and Brunger M J 2013 *Plasma Sources Sci. Technol.* **22** 013002
- [6] Brunetti R et al 2005 *New Astron. Rev.* **49** 265
- [7] Calvo J et al 2017 *J. Cosmol. Astropart. Phys.* **JCAP03(2017)** 003
- [8] Montie T C, Kelly-Wintenberg K and Roth J R 2000 *IEEE Trans. Plasma Sci.* **28** 41
- [9] Bekeschus S, Schmidt A, Weltmann K-D and von Woedtke T 2016 *Clin. Plasma Med.* **4** 19
- [10] von Woedtke T, Metelmann H-R and Weltmann K-D 2014 *Contrib. Plasma Phys.* **54** 104
- [11] Stoffels E, Sakiyama Y and Graves D B 2008 *IEEE Trans. Plasma Sci.* **36** 1441
- [12] Muñoz A, Blanco F, Garcia G, Thorn P A, Brunger M J, Sullivan J P and Buckman S J 2008 *Int. J. Mass Spectrom.* **277** 175
- [13] Francis Z, Incerti S, Capra R, Mascialino B, Montarou G, Stepan V and Villagrasa C 2011 *Appl. Radiat. Isot.* **69** 220
- [14] Rabie M and Franck C M 2018 *Environ. Sci. Technol.* **52** 369
- [15] Bartschat K and Kushner M J 2016 *Proc. Natl Acad. Sci. USA* **113** 7026
- [16] Kong M G, Kroesen G, Morfill G, Nosenko T, Shimizu T, van Dijk J and Zimmermann J L 2009 *New J. Phys.* **11** 115012
- [17] Christophorou L G and Olthoff J K 2001 *Advances in Atomic, Molecular, and Optical Physics* vol 44 (Amsterdam: Elsevier) pp 59–98
- [18] Brandenburg R 2017 *Plasma Sources Sci. Technol.* **26** 053001
- [19] Roussel-Dupré R, Colman J J, Symbalisty E, Sentman D and Pasko V P 2008 *Space Sci. Rev.* **137** 51
- [20] Misra N N, Martynenko A, Chemat F, Paniwnyk L, Barba F J and Jambrak A R 2018 *Crit. Rev. Food Sci. Nutr.* **58** 1832
- [21] Marinković B P, Bredehöft J H, Vujčić V, Jevremović D and Mason N J 2017 *Atoms* **5** 46
- [22] Frost L S and Phelps A V 1962 *Phys. Rev.* **127** 1621
- [23] Engelhardt A G and Phelps A V 1964 *Phys. Rev.* **133** A375
- [24] Engelhardt A G, Phelps A V and Risk C G 1964 *Phys. Rev.* **135** A1566
- [25] Phelps A V 1968 *Rev. Mod. Phys.* **40** 399
- [26] Christophorou L G and Hunter S R 1984 *Electron Molecule Interactions and Their Applications* vol 2 ed L G Christophorou (New York: Academic Press)
- [27] Milloy H B and Crompton R W 1977 *Phys. Rev. A* **15** 1847
- [28] Crompton R W 1994 *Advances in Atomic, Molecular, and Optical Physics* vol 32 (Amsterdam: Elsevier) pp 97–148
- [29] Petrović Z Lj, Šuvakov M, Nikitović Ž, Dujko S, Šašić O, Jovanović J, Malović G and Stojanović V 2007 *Plasma Sources Sci. Technol.* **16** S1
- [30] Robson R E, White R D and Ness K F 2011 *J. Chem. Phys.* **134** 064319
- [31] Ness K F, Robson R E, Brunger M J and White R D 2012 *J. Chem. Phys.* **136** 024318
- [32] de Urquijo J, Basurto E, Juárez A M, Ness K F, Robson R E, Brunger M J and White R D 2014 *J. Chem. Phys.* **141** 014308
- [33] Pitchford L C et al 2017 *Plasma Proc. Polym.* **14** 1600098
- [34] Jovanović J V, Stojanović V, Raspopović Z, de Urquijo J and Petrović Z Lj 2019 *Plasma Sources Sci. Technol.* **28** 045006
- [35] Grofulović M, Alves L L and Guerra V 2016 *J. Phys. D: Appl. Phys.* **49** 395207
- [36] Schmidt B, Berkhan K, Götz B and Müller M 1994 *Phys. Scr.* **T53** 30
- [37] Nakamura Y and Kurachi M 1988 *J. Phys. D: Appl. Phys.* **21** 718
- [38] Morgan W L 1992 *Plasma Chem. Plasma Process.* **12** 449
- [39] Gibson D K 1970 *Aust. J. Phys.* **23** 683
- [40] Davies D K, Kline L E and Bies W E 1989 *J. Appl. Phys.* **65** 3311
- [41] Rabie M, Haeffliger P, Chachereau A and Franck C M 2015 *J. Phys. D: Appl. Phys.* **48** 075201
- [42] Mirić J, Simonović I, Petrović Z Lj, White R D and Dujko S 2017 *Eur. Phys. J. D* **71** 289
- [43] Zawadzki M, Chachereau A, Kočišek J, Franck C M and Fedor J 2018 *J. Chem. Phys.* **149** 204305
- [44] Petrović Z Lj, Dujko S, Marić D, Malović G, Nikitović Ž, Šašić O, Jovanović J, Stojanović V and Radmilović-Radenović M 2009 *J. Phys. D: Appl. Phys.* **42** 194002
- [45] Crompton R W 1967 *J. Appl. Phys.* **38** 4093
- [46] Thomas W R L 1969 *J. Phys. B: At. Mol. Phys.* **2** 551
- [47] Tagashira H, Sakai Y and Sakamoto S 1977 *J. Phys. D: Appl. Phys.* **10** 1051
- [48] Sakai Y, Tagashira H and Sakamoto S 1977 *J. Phys. D: Appl. Phys.* **10** 1035
- [49] Boeuf J P and Marode E 1984 *J. Phys. D: Appl. Phys.* **17** 1133
- [50] Blevin H A and Fletcher J 1984 *Aust. J. Phys.* **37** 593
- [51] Robson R E 1986 *J. Chem. Phys.* **85** 4486
- [52] Kondo K and Tagashira H 1990 *J. Phys. D: Appl. Phys.* **23** 1175
- [53] Robson R E 1991 *Aust. J. Phys.* **44** 685
- [54] Robson R E 1995 *Aust. J. Phys.* **48** 677
- [55] Nakamura Y 2007 *Proc. 28th ICPiG (Prague)* pp 224–6
- [56] Dujko S, White R D and Petrović Z Lj 2008 *J. Phys. D: Appl. Phys.* **41** 245205
- [57] Robson R E, White R D and Hildebrandt M 2017 *Fundamentals of Charged Particle Transport in Gases and Condensed Matter* (Boca Raton, FL: CRC Press)
- [58] Dahl D A, Teich T H and Franck C M 2012 *J. Phys. D: Appl. Phys.* **45** 485201
- [59] Dahl D A and Franck C M 2013 *J. Phys. D: Appl. Phys.* **46** 445202
- [60] Chachereau A, Rabie M and Franck C M 2016 *Plasma Sources Sci. Technol.* **25** 045005
- [61] Chachereau A, Fedor J, Janečková R, Kočišek J, Rabie M and Franck C M 2016 *J. Phys. D: Appl. Phys.* **49** 375201
- [62] Haeffliger P, Hösl A and Franck C M 2018 *J. Phys. D: Appl. Phys.* **51** 355201
- [63] Haeffliger P and Franck C M 2018 *Rev. Sci. Instrum.* **89** 023114
- [64] Pachin J, Hösl A and Franck C M 2019 *J. Phys. D: Appl. Phys.* **52** 235204
- [65] Ridenti M A, Vivaldini T C, Lima I B and Pascholati P R 2010 *AIP Conf. Proc. (AIP)* vol 1245 pp 92–7
- [66] Aschwanden T 1985 Die ermittlung physikalischer entladungsparameter in isoliergasen und isoliergasgemischen

- mit einer verbesserten Swarm-methode *PhD Thesis* ETH Zurich
- [67] Phelps A V and Pitchford L C 1985 *Phys. Rev. A* **31** 2932
- [68] Ruiz-Vargas G, Yousfi M and de Urquijo J 2010 *J. Phys. D: Appl. Phys.* **43** 455201
- [69] Korolov I, Vass M, Bastykova N K and Donkó Z 2016 *Rev. Sci. Instrum.* **87** 063102
- [70] Donkó Z, Hartmann P, Korolov I, Jeges V, Bošnjaković D and Dujko S 2019 *Plasma Sources Sci. Technol.* **28** 095007
- [71] Pinhão N R, Loffhagen D, Vass M, Hartmann P, Korolov I, Dujko S, Bošnjaković D and Donkó Z 2020 *Plasma Sources Sci. Technol.* **29** 045009
- [72] Hasegawa H, Date H and Shimoizuma M 2007 *J. Phys. D: Appl. Phys.* **40** 2495
- [73] Robson R E 1985 *Phys. Rev. A* **31** 3492
- [74] Philippa B, White R D and Robson R E 2011 *Phys. Rev. E* **84** 041138
- [75] Kumar K, Skullerud H R and Robson R E 1980 *Aust. J. Phys.* **33** 343
- [76] Stokes P W, Simonović I, Philippa B, Cocks D G, Dujko S and White R D 2018 *Sci. Rep.* **8** 1
- [77] Robson R E and Ness K F 1986 *Phys. Rev. A* **33** 2068
- [78] White R D, Ness K F and Robson R E 2002 *Appl. Surf. Sci.* **192** 26
- [79] de Urquijo J, Arriaga C A, Cisneros C and Alvarez I 1999 *J. Phys. D: Appl. Phys.* **32** 41
- [80] Basurto E, Hernández-Ávila J L, Juárez A M and de Urquijo J 2013 *J. Phys. D: Appl. Phys.* **46** 355207
- [81] de Urquijo J, Juárez A M, Rodríguez-Luna J C and Ramos-Salas J S 2007 *IEEE Trans. Plasma Sci.* **35** 1204
- [82] Šašić O, de Urquijo J, Juárez A M, Dupljanin S, Jovanović J, Hernández-Ávila J L, Basurto E and Petrović Z Lj 2010 *Plasma Sources Sci. Technol.* **19** 034003
- [83] Bekstein A, de Urquijo J, Ducasse O, Rodríguez-Luna J C and Juárez A M 2012 *J. Phys.: Conf. Ser.* **370** 012006
- [84] de Urquijo J, Alvarez I, Basurto E and Cisneros C 1999 *J. Phys. D: Appl. Phys.* **32** 1646
- [85] Datskos P G, Carter J G and Christophorou L G 1992 *J. Appl. Phys.* **71** 15
- [86] Simonović I, Bošnjaković D, Petrović Z Lj, White R D and Dujko S 2020 *Eur. Phys. J. D* **74** 1
- [87] Simonović I, Bošnjaković D, Petrović Z Lj, Stokes P W, White R D and Dujko S 2020 *Phys. Rev. E* **101** 023203
- [88] Boyle G J, Tattersall W J, Cocks D G, Dujko S and White R D 2015 *Phys. Rev. A* **91** 052710
- [89] Boyle G J, McEachran R P, Cocks D G and White R D 2015 *J. Chem. Phys.* **142** 154507
- [90] de Urquijo J, Casey M J E, Serkovic-Loli L N, Cocks D G, Boyle G J, Jones D B, Brunger M J and White R D 2019 *J. Chem. Phys.* **151** 054309
- [91] Hernández-Ávila J L, Basurto E and de Urquijo J 2004 *J. Phys. D: Appl. Phys.* **37** 3088
- [92] Hernández-Ávila J L, Basurto E and de Urquijo J 2004 UNAM database <http://lxcnet.net> accessed 03 January 2018
- [93] Küçükarpaci H N and Lucas J 1981 *J. Phys. D: Appl. Phys.* **14** 2001
- [94] Küçükarpaci H N and Lucas J 1981 IST-Lisbon database <http://lxcnet.net> accessed 03 January 2019
- [95] Biagi S F Magboltz version 8.97 <http://magboltz.web.cern.ch/magboltz/> accessed 31 December 2017
- [96] Haeffliger P and Franck C M 2018 ETHZ (ETH Zurich, high voltage laboratory) database <http://lxcnet.net> accessed 03 January 2019
- [97] Foster S 2018 Self-consistency of electron-THFA gaseous cross-sections via Swarm techniques *Undergraduate Honors Thesis* James Cook University
- [98] Xiao D M, Zhu L L and Chen Y Z 1999 *J. Phys. D: Appl. Phys.* **32** L18
- [99] Nakamura Y 1988 *J. Phys. D: Appl. Phys.* **21** 67
- [100] Naidu M S and Prasad A N 1972 *J. Phys. D: Appl. Phys.* **5** 1090
- [101] Biagi S F 2014 Biagi database (Magboltz version 10.6) <http://lxcnet.net/Biagi> accessed 03 January 2019
- [102] Christophorou L G and Olthoff J K 2000 *J. Phys. Chem. Ref. Data* **29** 267
- [103] de Urquijo J, Basurto E and Hernández-Ávila J L 2001 *J. Phys. D: Appl. Phys.* **34** 2151
- [104] Xiao D M, Li X G and Xu X 2001 *J. Phys. D: Appl. Phys.* **34** L133
- [105] Petrović Z Lj, Marić D, Savić M, Marjanović S, Dujko S and Malović G 2017 *Plasma Proc. Polym.* **14** 1600124
- [106] Crompton R W and Jory R L 1962 *Aust. J. Phys.* **15** 451
- [107] Crompton R W, Elford M T and Gascoigne J 1965 *Aust. J. Phys.* **18** 409
- [108] Elford M T 1971 *Aust. J. Phys.* **24** 705
- [109] Crompton R W and Elford M T 1973 *Aust. J. Phys.* **26** 771
- [110] Robson R E, White R D and Petrović Z Lj 2005 *Rev. Mod. Phys.* **77** 1303
- [111] Mladenović Ž, Gocić S, Marić D and Petrović Z Lj 2018 *Eur. Phys. J. Plus* **133** 344

PAPER

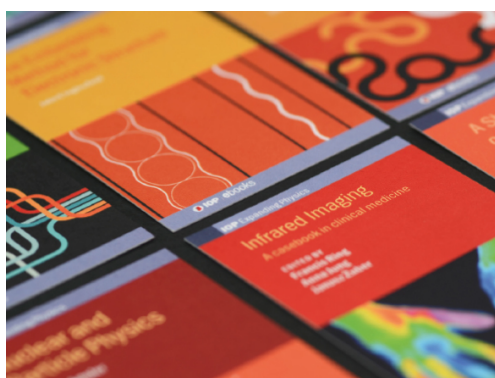
Third-order transport coefficients for electrons in N_2 and CF_4 : effects of non-conservative collisions, concurrence with diffusion coefficients and contribution to the spatial profile of the swarm

To cite this article: I Simonovi *et al* 2022 *Plasma Sources Sci. Technol.* **31** 015003

View the [article online](#) for updates and enhancements.

You may also like

- [Experimental and theoretical study of RF capacitively coupled plasma in \$Ar-CF_4-CF_3I\$ mixtures](#)
O V Proshina, T V Rakhimova, D V Lopaev *et al.*
- [Electron swarm properties under the influence of a very strong attachment in \$SF_6\$ and \$CF_3I\$ obtained by Monte Carlo rescaling procedures](#)
J Miri, D Bošnjakovi, I Simonovi *et al.*
- [Comparison of vacuum ultra-violet emission of \$Ar/CF_4\$ and \$Ar/CF_3I\$ capacitively coupled plasmas](#)
A Zotovich, O Proshina, Z el Otell *et al.*



IOP | ebooks™

Bringing together innovative digital publishing with leading authors from the global scientific community.

Start exploring the collection—download the first chapter of every title for free.

Third-order transport coefficients for electrons in N_2 and CF_4 : effects of non-conservative collisions, concurrence with diffusion coefficients and contribution to the spatial profile of the swarm

I Simonović¹ , D Bošnjaković¹ , Z Lj Petrović^{2,3} , R D White⁴  and S Dujko^{1,*} 

¹ Institute of Physics Belgrade, University of Belgrade, Pregrevica 118, 11080 Belgrade, Serbia

² University of Ulster, Newtownabbey, Antrim, Northern Ireland, United Kingdom

³ Serbian Academy of Sciences and Arts, Knez Mihailova 35, 11000 Belgrade, Serbia

⁴ College of Science and Engineering, James Cook University, Townsville, QLD 4811, Australia

E-mail: sasha@ipb.ac.rs

Received 20 September 2021, revised 23 November 2021

Accepted for publication 6 December 2021

Published 11 January 2022



Abstract

Using a multi-term solution of the Boltzmann equation and Monte Carlo simulation technique we study behaviour of the third-order transport coefficients for electrons in model gases, including the ionisation model of Lucas and Saelee and modified Ness–Robson model of electron attachment, and in real gases, including N_2 and CF_4 . We observe negative values in the E/n_0 -profiles of the longitudinal and transverse third-order transport coefficients for electrons in CF_4 (where E is the electric field and n_0 is the gas number density). While negative values of the longitudinal third-order transport coefficients are caused by the presence of rapidly increasing cross sections for vibrational excitations of CF_4 , the transverse third-order transport coefficient becomes negative over the E/n_0 -values after the occurrence of negative differential conductivity. The discrepancy between the two-term approximation and the full multi-term solution of the Boltzmann equation is investigated for electrons in N_2 and CF_4 . While the accuracy of the two-term approximation is sufficient to investigate the behaviour of the third-order transport coefficients in N_2 , it produces large errors and is not even qualitatively correct for electrons in CF_4 . The influence of implicit and explicit effects of electron attachment and ionisation on the third-order transport tensor is investigated. In particular, we discuss the effects of attachment heating and attachment cooling on the third-order transport coefficients for electrons in the modified Ness–Robson model, while the effects of ionisation are studied for electrons in the ionisation model of Lucas and Saelee, N_2 and CF_4 . The concurrence between the third-order transport coefficients and the components of the diffusion tensor, and the contribution of the longitudinal component of the third-order transport tensor to the spatial profile of the swarm are also investigated. For electrons in CF_4 and CH_4 , we found that the contribution of the component of the third-order transport tensor to the spatial profile of the swarm between approximately 50 Td and 700 Td, is almost identical to the corresponding contribution for electrons in N_2 . This suggests that the recent measurements of third-order transport coefficients for electrons in N_2 may be extended and generalized to other gases, such as CF_4 and CH_4 .

* Author to whom any correspondence should be addressed.

Keywords: third-order transport coefficients, Boltzmann equation, Monte Carlo simulation, electron transport, ionisation, electron attachment

(Some figures may appear in colour only in the online journal)

1. Introduction

Non-equilibrium plasmas have a wide range of important applications including micro and nano-electronic device fabrication [1–4], surface etching [5, 6], sputtering [7, 8], chemical processing [9, 10], and plasma medicine [11–13]. The modelling of non-equilibrium plasma is important for further development and optimization of these applications [14–17]. However, this can be quite challenging due to a wide variety of effects that determine the nature of non-equilibrium plasma. These effects include collisions of electrons and ions with neutral particles of the background fluid [18–20], kinetics of excited species [21–23], generation of fast neutrals [24], space charge effects [25, 26], and plasma-surface interaction [27, 28]. Despite their simplicity, charged-particle swarms are at the heart of non-equilibrium plasma modelling [2, 18, 29, 30]. Specifically, transport coefficients that describe the dynamics of a swarm of charged particles are used as input data into the fluid models of non-equilibrium plasma [31–38]. In addition, transport coefficients are required in the swarm procedure for determining the complete and consistent sets of cross-sections for collisions of charged particles with atoms and molecules of the background fluid [39–42]. These sets of cross-sections are employed as input data into the particle models of non-equilibrium plasma [43–49]. Due to the sensitivity of plasma models to transport coefficients and cross-section sets in the case of fluid and particle models, respectively, a great amount of attention has been dedicated to the calculation and measurement of transport coefficients of electrons and ions in numerous atomic and molecular gases. However, this attention has been limited to the lower-order transport coefficients such as rate coefficients for non-conservative processes, drift velocity, and diffusion tensor components [18, 19, 50].

Transport coefficients of third and higher order have been implemented to analyse ion swarm experiments [51–55]. However, they have been almost systematically ignored in the traditional analysis of electron swarm experiments, as they are difficult to measure and difficult to study by employing theoretical methods [56–58]. However, Kawaguchi and co-workers have recently measured third-order transport coefficients for electrons in molecular nitrogen by employing the arrival time spectra experiment [59]. In addition, they have shown that it is necessary to consider the longitudinal component of the third-order transport tensor Q_L in order to correctly determine the longitudinal component of the diffusion tensor D_L from the arrival time spectra data. The difference between the values of D_L , which are estimated after neglecting Q_L , and the corresponding values, which are determined from the expression that includes Q_L , is greater than the sum

of their experimental errors at high electric fields. Moreover, it is known that the third-order transport coefficients are required for the conversion of hydrodynamic flux transport coefficients into transport parameters that are determined from the steady state Townsend experiment [60]. Third-order transport coefficients are more sensitive to energy dependence of the cross sections for the scattering of charged particles on the constituents of the background medium than drift velocity and diffusion tensor [56, 61, 62]. For this reason, third-order transport coefficients would be very useful in the swarm procedure for determining the complete sets of cross sections, if these transport coefficients were calculated and measured with a sufficient precision. Kawaguchi *et al* [59] have shown that the third-order transport coefficients are sensitive to the anisotropy of electron scattering. Thus, inclusion of the third-order transport coefficients would help in testing the implementation of anisotropic scattering in transport calculations, if the values of these transport coefficients were known from experiments [63]. This is important as the correct implementation of anisotropic scattering is required for determining the values of the rate coefficient for electron impact ionisation at high electric fields, with high precision [63, 64].

The structure of the third-order transport tensor in the electric field only configuration was determined by Whealton and Mason [65], Vrhovac *et al* [56] and Koutselos [52]. Simonović and co-workers have determined the structure of this tensor in all configurations of electric and magnetic field, and they have investigated the physical interpretation of the individual components of this tensor [58]. Koutselos studied the third-order transport coefficients for ions in atomic gases, by employing molecular dynamics simulations and a three-temperature method for solving the Boltzmann equation [52, 66–68]. Third-order transport coefficients for electrons in noble gases were investigated by Penetrante and Bardsley [61], Vrhovac *et al* [56] and Simonović *et al* [69]. Penetrante and Bardsley used the two-term approximation for solving the Boltzmann equation and Monte Carlo (MC) simulations, Vrhovac *et al* employed the momentum transfer theory and generalized Einstein relations, while Simonović *et al* used a multi-term theory for solving the Boltzmann equation. Stokes and co-workers investigated the effects of localized and delocalized electron states on the third-order transport coefficients [70]. Recently, Kawaguchi *et al* [71] have shown that the third-order transport coefficients can be measured in the arrival time spectra experiment by employing MC simulations, and they have determined the values of these transport coefficients for electrons in CH_4 and SF_6 by using the same method. They have subsequently measured the longitudinal component of the third-order transport tensor for electrons in N_2 by employing the arrival time spectra experiment. Kawaguchi

et al have further verified these results by using MC simulations [59, 63].

Although the lower-order transport coefficients have been carefully investigated in the literature, the third-order transport coefficients are still largely unexplored. For this reason, a number of questions concerning the properties of these transport coefficients and their dependence on elementary scattering processes are still open. How sensitive are these transport coefficients to effects of non-conservative collisions such as ionisation and electron attachment? Are the differences between the flux and bulk values of the third order transport coefficients higher or lower than the corresponding differences in the lower order transport coefficients? Is there any concurrence between these transport coefficients and those of lower-order? If such concurrence exists, how can it be accounted for? Can third-order transport coefficients be negative, and what would the negative values of these transport coefficients mean physically? Some of these issues will be addressed in this work. Implicit and explicit effects of electron attachment and ionisation on the third-order transport tensor are investigated, for electrons in Ness–Robson model and Lucas–Saelee model, respectively, by employing MC simulations and a multi-term method for solving the Boltzmann equation. In addition, explicit effects of ionisation on this transport tensor for electrons in N_2 and CF_4 are studied. Negative values of the third-order transport coefficients for electrons in CF_4 are also investigated. The concurrence between these transport coefficients and diffusion is analysed for electrons in N_2 and CF_4 . The values of the longitudinal component of the third-order transport tensor for electrons in N_2 , that are determined in this work, are compared with results of Kawaguchi *et al*. The contribution of the third-order transport coefficients to the spatial profile of the swarm is determined for electrons in N_2 , CF_4 and CH_4 over a wide range of the reduced electric field. The third-order transport coefficients are defined in section 2. The methods for calculating these transport coefficients by employing a multi-term solution of the Boltzmann equation and MC simulations are discussed in sections 3.1 and 3.2, respectively. The cross sections for model and real gases, that are used as input data in this work, are discussed in section 4.1. The variation of the flux third-order transport tensor with the reduced electric field for electrons in N_2 and CF_4 is analysed in section 4.2. The impact of electron attachment on the third-order transport coefficients for electrons in the modified Ness–Robson model is studied in section 4.3.1, while the influence of electron impact ionisation on these transport coefficients for electrons in Lucas–Saelee model, N_2 and CF_4 is investigated in section 4.3.2. The longitudinal component of the third-order transport tensor, that is determined in this study, is compared with the measurements and calculations of Kawaguchi and co-workers in section 4.4. Concurrence between the third-order transport coefficients and individual components of the diffusion tensor for electrons in N_2 and CF_4 is analysed in this section as well. In the same section the contribution of the third-order transport coefficients to the spatial profile of the swarm is determined for electrons in N_2 , CF_4 and CH_4 . The concluding remarks are given in section 5.

2. Theory

Transport coefficients are defined for a swarm of charged particles in hydrodynamic conditions. A swarm is an ensemble of charged particles that moves in a neutral background fluid under the influence of an external electric and/or magnetic field. The density of charged particles is considered to be small, so that their mutual interactions, as well as the effects induced by the space-charge, are neglected. The swarm gains energy from the external electric field and it dissipates this energy input into collisions with the particles of the background fluid. However, the probability of having collisions with molecules perturbed/excited by the swarm itself is negligible due to a low swarm particle density.

If the external fields are uniform in space, the swarm relaxes to a stationary state in which the amount of energy that is gained per unit time, is equal to the amount of energy that is dissipated in collisions during this time. The influence of the swarm on the background fluid and fields is neglected, due to the low density of charged particles, and it is considered that this fluid is in a state of thermodynamic equilibrium. Hydrodynamic conditions are fulfilled for a swarm of charged particles if the background fluid and the electric/magnetic fields are spatially homogeneous, and if the swarm is far from the boundaries of the system and far from sources and sinks of charged particles. Under these conditions the phase space distribution function can be expanded into a density gradient series as [72]:

$$f(\mathbf{r}, \mathbf{c}, t) = \sum_{k=0}^{\infty} \mathbf{f}^{(k)}(\mathbf{c}) \odot (-\nabla)^k n(\mathbf{r}, t), \quad (1)$$

where \mathbf{r} , \mathbf{c} and t are radius vector, velocity vector and time, respectively, $\mathbf{f}^{(k)}(\mathbf{c})$ are tensors of rank k , \odot is tensor contraction of order k , while $n(\mathbf{r}, t)$ is number density of charged particles. Under hydrodynamic conditions the flux of velocity of charged particles can be written as [56]:

$$\begin{aligned} \mathbf{\Gamma}(\mathbf{r}, t) = & \mathbf{W}^{(f)} n(\mathbf{r}, t) - \hat{\mathbf{D}}^{(f)} \cdot \nabla n(\mathbf{r}, t) \\ & + \hat{\mathbf{Q}}^{(f)} \odot (\nabla \otimes \nabla) n(\mathbf{r}, t) + \dots, \end{aligned} \quad (2)$$

where $\mathbf{W}^{(f)}$, $\hat{\mathbf{D}}^{(f)}$ and $\hat{\mathbf{Q}}^{(f)}$ are flux drift velocity, flux diffusion tensor and flux third-order transport tensor, respectively, and \otimes is the tensor product. The equation (2) is truncated at the third term, as this is sufficient for defining the flux third-order transport tensor. Explicit expressions for the flux transport coefficients in terms of the phase space distribution function are given in reference [58].

Bulk transport coefficients appear in the generalized diffusion equation [56], which has been truncated at the third-order gradients for our needs:

$$\begin{aligned} \frac{\partial n(\mathbf{r}, t)}{\partial t} + & \mathbf{W}^{(b)} \cdot \nabla n(\mathbf{r}, t) - \hat{\mathbf{D}}^{(b)} : (\nabla \otimes \nabla) n(\mathbf{r}, t) \\ & + \hat{\mathbf{Q}}^{(b)} \vdots (\nabla \otimes \nabla \otimes \nabla) n(\mathbf{r}, t) = R_i n(\mathbf{r}, t), \end{aligned} \quad (3)$$

where $\mathbf{W}^{(b)}$, $\hat{\mathbf{D}}^{(b)}$, $\hat{\mathbf{Q}}^{(b)}$ and R_i are bulk drift velocity, bulk diffusion tensor, bulk third-order transport tensor and effective

rate coefficient for non-conservative processes, respectively, while \vdots and \ddots represent tensor contractions of second and third-order, respectively. Bulk transport coefficients can be expressed in terms of flux transport coefficients as [58]:

$$\mathbf{W}^{(b)} = \mathbf{W}^{(f)} + \mathbf{S}^{(1)}, \quad \hat{\mathbf{D}}^{(b)} = \hat{\mathbf{D}}^{(f)} + \mathbf{S}^{(2)}, \quad \hat{\mathbf{Q}}^{(b)} = \hat{\mathbf{Q}}^{(f)} + \mathbf{S}^{(3)}, \quad (4)$$

where $\mathbf{S}^{(k)}$ is the coefficient in the hydrodynamic expansion of the source term, that is contracted with k th derivative of the density gradient. For a swarm of electrons in the presence of electron impact ionisation and/or electron attachment, the source term is defined as:

$$S(\mathbf{r}, t) = \int n_0 c(\sigma_i(\epsilon) - \sigma_a(\epsilon)) f(\mathbf{r}, \mathbf{c}, t) d\mathbf{c}, \quad (5)$$

where n_0 , ϵ , $\sigma_i(\epsilon)$ and $\sigma_a(\epsilon)$ are number density of the background molecules, electron energy, and cross sections for ionisation and electron attachment, respectively.

Implicit effects of non-conservative collisions arise due to population and depopulation of different parts of the distribution function in velocity space, that are caused by the energy dependence of collision frequencies of non-conservative processes. These effects refer to the influence of non-conservative collisions on tensors $\mathbf{f}^{(k)}(\mathbf{c})$ in equation (1). Explicit effects of non-conservative processes arise due to the spatial dependence of collision frequencies for these processes. This spatial dependence is caused by the energy dependence of the collision frequencies for non-conservative collisions and spatial variation of energy of charged particles. Explicit effects of non-conservative collisions are represented by tensors $\mathbf{S}^{(k)}$ from the equation (4) and they determine the difference between flux and bulk transport coefficients.

The influence of implicit and explicit effects of non-conservative collisions on low order transport coefficients has been thoroughly studied in previous publications [73, 75]. Implicit effects of ionisation on the third-order transport coefficients refer to the influence of ionisation cooling on the asymmetric component of the diffusive flux, which is represented by the flux third-order transport tensor. Due to explicit effects of ionisation more electrons are created at the front of the swarm than at the back of the swarm, which in turn elongate the spatial distribution of electrons along both longitudinal and transverse directions at the leading edge of the swarm. Similarly, the implicit effects of electron attachment relate to the influence of depopulation of low-energy part of the distribution function, in case of attachment heating, and depopulation of high-energy part of the distribution function, in case of attachment cooling, on the asymmetric component of the diffusive flux. Explicit effects of electron attachment on the third-order transport coefficients refer to the influence of the spatial variation of electron losses to the compression of the spatial distribution of the swarm in those regions of space where electron attachment is more frequent.

The studied system is a swarm of electrons which move in a homogeneous background gas under the influence of a homogeneous and constant electric field that is oriented along the z axis. In this field configuration the flux third-order transport tensor has three independent components Q_{zzz} , Q_{xxz} and Q_{zxx} . In this field configuration, the following relations are

imposed on the off-diagonal components of the flux third-order transport tensor: $Q_{xxz} = Q_{xzx} = Q_{yyz} = Q_{yzy}$ and $Q_{zxx} = Q_{zxy} = Q_{zyx} = Q_{zyy}$ [52, 56, 58, 65]. The structure of the third-order transport tensor and physical interpretation of its individual components are extensively discussed in our recent work [58]. In particular, contribution of the third-order transport coefficients to the spatial profile of the swarm is represented by the following approximate expression [58]:

$$n^{(1)}(\mathbf{r}, t) = n^{(0)}(\mathbf{r}, t) \left[1 + \frac{tQ_L^{(b)}}{\sigma_z^3} \chi_z (\chi_z^2 - 3) + \frac{3tQ_T^{(b)}}{\sigma_x^2 \sigma_y} \chi_z (\chi_x^2 + \chi_y^2 - 2) \right], \quad (6)$$

where $n^{(0)}(\mathbf{r}, t)$ is the solution of the diffusion equation in which third and higher order transport coefficients are neglected, $Q_L = Q_{zzz}$, $Q_T = \frac{1}{3}(Q_{xxz} + Q_{xzx} + Q_{zxx})$, $\sigma_z = \sqrt{2D_L^{(b)}t}$ and $\sigma_x = \sigma_y = \sqrt{2D_T^{(b)}t}$, while χ_z , χ_x , χ_y are defined as:

$$\chi_z = \frac{z - W^{(b)}t}{\sigma_z}, \quad \chi_x = \frac{x}{\sigma_x}, \quad \chi_y = \frac{y}{\sigma_y}. \quad (7)$$

The equation (6) can be derived from the Fourier transform of the generalized diffusion equation in which third-order transport coefficients are included [58]. It can be seen from equation (6) that contribution of the longitudinal component of the third-order transport tensor to the spatial profile of the swarm is proportional to $Q_L^{(b)}/(D_L^{(b)})^{3/2}$. In statistics the asymmetry of the probability distribution of a random variable about its expected value is represented by skewness [74]. There are several ways to express skewness in statistics including the third central moment and the third standardized moment of a random variable [74]. It can be shown that the bulk third-order transport tensor is proportional to the third central moment of the position vector, while $Q_L^{(b)}/(D_L^{(b)})^{3/2}$ is proportional to the longitudinal component of the third standardized moment of the position vector. Likewise, the $Q_T^{(b)}/(D_T^{(b)}(D_L^{(b)})^{1/2})$ term is proportional to the off-diagonal component of the same standardized moment with the combination of indices π_{xxz} , where π_{abc} represents any permutation of a , b and c .

The flux third-order transport tensor is defined by the flux gradient relation. The last two indices of this tensor are contracted with partial derivatives of the charged-particle number density with respect to spatial coordinates. The third-order bulk transport tensor is however defined by the generalised diffusion equation, in which the three indices of this tensor are contracted with partial derivatives. For this reason, all three indices of the bulk third-order transport tensor commute, as this transport property is symmetrized in the equation in which it is defined. The same reasoning applies to the bulk diffusion tensor and higher order bulk transport tensors. Using these arguments, in the case of bulk third-order transport coefficients and when the swarm of charged-particles is acted on solely by an electric field, we can identify only two independent bulk components $Q_L^{(b)}$ and $Q_T^{(b)}$. In a more general configuration of electric and magnetic fields, we can identify those components

of the bulk third-order transport tensor that are symmetrized along all three indices. These are third-order transport coefficients that can be distinguished in our MC simulations, as we calculate transport coefficients using expressions derived from the generalized diffusion equation [58].

3. Methodology

3.1. Multi-term solution of the Boltzmann equation

The Boltzmann equation describes the evolution of the phase space distribution function $f(\mathbf{r}, \mathbf{c}, t)$. For a swarm of electrons the Boltzmann equation can be written as:

$$\frac{\partial f(\mathbf{r}, \mathbf{c}, t)}{\partial t} + \mathbf{c} \cdot \frac{\partial f(\mathbf{r}, \mathbf{c}, t)}{\partial \mathbf{r}} + \frac{q}{m} \mathbf{E} \cdot \frac{\partial f(\mathbf{r}, \mathbf{c}, t)}{\partial \mathbf{c}} = -J(f, f_0), \quad (8)$$

where q and m are electron charge and electron mass respectively, \mathbf{E} is electric field and J is collision operator. This operator represents change of the electron distribution function per unit time, due to collisions with particles of the background medium. These particles are described by the distribution function f_0 .

In the multi-term method for solving Boltzmann's equation the phase space distribution function is expanded in terms of spherical harmonics and Sonine polynomials in angular and radial parts of the velocity space, respectively. Thus, under hydrodynamic conditions $f(\mathbf{r}, \mathbf{c}, t)$ is expanded as follows [75–79]:

$$f(\mathbf{r}, \mathbf{c}, t) = \omega(\alpha, c) \sum_{s=0}^{\infty} \sum_{\lambda=0}^s \sum_{\mu=-\lambda}^{\lambda} \sum_{l=0}^{\infty} \sum_{m=-l}^l F(\nu l m | s \lambda \mu; \alpha) \times R_{\nu l}(\alpha, c) Y_m^{[l]}(\hat{\mathbf{c}}) G_{\mu}^{(s\lambda)} n(\mathbf{r}, t), \quad (9)$$

where $F(\nu l m | s \lambda \mu; \alpha)$ are moments of the distribution function, $\hat{\mathbf{c}}$ is unit vector in velocity space, $Y_m^{[l]}(\hat{\mathbf{c}})$ are spherical harmonics, $G_{\mu}^{(s\lambda)}$ is the spherical form of the gradient tensor operator, while α , $\omega(\alpha, c)$ and $R_{\nu l}(\alpha, c)$ are given by:

$$\alpha^2 = \frac{m}{kT_b}, \quad (10)$$

$$\omega(\alpha, c) = \left(\frac{\alpha^2}{2\pi} \right)^{3/2} e^{-\alpha^2 c^2 / 2}, \quad (11)$$

$$R_{\nu l}(\alpha c) = N_{\nu l} \left(\frac{\alpha c}{\sqrt{2}} \right)^2 S_{l+1/2}^{(\nu)}(\alpha^2 c^2 / 2), \quad (12)$$

where k is the Boltzmann constant, T_b is the basis temperature, which is a parameter for optimizing convergence, $S_{l+1/2}^{(\nu)}$ is Sonine polynomial, while $N_{\nu l}$ is given by:

$$N_{\nu l}^2 = \frac{2\pi^{3/2} \nu!}{\Gamma(\nu + l + 3/2)}, \quad (13)$$

where $\Gamma(\nu + l + 3/2)$ is gamma function.

The Boltzmann equation is decomposed into a hierarchy of kinetic equations by applying the relations of orthogonality for spherical harmonics and Sonine polynomials [76]. The moments of the distribution function $F(\nu l m | s \lambda \mu; \alpha)$ can

be obtained by solving this system of kinetic equations [75, 80]. The resulting hierarchy of kinetic equations is truncated at finite values of $l = l_{\max}$ and $\nu = \nu_{\max}$. Unlike the two-term approximation, in which small anisotropy in velocity space is assumed and l_{\max} is set to 1, in the multi-term method l_{\max} is increased until full convergence of transport coefficients is obtained, after which the obtained hierarchy is solved numerically.

Spherical form of the velocity vector is defined as [76]:

$$c_m^{[1]} = \sqrt{\frac{4\pi}{3}} c Y_m^{[1]}(\hat{\mathbf{c}}). \quad (14)$$

Cartesian components of a vector can be expressed via spherical form as:

$$c_x = \frac{i}{\sqrt{2}} (c_1^{[1]} - c_{-1}^{[1]}), \quad (15)$$

$$c_y = \frac{1}{\sqrt{2}} (c_1^{[1]} + c_{-1}^{[1]}), \quad (16)$$

$$c_z = -ic_0^{[1]}. \quad (17)$$

Spherical form of the flux of velocity of electrons can be written as [80]:

$$\Gamma_m^{(1)}(\mathbf{r}, t) = \frac{1}{\alpha} \sum_{s=0}^{\infty} \sum_{\lambda=0}^s \sum_{\mu=-\lambda}^{\lambda} F(01m | s \lambda \mu) G_{\mu}^{(s\lambda)} n(\mathbf{r}, t). \quad (18)$$

Explicit expressions for the individual components of the flux third-order transport tensor can be determined from the Cartesian components of the flux of velocity from equation (18) after identifying terms that are contracted with the corresponding partial derivatives [58].

Expressions for three independent components of the flux third-order transport tensor in the electric field only configuration defined to be in the z direction, are given by:

$$Q_{xxz}^{(f)} = \frac{1}{\sqrt{2}\alpha} [\text{Im}(F(011 | 221; \alpha)) - \text{Im}(F(01 - 1 | 221; \alpha))], \quad (19)$$

$$Q_{zxx}^{(f)} = -\frac{1}{\alpha} \left[\frac{1}{\sqrt{3}} \text{Im}(F(010 | 200; \alpha)) + \frac{1}{\sqrt{6}} \text{Im}(F(010 | 220; \alpha)) \right] + \frac{1}{\alpha} \text{Im} [F(010 | 222; \alpha)], \quad (20)$$

$$Q_{zzz}^{(f)} = \frac{1}{\alpha} \left[\sqrt{\frac{2}{3}} \text{Im}(F(010 | 220; \alpha)) - \frac{1}{\sqrt{3}} \text{Im}(F(010 | 200; \alpha)) \right], \quad (21)$$

where Im denotes imaginary parts of the moments of the phase space distribution function.

3.2. Monte Carlo simulations

In MC simulations, we track the space and time evolution of a swarm of electrons. The extensive use of random numbers is required in order to determine the exact moment and the type of the individual collisions of electrons with the background molecules, as well as the direction of the post collisional electron velocity. The transport coefficients are computed from the corresponding polynomials of the electron coordinates and velocity components, which are averaged over the entire swarm. The details of our MC code are discussed in our previous publications [75, 81–83]. Bulk third-order transport coefficients are calculated as:

$$\mathbf{Q}^{(b)} = \frac{1}{3!} \frac{d}{dt} \langle \mathbf{r}^* \mathbf{r}^* \mathbf{r}^* \rangle, \quad (22)$$

while the flux third-order transport coefficients are determined from:

$$\mathbf{Q}^{(f)} = \frac{1}{3!} \left\langle \frac{d}{dt} (\mathbf{r}^* \mathbf{r}^* \mathbf{r}^*) \right\rangle, \quad (23)$$

where $\mathbf{r}^* = \mathbf{r} - \langle \mathbf{r} \rangle$, and the brackets $\langle \rangle$ represent ensemble averages. Expressions for transport coefficients, that are used in our MC method, are derived from the generalized diffusion equation, in which all tensor indices are contracted with partial derivatives. Thus, in the generalized diffusion equation symmetrization of the third-order transport tensor with respect to all indices is performed. For this reason, we cannot determine individual off-diagonal components of the third-order transport tensor or individual off-diagonal components of the diffusion tensor in our MC simulations [75]. Instead, we can determine individual diagonal components such as $Q_L = Q_{zzz}$ and averages of those off-diagonal components that have the same combination of indices like $Q_T = (Q_{xxz} + Q_{xzx} + Q_{zxx})/3$. It should be noted that Q_{xxz} and Q_{xzx} are equal due to the commutativity of the last two indices of the third-order transport tensor [52, 56, 58, 65]. Explicit expressions for $Q_L^{(b)}$ and $Q_T^{(b)}$ in the electric field only configuration are given by:

$$Q_L^{(b)} = \frac{1}{6} \frac{d}{dt} (\langle z^3 \rangle - 3\langle z \rangle \langle z^2 \rangle + 2\langle z \rangle^3), \quad (24)$$

$$Q_T^{(b)} = \frac{1}{6} \frac{d}{dt} (\langle zx^2 \rangle - \langle z \rangle \langle x^2 \rangle), \quad (25)$$

while the corresponding flux components $Q_L^{(f)}$ and $Q_T^{(f)}$ are given in [58].

It is important to note that numerical differentiation in time is not used for the calculation of $Q_L^{(b)}$ and $Q_T^{(b)}$, because of the statistical fluctuations of the corresponding expressions in brackets. Direct numerical differentiation of these expressions would create fluctuations that are much more intense than the fluctuations of the initial expressions. Instead, the expression in brackets is fitted to a linear function. The corresponding time derivative is determined as the slope of this linear function. This is justified because $Q_L^{(b)}$ and $Q_T^{(b)}$ are independent of time after relaxation of the swarm, and the corresponding expressions in brackets in equation (24) and (25) are linear functions in time. This method for calculating $Q_L^{(b)}$ and $Q_T^{(b)}$

has been further verified by comparing values of the bulk third-order transport coefficients, that are obtained by this method, with the corresponding values that are determined by employing numerical differentiation in time. An additional check was obtained by comparing $Q_L^{(b)}$ and $Q_T^{(b)}$ with $Q_L^{(f)}$ and $Q_T^{(f)}$, respectively, under conditions where non-conservative processes are absent.

4. Results and discussion

4.1. Preliminaries

In this paper, we consider the transport of electrons in the Lucas–Saelee model, modified Ness–Robson model, N_2 and CF_4 . The Ness–Robson model was developed for testing the multi-term method for solving the Boltzmann equation in the presence of electron attachment [80]. Nolan and co-workers presented a new gas model that is based on the Ness–Robson model and the Lucas–Saelee model [73]. In this model the collision frequency of elastic collisions is independent of energy while the cross section for inelastic collisions is the same as in the Lucas–Saelee model. In modifying the Ness–Robson model, which is introduced by Nolan *et al* [73], both inelastic collisions and ionisation are present. The ratio of the cross section for inelastic collisions to the cross section for ionisation is determined by the F parameter, as in the Lucas–Saelee model. Two different versions of the modified Ness–Robson model [73] with different functional dependences of the cross section for electron attachment are considered in this work. In both considered versions of the modified Ness–Robson model the parameter F is set to zero, implying the absence of ionisation. The details of the modified Ness–Robson model, in the absence of ionisation, are given by the following equations:

$$\begin{aligned} \sigma_{el}(\epsilon) &= 4\epsilon^{-1/2} \text{ \AA}^2 \quad (\text{elastic collision}) \\ \sigma_{ex}(\epsilon) &= \begin{cases} 0.1(\epsilon - 15.6) \text{ \AA}^2, & \epsilon \geq 15.6 \text{ eV} \\ 0, & \epsilon < 15.6 \text{ eV} \end{cases} \quad (\text{inelastic collision}) \\ \sigma_a(\epsilon) &= a\epsilon^p \quad (\text{electron attachment}) \\ m/m_0 &= 10^{-3}, \\ T_0 &= 0 \text{ K}, \end{aligned} \quad (26)$$

where $\sigma_{el}(\epsilon)$, $\sigma_{ex}(\epsilon)$, $\sigma_a(\epsilon)$ are cross sections for elastic collisions, inelastic collisions and electron attachment, respectively, given as functions of electron energy ϵ , T_0 is the temperature of the background gas, while m and m_0 are masses of electrons and of the molecules of the background gas, respectively. In the above equations, the values of the electron energy are given in eV. Parameters a and p determine the magnitude and the functional dependence of the cross section for electron attachment, respectively. The values of p that are considered in this work include -1.0 and 0.5 . These values correspond to attachment heating and attachment cooling, respectively. The percentage differences between the third-order transport

coefficients determined for each of these two models and the corresponding values in the model where $p = -0.5$ are considered in this work. In the third model the collision frequency for electron attachment is independent of energy. The values of parameter a , that are used in this work, include $8 \times 10^{-3} \text{ \AA}^2$ and $5 \times 10^{-4} \text{ \AA}^2$. The first value is used for the attachment heating model, while the second value is used for the attachment cooling model. In the model with constant collision frequency for electron attachment, this non-conservative process is equally frequent at all values of the electron energy, and it does not affect transport coefficients of any order (excluding the rate coefficient for electron attachment). In this model the values of the third-order transport tensor are the same as in the conservative Lucas–Saelee model, where $F = 0$.

The Lucas–Saelee ionisation model was introduced in order to investigate the influence of electron-impact ionisation on the electron transport by using MC simulations [84]. Ness and Robson investigated the electron transport in this model, in order to test the validity of the theory and associated computer code for solving the Boltzmann equation, in the presence of non-conservative processes [80]. The details of the Lucas–Saelee model are given by the following equations:

$$\begin{aligned} \sigma_{\text{el}}(\epsilon) &= 4\epsilon^{-1/2} \text{ \AA}^2 \quad (\text{elastic collision}) \\ \sigma_{\text{ex}}(\epsilon) &= \begin{cases} 0.1(1-F)(\epsilon - 15.6) \text{ \AA}^2, & \epsilon \geq 15.6 \text{ eV} \\ 0, & \epsilon < 15.6 \text{ eV} \end{cases} \quad (\text{inelastic collision}) \\ \sigma_{\text{I}}(\epsilon) &= \begin{cases} 0.1F(\epsilon - 15.6) \text{ \AA}^2, & \epsilon \geq 15.6 \text{ eV} \\ 0, & \epsilon < 15.6 \text{ eV} \end{cases} \quad (\text{ionisation}) \\ P(q, \epsilon') &= 1, m/m_0 = 10^{-3}, \\ T_0 &= 0 \text{ K}, \end{aligned} \quad (27)$$

where $\sigma_{\text{I}}(\epsilon)$ is the cross section for ionisation, $P(q, \epsilon)$ is the ionisation partition function, and F is the parameter that determines the magnitudes of cross sections for inelastic collisions and ionisation. As the scattering is isotropic in this model $\sigma_{\text{el}}(\epsilon)$, $\sigma_{\text{ex}}(\epsilon)$, and $\sigma_{\text{I}}(\epsilon)$ represent total cross sections. Arguments of the ionisation partition function $P(q, \epsilon')$, q and ϵ' , are the ratio of total postcollisional energy, that is given to the ejected electron, and the energy of the initial electron before ionisation, respectively. In this model, ionisation partition function is set to unity, indicating that all values $0 \leq q \leq 1$ are equally probable.

The set of cross sections for electron scattering in N_2 , which is used in this work, is detailed in [64]. It includes elastic momentum transfer cross section, as well as the total cross section for rotational excitations, and cross sections for vibrational excitations, electronic excitations and electron-impact ionisation. The set of cross sections for electron scattering in CF_4 , which is employed in this work, was developed

and discussed by Kurihara and co-workers [85]. It includes elastic momentum transfer cross section, cross sections for vibrational excitations, electronic excitations, electron attachment, and ionisation. For some aspects of this work, it was necessary to consider the electron transport in CH_4 . These results are obtained by using the cross sections developed by Šašić et al [86].

The results for the model and the real gases were obtained from the MC simulations and numerical multi-term solution of the Boltzmann equation. In particular, it was necessary to follow a large number of electrons (at least 10^7) in our MC simulations in order to calculate third-order transport coefficients accurately, due to high statistical fluctuations of individual terms appearing in expressions (24) and (25). It was also necessary to determine the phase space distribution function with a high degree of precision in order to calculate the third-order transport coefficients from the multi-term method. While the number of spherical harmonics indicates the degree of anisotropy of the phase space distribution function in velocity space, the number of Sonine polynomials is indicative of the deviation of the energy dependence of the distribution function from a Maxwellian at a particular temperature T_b , not necessarily equal to the gas temperature T_0 . Third-order transport coefficients are more sensitive to the shape of the phase space distribution function than transport coefficients of lower order. For this reason it was necessary to include a large number of spherical harmonics and Sonine polynomials to achieve the convergence of the third-order transport coefficients, in the presence of strong inelastic and/or non-conservative collisions. For example, the required numbers of l_{max} and ν_{max} were 8 and 90, respectively, for electrons in CF_4 . This was especially pronounced in the energy region where the cross sections for vibrational excitations are rapidly rising functions of electron energy, while the cross section for elastic collisions is being reduced with increasing electron energy. The solutions of the Boltzmann equation are not determined for $E/n_0 > 300 \text{ Td}$, as the convergence of the transport coefficients was poor in this field region. For this reason, we have only displayed the MC results in the field range above 300 Td.

4.2. Variation of the flux third-order transport coefficients with E/n_0 for electrons in N_2 and CF_4

In figures 1(a) and (b) we show the mean energy for an electron swarm in N_2 , and CF_4 , respectively, as a function of the reduced electric field, E/n_0 . At the lowest fields the mean energy is thermal in both gases, while it is rising with increasing E/n_0 at higher fields. The slope of the mean energy is determined by collisions of electrons with atoms/molecules of the background gas [85]. The profiles of the mean energy are useful for analysing the field dependence of the third-order transport coefficients. From these profiles one can determine which collisional processes dominate electron transport in a given field range.

In this section, we study the behaviour of the components of the flux third-order transport tensor for electrons in N_2 and CF_4 in the presence of an electric field. It has been previously shown that the rise of E/n_0 under constant collision frequency

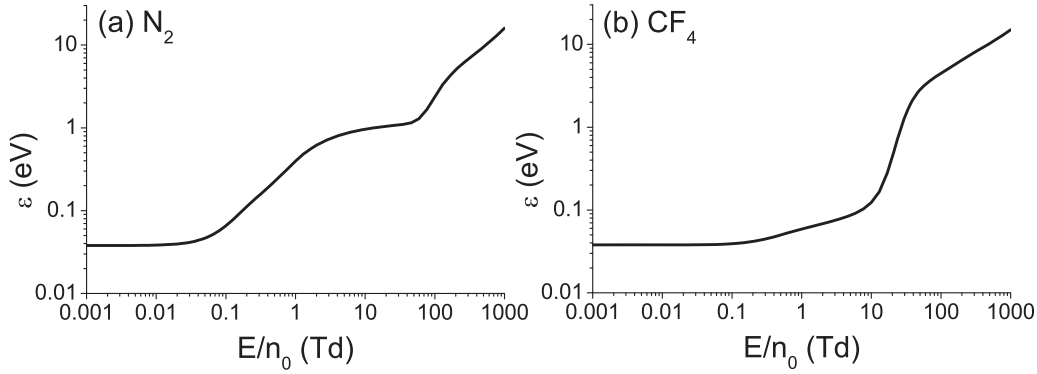


Figure 1. Mean energy of electron swarm in (a) N_2 and (b) CF_4 , as a function of the reduced electric field. These results are obtained by using multi term theory for solving the Boltzmann equation up to about 300 Td and by employing MC simulations at higher fields.

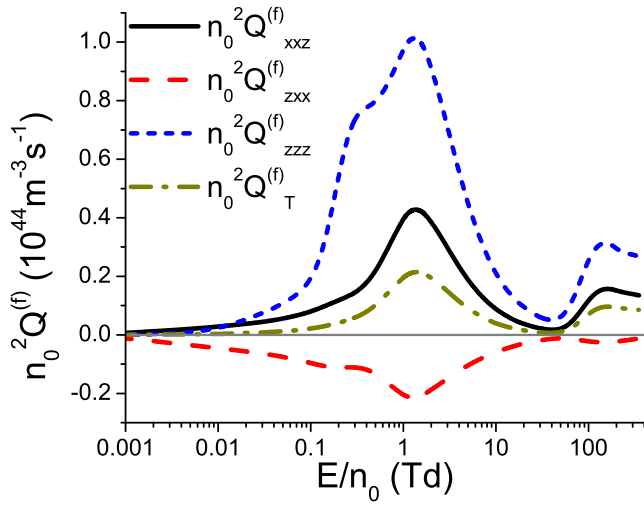


Figure 2. Independent components of the flux third-order transport tensor and $n_0^2 Q_T^{(f)}$ as functions of E/n_0 for electrons in N_2 . The results are obtained from numerical multi-term solutions of the Boltzmann equation.

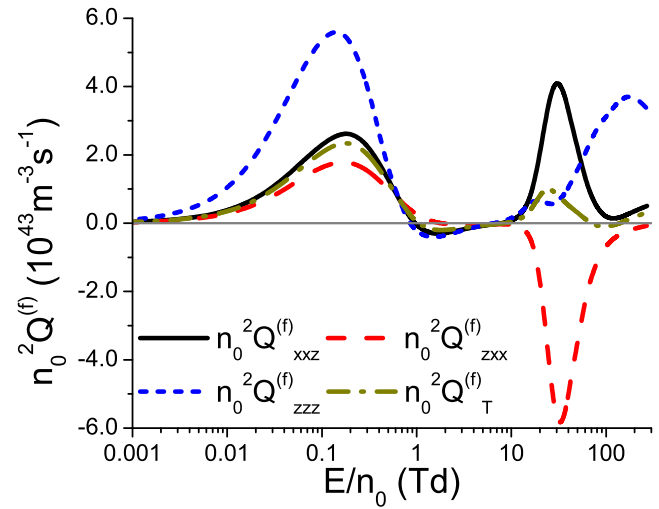


Figure 3. Independent components of the third-order transport tensor and $n_0^2 Q_T^{(f)}$ as functions of E/n_0 for electrons in CF_4 . The results are obtained from numerical multi-term solutions of the Boltzmann equation.

conditions leads to an increase of the components of the third-order transport coefficient tensor [58]. It has also been shown that the increase of the collision frequency with increasing energy may lead to a decrease of the components of this tensor, as well as to negative values of these components, if the rise of the collision frequency is steep enough [58, 69]. For this reason, the E/n_0 -profile of the third-order transport coefficients is determined by the complex interplay between the electric field, which accelerates electrons and acts to direct their movement along the field lines, and collisions between electrons and atoms/molecules of the background gas, which dissipate electron energy and momentum. Although it is possible to analyse E/n_0 profiles of the third-order transport coefficients directly from the mean energy of electrons and collision frequencies for individual collisional processes, such analysis is often quite complicated and tedious. Therefore, in this section we briefly discuss the general E/n_0 -profiles of the third-order transport coefficients for electrons in N_2 and CF_4 , while a more detailed analysis is reserved only for the unusual and unexpected aspects of the behaviour of these transport properties.

A more detailed study of the behaviour of $Q_{zz}^{(f)}$ and $Q_T^{(f)}$ for electrons in N_2 and CF_4 is presented in section 4.4.

In figure 2 we show the independent components of the third-order flux transport tensor for electrons in N_2 as functions of E/n_0 . In addition, we also show the variation of $n_0^2 Q_T^{(f)}$ with E/n_0 . The $Q_{zxx}^{(f)}$ component is negative, while the remaining quantities are positive over the entire E/n_0 range considered. Negative values of $Q_{zxx}^{(f)}$ can be attributed to the rise of the collision frequency for elastic and inelastic collisions with increasing electron energy. This phenomenon has been observed for electrons in both model and real gases [58, 62, 69]. It can be seen from figure 2 that the absolute values of quantities have a similar qualitative dependence on E/n_0 . Specifically, the absolute values of these transport coefficients have two local maximums at about 1.3 Td and 150 Td, and a local minimum at around 46 Td.

In figure 3 we show the three independent components of the flux third-order transport tensor for electrons in CF_4 as functions of E/n_0 . In the same figure we show the variation of $n_0^2 Q_T^{(f)}$ with E/n_0 . At the lowest fields, all quantities are

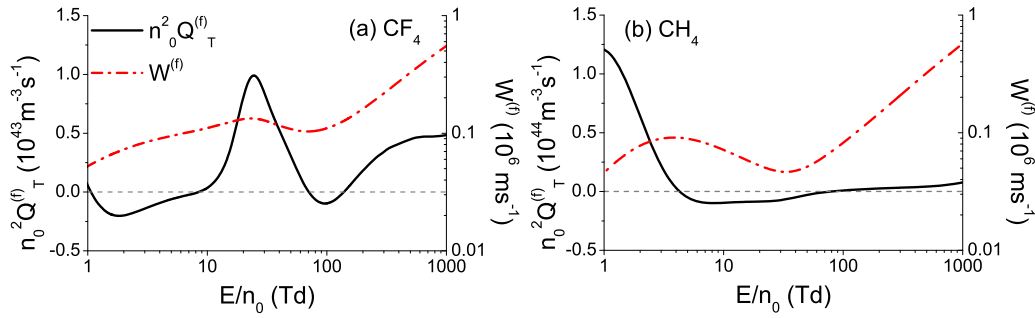


Figure 4. Transverse flux third-order transport coefficients $n_0^2 Q_T^{(f)}$ and the flux drift velocity $W^{(f)}$ as functions of E/n_0 for electrons in (a) CF_4 and (b) CH_4 . The results are obtained by employing the multi-term theory for solving the Boltzmann equation up to about 300 Td for electrons in CF_4 , and up to 600 Td for electrons in CH_4 , and by using MC simulations at higher fields.

positive, and increasing functions E/n_0 up to about 0.14 Td in the case of $Q_{zzz}^{(f)}$, and up to about 0.18 Td in the case of the remaining quantities. At higher fields these quantities are being reduced and they become negative. The $Q_{xx}^{(f)}$ component becomes negative at about 2 Td. The remaining transport coefficients become negative at about 0.9 Td, and they reach a local minimum at around 1.6 Td. These quantities become positive again at about 7.5 Td. The $Q_{xxz}^{(f)}$ and $Q_{zzz}^{(f)}$ components remain positive until the end of the considered range of E/n_0 , while the $Q_{zzx}^{(f)}$ component remains negative. The $Q_{zzz}^{(f)}$ component has two local maximums at about 20 Td and 170 Td and a local minimum at around 27 Td. The $Q_{xxz}^{(f)}$ component and $Q_T^{(f)}$ have a local maximum at about 31 Td and 25 Td, and a local minimum at around 120 Td and 100 Td, respectively. The $Q_{zzx}^{(f)}$ component has a local minimum at about 33 Td. At the lowest E/n_0 , all quantities that are displayed in figure 3 are rising functions of E/n_0 . This can be attributed to a negligible rise of the mean energy with increasing field in this E/n_0 region, which leads to a small change of the mean collision frequency for elastic and inelastic collisions. At higher fields, the rise of the mean energy and mean collision frequency for vibrational excitations with increasing E/n_0 , become more significant, which in turn induces a decrease of the third-order transport coefficients.

We now focus on the negative values of the third-order transport coefficients for electrons in CF_4 . As discussed elsewhere [58, 70], the bulk third-order transport tensor represents asymmetric deviation of the spatial distribution of the swarm from an ideal Gaussian. This deviation is caused by different rates of spread of electrons at the swarm front and at the back of the swarm. Due to this difference, different parts of the normalized spatial distribution of electrons may seem elongated or compressed when compared to an ideal Gaussian. Specifically, $Q_{zzz}^{(b)}$ component describes elongation/contraction of the spatial distribution of electrons at the leading edge of the swarm, and the opposite deformation at its trailing edge. A negative value of the $Q_{zzz}^{(b)}$ component implies that the normalized spatial distribution of electrons is compressed (when compared to an ideal Gaussian) along the longitudinal direction at the front of the swarm and expanded along the same direction at the back of the swarm. Similarly, a negative value of $Q_T^{(b)}$ implies that the normalized spatial distribution of electrons is compressed (relative to an ideal Gaussian) along the transverse direction at

the swarm front and expanded along the same direction at the back of the swarm. It is important to emphasize that the spatial distribution of electrons is not being actually compressed in time. Instead, in some regions of space the effective rate of spread of electrons, that is represented by both third-order transport coefficients and diffusion, is smaller than the corresponding rate of spread that would be represented by diffusion alone. In these regions of space, the normalized spatial distribution of electrons seems compressed when compared to an ideal Gaussian. For E/n_0 less than approximately 10 Td, the impact of non-conservative collisions is minimal, and thereby the bulk values of the third-order transport coefficients are equal to the corresponding flux values (see figure 13). In the field region around 0.9 Td, where $Q_{zzz}^{(f)}$, $Q_{xxz}^{(f)}$ and $Q_T^{(f)}$ become negative, electrons with energies that are 3 times higher than the mean energy are in the energy region around 0.2 eV, where the cross sections for two vibrational excitations of the CF_4 molecule reach their global maximums [85]. These cross sections are denoted as Q_{v1} and Q_{v3} in table 1 or reference [85] and their thresholds are 0.108 eV and 0.168 eV, respectively. Moreover, Q_{v1} becomes greater than the elastic momentum transfer cross section in the energy range between approximately 0.12 eV and 0.58 eV. The same holds for Q_{v3} in the energy range between approximately 0.17 eV and 2.6 eV. Thus, in the field region around 0.9 Td where $Q_{xxz}^{(f)}$, $Q_{zzz}^{(f)}$ and $Q_T^{(f)}$ become negative, the high energy tail of the distribution function is in the energy range where the electron transport is dominated by vibrational excitations. As the mean energy of electrons is increasing in the positive direction (direction of the force acting upon electrons), the intense energy losses due to the vibration excitations create a strong resistance to the spreading of the swarm at its front in the longitudinal and transverse directions. This resistance leads to the compression of the spatial distribution of electrons at the front of the swarm along both longitudinal and transverse directions, while this spatial distribution is more expanded along both these directions at the back of the swarm. Such deviation of the spatial profile of electrons from an ideal Gaussian is manifested through negative values of Q_{zzz} and Q_T (in both flux and bulk case).

In figures 4(a) and (b), we show the variation of $n_0^2 Q_T^{(f)}$ and $W^{(f)}$ with E/n_0 for electrons in CF_4 and CH_4 , respectively. It should be noted that some general aspects of the behaviour of

third-order transport coefficients for electrons in CH_4 were discussed in our previous publication [62]. CH_4 was introduced here in order to observe relationship of negative values of the higher order transport coefficients with the negative differential conductivity (NDC) for drift velocity. We observe from figures 4(a) and (b) that the drift velocity of electrons in both CF_4 and CH_4 exhibits NDC. NDC refers to the decrease in drift velocity with an increase in the reduced electric field E/n_0 . To understand NDC, it is necessary to consider the rates of momentum and energy transfer in elastic and inelastic collisions [87]. Interestingly, Q_T has negative values between approximately 70 Td and 140 Td in CF_4 . This approximately corresponds to the field region beyond the end of the NDC where drift velocity begins to rise rapidly (almost reaching its maximum value before the NDC). A similar relationship exists in the E/n_0 -profile of the electron drift velocity in CH_4 . However, in CH_4 , Q_T becomes negative at the beginning of the NDC much earlier than in CF_4 .

The qualitative behaviour of the individual off-diagonal components of the third-order transport tensor over the range of E/n_0 , where NDC occurs, is different for electrons in CF_4 and CH_4 . For electrons in CF_4 the $Q_{xxz}^{(f)}$ component is positive, while the $Q_{zxx}^{(f)}$ component is negative, over the entire range of E/n_0 , corresponding to the NDC. For the electrons in CH_4 , however, the $Q_{xxz}^{(f)}$ component becomes negative shortly after the start of the NDC, while $Q_{zxx}^{(f)}$ becomes positive at a slightly larger field. The $Q_{xxx}^{(f)}$ component becomes positive again for electrons in CH_4 , for the value of E/n_0 where $Q_T^{(f)}$ becomes positive. Thus, it is difficult to find out more about the behaviour of individual off-diagonal components of the third-order transport tensor, from the presence of NDC in the E/n_0 -profile of drift velocity in a given field region, due to the complexity of various factors that determine the behaviour of the third-order transport coefficients. However, it is evident that negative values of $Q_T^{(f)}$ can arise in the vicinity of the field region where NDC occurs. Negative values of $Q_T^{(f)}$ imply the compression of the spatial profile of the swarm along the transverse direction at the front of the swarm, and the expansion of this profile along the same direction at the back of the swarm [58]. This implies that the rapid increase of collision frequency for elastic collisions, which leads to a greater randomization of velocity vectors of the individual electrons and the occurrence of NDC, can also hinder transverse spreading of electrons at the swarm front, where the mean energy of electrons is higher than that at the back of the swarm. This is manifested through negative values of $Q_T^{(f)}$. However, this does not lead to negative values of $Q_L^{(f)}$, as they occur only when the spatial profile of the swarm is skewed in the direction opposite to the direction of drift velocity. This kind of deformation requires a strong resistance to the motion of electrons in the direction of drift velocity, which is more easily achieved with inelastic and non-conservative collisions, when the corresponding cross sections are large enough. It can be seen that $Q_T^{(f)}$ is negative in the majority of region where $Q_L^{(f)}$ is negative for electrons in CF_4 , as it is easier to achieve negative values of $Q_T^{(f)}$ than negative values of $Q_L^{(f)}$. Thus, one may conclude that the concurrence

between drift velocity and $Q_T^{(f)}$ can be attributed to the corresponding collisions which lead to the occurrence of NDC and to the compression of the spatial distribution of the swarm along the transverse direction at the front of the swarm. However, we observe that for the electrons in CF_4 negative values of $Q_T^{(f)}$ occur only in a small field range after the NDC. Therefore, the presence of NDC at a certain value of E/n_0 does not necessarily result in a negative value of $Q_T^{(f)}$ for these electric fields, but again the conditions in the momentum and energy balances that lead to NDC also favour negative values of Q_T depending on the balance of different competing processes. The concurrence between the transport coefficients of the third-order and the drift velocity is therefore much less pronounced than the concurrence between the transport coefficients of the third-order and diffusion. It would be interesting to investigate the behaviour of $Q_T^{(f)}$ and $Q_T^{(b)}$ in strongly attaching gases under conditions in which NDC occurs only for bulk drift velocity, due to electron attachment [88, 89]. This will be considered in the near future.

It is striking that although similar in the shape of the cross sections the two gases exhibit very different dependences of the NDC. For CF_4 the NDC minimum is much shallower and occurs at higher E/n_0 . The depth of the NDC is normally promoted by the separate control of the mean energy and momentum transfer by cross sections that control the energy exchange and momentum transfer. Positioning of vibrational excitation cross sections and overlap of their influences will at the same time affect the magnitude of the peak in drift velocity induced by the inelastic processes and also the onset and overall effect of the NDC.

In figures 5 and 6, we show comparison between the two-term and converged multi-term solutions of the Boltzmann equation for electrons in N_2 and CF_4 , respectively. The E/n_0 profiles of the independent components of the flux third-order transport tensor, including $n_0^2 Q_{xxz}^{(f)}$, $n_0^2 Q_{zxx}^{(f)}$ and $n_0^2 Q_{zzz}^{(f)}$ are shown. In addition, the variation of $n_0^2 Q_T^{(f)}$ with E/n_0 is also shown. Comparing two-term and multi-term results for electrons in N_2 , it is evident that for the low values of E/n_0 the agreement is good while the maximum error in the two-term approximation occurs at the highest fields. For electrons in CF_4 , however, there is a significant difference between the two-term and multi-term solutions of the Boltzmann equation over the entire range of E/n_0 considered in this work, except in the limit of the lowest E/n_0 . In contrast to N_2 , the two-term and multi-term results are qualitatively different in CF_4 , indicating that sometimes the two-term theory predicts physics that is not entirely correct. The maximum errors of the two-term approximation occur over the range of E/n_0 values where $n_0^2 Q_{zzz}^{(f)}$ is negative. This happens at electron energies where elastic momentum transfer is approximately at a minimum while inelastic collisions which lead to the vibrational excitations of CF_4 molecule became significant and are approximately at their maximum. This induces a large asymmetry of the distribution function in velocity space which makes the two-term approximation inadequate for studying the third-order transport coefficients. Thus, it is important to note that neglecting higher terms in the spherical harmonic expansion of the phase

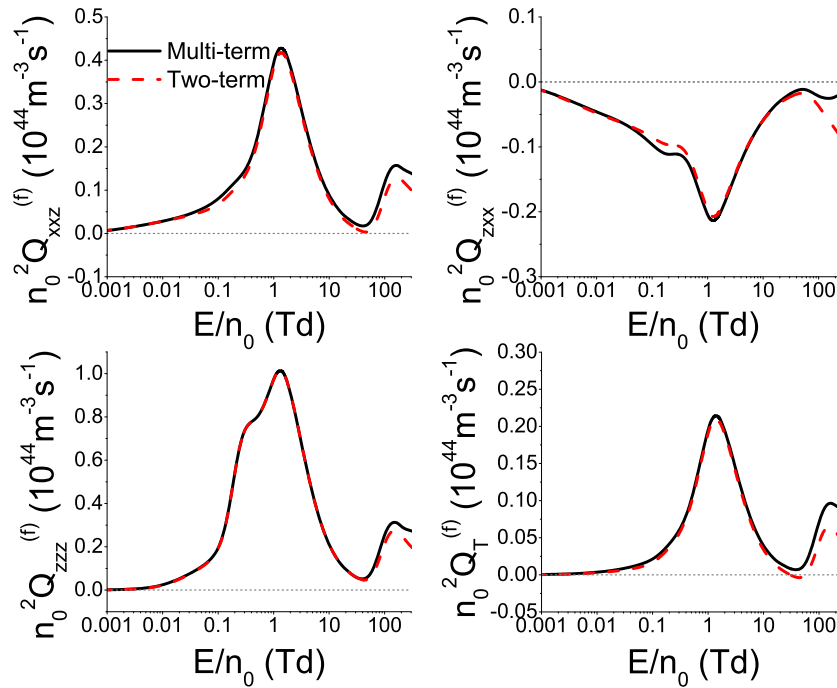


Figure 5. Comparison between the flux third-order transport coefficients obtained by the two-term approximation and multi-term theory for solving the Boltzmann equation. Calculations are performed for electrons in N_2 .

space distribution function has a much more pronounced effect for third order transport coefficients than for lower order transport coefficients. For electrons in CF_4 the third-order transport coefficients determined by using the two-term approximation are not even qualitatively correct.

4.3. The influence of non-conservative processes on the third-order transport coefficients

4.3.1. The influence of electron attachment on the third-order transport coefficients for electrons in the modified Ness–Robson model. The bulk and flux values of the longitudinal and transverse components of the third-order transport tensor for electrons in the Ness–Robson attachment heating model, are shown in figures 7(a) and (b), respectively. In this model the slower electrons at the back of the swarm are preferentially attached. As a consequence, the bulk values of Q_L and Q_T exceed the corresponding flux values for lower values of E/n_0 , e.g. up to about 3.8 Td for Q_L and 5 Td for Q_T .

For higher values of E/n_0 , up to about 8 Td for Q_L and 17 Td for Q_T , the flux values are greater than the corresponding bulk values, although this effect is in the limit of statistical error of MC simulations in the case of Q_T . This can be attributed to a combination of two factors. The first factor is the decreased number of low-energy electrons at the back of the swarm, due to the rise of the mean energy with increasing field. The second factor is the increased number of low-energy electrons at the front of the swarm, due to the influence of inelastic collisions, which are more frequent at the front of the swarm. In the limit of the highest fields, higher than 8 Td for Q_L and 17 Td for Q_T , the difference between flux and bulk values of the third-order transport coefficients is negligible for electrons in this model gas.

The bulk and flux values of the longitudinal and transverse components of the third-order transport tensor for electrons in the Ness–Robson attachment cooling model, are shown in figures 8(a) and (b), respectively. In this model the faster electrons at the front of the swarm, where the mean energy is higher, are preferentially attached. As a consequence, for lower values of E/n_0 bulk values are lower than the corresponding flux values. We observe that this effect is within the statistical uncertainty of MC simulations for Q_T . However, for higher values of E/n_0 (from approximately 5 Td) bulk values are larger than the corresponding flux values in case of Q_L , although this difference is lower than the statistical error of MC simulations. For $E/n_0 \geq 10$ Td $Q_L^{(f)}$ and $Q_L^{(b)}$ are practically equal. Similar behaviour is observed for Q_T , because for $E/n_0 \geq 7$ Td $Q_T^{(f)}$ and $Q_T^{(b)}$ coincide. Between 5 Td and 10 Td, $Q_L^{(b)}$ exceeds $Q_L^{(f)}$ due to the interplay of inelastic collisions and the increase of the mean electron energy with increasing E/n_0 , as in the case of the attachment heating model.

In figure 9 the percentage difference in the longitudinal component of the third-order transport tensor calculated using the modified Ness–Robson models with the attachment heating and with a constant collision frequency for electron attachment, are shown. Panel (a) shows the difference between the flux values, while the panel (b) displays the difference between the bulk values. The percentage differences are calculated using the expression: $Q_L^{\text{heating}}/Q_L^{\text{constant}} - 1$. The difference between flux values of Q_L in these two models is caused by the implicit effects of electron attachment, while the difference between the corresponding bulk values is induced by a combined effect of implicit and explicit effects of electron attachment. Comparing panels (a) and (b) in the limit of the

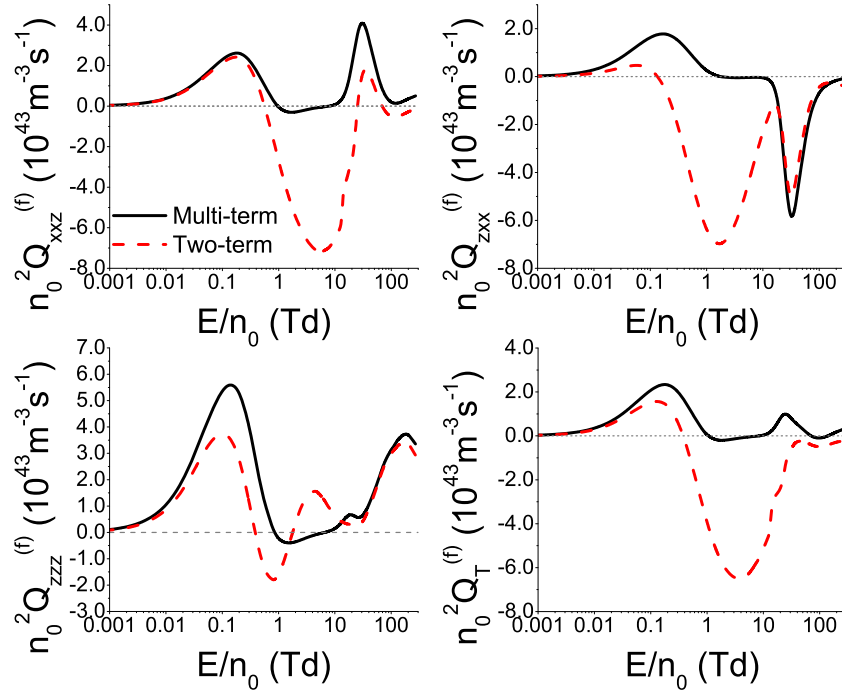


Figure 6. Comparison between the flux third-order transport coefficients obtained by the two-term approximation and multi-term theory for solving the Boltzmann equation. Calculations are performed for electrons in CF_4 .

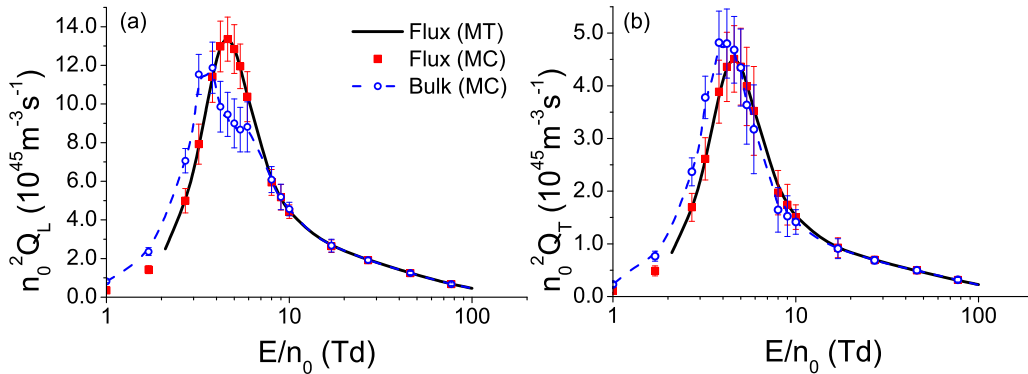


Figure 7. Comparison of the bulk and flux values of (a) $n_0^2 Q_L$ and (b) $n_0^2 Q_T$ for electrons in the modified Ness–Robson attachment heating model. The results are obtained from numerical multi-term solutions of the Boltzmann equation (MT) and MC simulations.

lowest E/n_0 , we observe that Q_L is much higher in the attachment heating model than in the model with a constant collision frequency for electron attachment, for both bulk and flux values. It is also evident that these differences are much more pronounced in the case of bulk third-order transport coefficients. These differences decrease with increasing E/n_0 and become even negative over a limited range of E/n_0 . As E/n_0 further increases, the differences tend to zero. It should be noted that negative values of these quantities can be attributed to the influence of inelastic collisions, although these values are within the statistical uncertainty of MC simulations.

Similarly, figure 10 shows the difference in Q_L calculated using the modified Ness–Robson models with the attachment cooling and with a constant collision frequency for electron attachment. Results for $Q_L^{(f)}$ and $Q_L^{(b)}$ are shown in panels (a) and (b), respectively. In this case, the following

expression is used for calculating the percentage difference: $Q_L^{\text{cooling}}/Q_L^{\text{constant}} - 1$. The values of this expression for the longitudinal components of both flux and bulk third-order transport tensor are decreasing functions of E/n_0 up to about 4 Td where they reach a local minimum, which is equal to around -20% and about -50% for $Q_L^{(f)}$ and $Q_L^{(b)}$, respectively. For higher values of E/n_0 these differences are being increased and they reach a local maximum at around 10 Td in the case of $Q_L^{(f)}$ and at about 8 Td in the case of $Q_L^{(b)}$. This local maximum has a positive value, although this value is within the statistical uncertainty of MC simulations. As E/n_0 further increases, these differences converge to zero.

4.3.2. The influence of ionisation on the third-order transport coefficients for electrons in Lucas–Saelee model, N_2 and CF_4 . The variation of the flux and bulk Q_L with E/n_0 of electrons

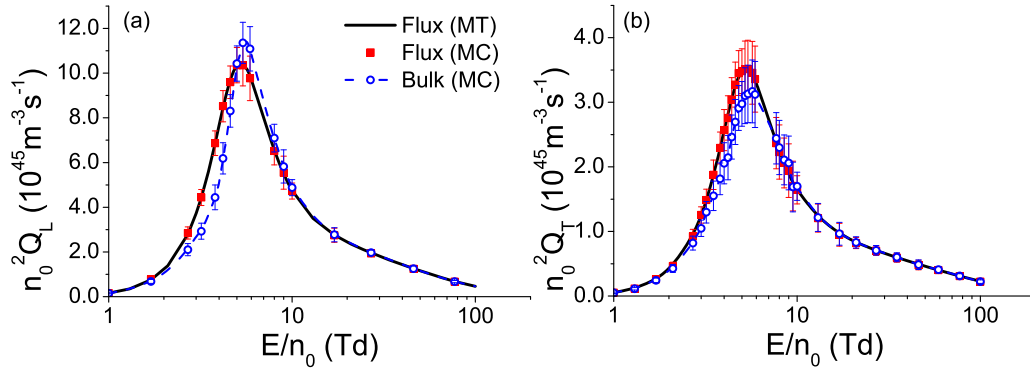


Figure 8. Comparison of the bulk and flux values of (a) $n_0^2 Q_L$ and (b) $n_0^2 Q_T$ for electrons in the modified Ness–Robson attachment cooling model. The results are obtained from numerical multi-term solutions of the Boltzmann equation (MT) and MC simulations.

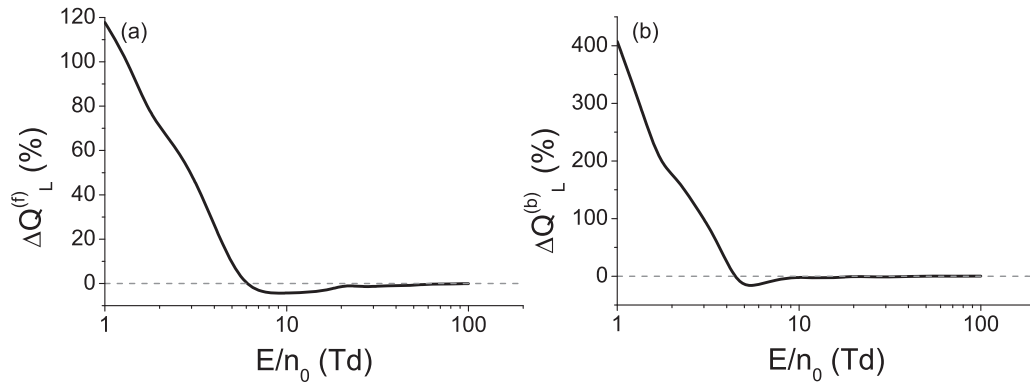


Figure 9. Percentage differences between the values of (a) $Q_L^{(f)}$ and (b) $Q_L^{(b)}$ for electrons in two different versions of the modified Ness–Robson model. Calculations are performed by the MC method in the modified Ness–Robson attachment heating model and in the modified Ness–Robson model with a constant collision frequency for electron attachment.

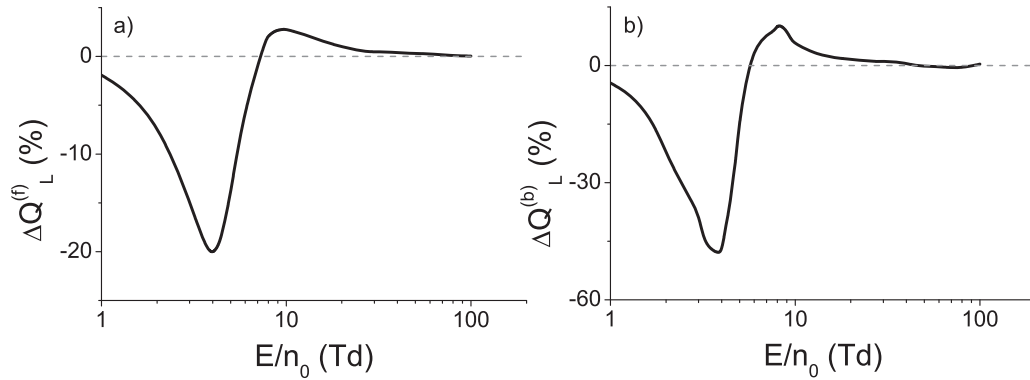


Figure 10. Percentage differences between the values of (a) $Q_L^{(f)}$ and (b) $Q_L^{(b)}$ for electrons in two different versions of the modified Ness–Robson model. Calculations are performed by the MC method in the modified Ness–Robson attachment cooling model and in the modified Ness–Robson model with a constant collision frequency for electron attachment.

in the Lucas–Saelee model for three values of the parameter F is displayed in figure 11(a). Likewise, figure 11(b) shows the flux and bulk Q_T as a function of E/n_0 . We observe that bulk values are larger than the corresponding flux values for $F = 0.5$ and $F = 1$, due to explicit effects of ionisation on the third-order transport coefficients. Comparing Q_L and Q_T , we see that the difference between bulk and flux values in this model is much higher for Q_T . This can be attributed to strong

inelastic and non-conservative collisions that provide strong resistance to the spread of the swarm in the direction of the drift velocity. This significantly inhibits the elongation of the spatial distribution of the swarm in the longitudinal direction under the influence of ionisation.

We observe from figure 11 that the flux values of Q_L and Q_T are reduced with increasing parameter F due to ionisation cooling of the swarm. This illustrates the implicit effects

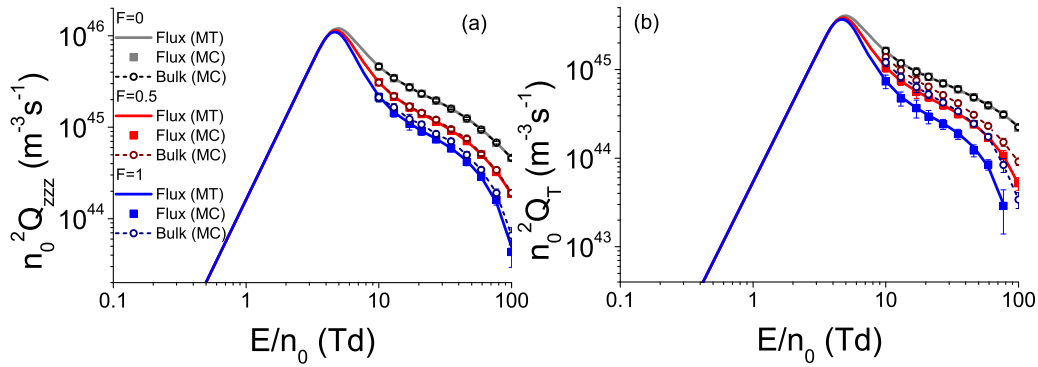


Figure 11. Comparison of the bulk and flux values of (a) $n_0^2 Q_{zzz}$ and (b) $n_0^2 Q_T$ for electrons in the ionisation model of Lucas and Saelee. The results are obtained from numerical multi-term solutions of the Boltzmann equation (MT) and MC simulations.

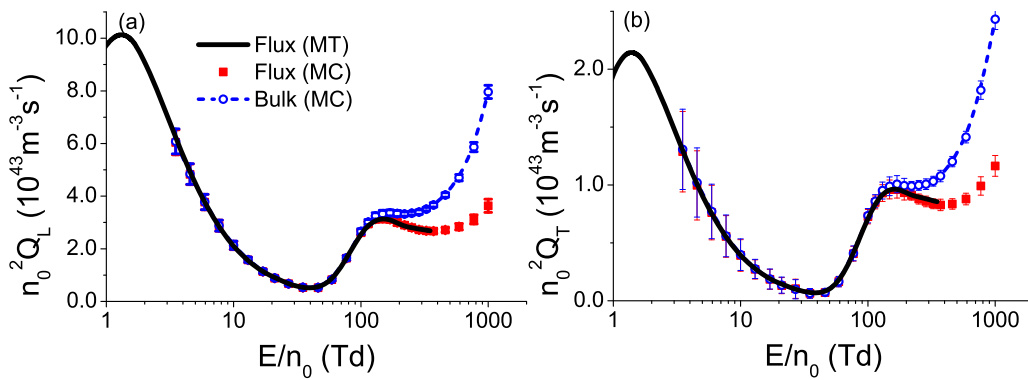


Figure 12. Comparison of the bulk and flux values of (a) $n_0^2 Q_L$ and (b) $n_0^2 Q_T$ for electrons in N_2 . The results are obtained from numerical multi-term solutions of the Boltzmann equation (MT) and MC simulations.

of ionisation on the third-order transport coefficients. We also note that bulk values of Q_L and Q_T are being reduced with increasing F . This indicates that the influence of the implicit effects of ionisation on the third-order transport tensor is stronger than the corresponding influence of the explicit effects.

Figures 12(a) and (b) display the differences between flux and bulk values of Q_L and Q_T respectively, for electrons in N_2 . The differences between the flux and bulk values of Q_L and Q_T for electrons in CF_4 are shown in figures 13(a) and (b), respectively. We observe that bulk values of Q_L and Q_T are larger than the corresponding flux values in both gasses at high electric fields, where electrons undergo many ionisation collisions. Comparing N_2 and CF_4 on one side, and the Lucas–Saelee ionisation model on the other side, we observe that the impact of the explicit effects on the longitudinal component of the third-order transport tensor is much stronger for real gases. This follows from the fact that the minimal impact of the explicit effects of ionisation on Q_L for electrons in the ionisation model of Lucas and Saelee can be attributed to the specific energy dependence of cross sections for inelastic collisions and ionisation. Generally speaking, the qualitative behaviour of the third-order transport coefficients with increasing E/n_0 is the same in the case of flux and bulk values. However, for electrons in N_2 , we observe that the bulk values of Q_L and Q_T

reach their last local minimum at the lower E/n_0 than the corresponding flux values. Specifically, $Q_L^{(b)}$ and $Q_T^{(b)}$ reach their last local minimum at about 220 Td, while $Q_L^{(f)}$ and $Q_T^{(f)}$ reach their last local minimum at around 370 Td. We also observe from figures 12 and 13 that the results evaluated by multi term solution to the Boltzmann equation and those obtained in MC simulations agree very well.

4.4. Concurrence of the third-order transport coefficients and diffusion, the contribution of $Q_L^{(b)}$ to the spatial profile of the swarm and the comparison of $Q_L^{(b)}$ values obtained in this work with results of previous authors

The concurrence between third-order transport coefficients and diffusion coefficients for electrons in N_2 and CF_4 is illustrated by figures 14(a) and (b). Preliminary results in the study of this concurrence for electrons in CH_4 and noble gases have already been discussed [62, 69].

Specifically, for higher values of E/n_0 we observe that $Q_L^{(f)}$ is a rising function of E/n_0 when $D_L^{(f)}$ increases as a convex (or linear) function of E/n_0 in the log–log scale. One may also observe that $Q_L^{(f)}$ is reduced when $D_L^{(f)}$ decreases, or when $D_L^{(f)}$ rises as a concave function of the field in the log–log scale. This concurrence is absent in the limit of the lowest E/n_0 because the third-order transport coefficients

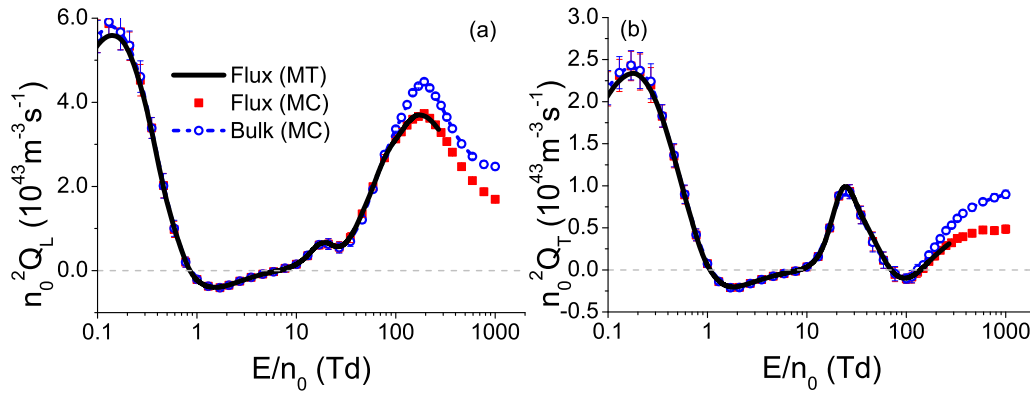


Figure 13. Comparison of the bulk and flux values of (a) $n_0^2 Q_L$ and (b) $n_0^2 Q_T$ for electrons in CF_4 . The results are obtained from numerical multi-term solutions of the Boltzmann equation (MT) and MC simulations.

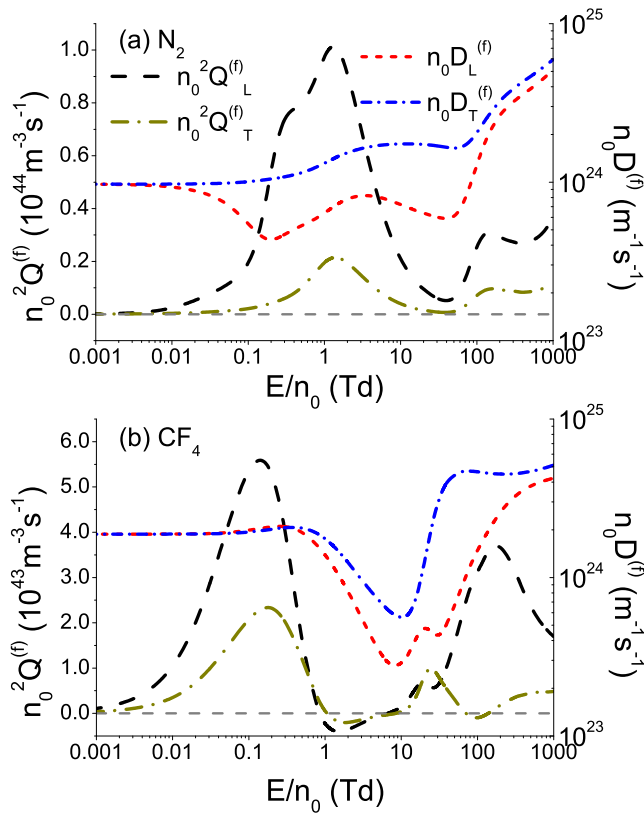


Figure 14. Concurrence of the third-order transport coefficients and diffusion coefficients for electrons in (a) N_2 and (b) CF_4 . For $E/n_0 \leq 300$ Td, the results are calculated from numerical multi-term solutions of the Boltzmann equation, while for $E/n_0 > 300$ Td the results are obtained from MC simulations.

vanish in this range of fields unlike diffusion coefficients which have non-zero thermal values.

As can be seen in figure 14(a) the concurrence between $Q_L^{(f)}$ and $D_L^{(f)}$ for electrons in N_2 is present in the entire field region above 0.21 Td. For electrons in CF_4 , we observe that the concurrence between $Q_L^{(f)}$ and $D_L^{(f)}$ is present in the subset of the field range above 0.02 Td, where $Q_L^{(f)}$ is positive (see figure 14(b)). However, this concurrence is absent in the field range between 1.6 Td and 8.5 Td, as $Q_L^{(f)}$ rises with increasing

E/n_0 although $D_L^{(f)}$ is being reduced in this field range. It is important to note that $Q_L^{(f)}$ has negative values over the range of E/n_0 in this field region. Further increase of the absolute value of $Q_L^{(f)}$, while this component is negative, would imply a further skewing of the spatial profile of the swarm in the negative direction (opposite to the drift velocity) along the longitudinal axis. Although the rise of the collision frequency for vibrational excitations with increasing E/n_0 is strong enough to cause a decrease of $D_L^{(f)}$, it is not strong enough to induce further skewing of the spatial profile of the swarm in the negative direction. It is interesting to note that the concurrence between $Q_L^{(f)}$ and $D_L^{(f)}$ is again present at about 8.5 Td, which is slightly above the field where $Q_L^{(f)}$ becomes positive again (at around 7 Td).

For electrons in N_2 , the qualitative trends of $D_L^{(f)}$ and $D_T^{(f)}$ are the same in the field range above 0.21 Td, where the concurrence between $Q_L^{(f)}$ and $D_L^{(f)}$ is clearly evident. Thus, it is difficult to determine if the E/n_0 profile of $Q_T^{(f)}$ is more related to the corresponding profile of $D_L^{(f)}$ or $D_T^{(f)}$ in the case of N_2 . For electrons in CF_4 , E/n_0 profile of $Q_T^{(f)}$ is related to the corresponding profile of $D_T^{(f)}$ in most of the field range where $Q_T^{(f)}$ is positive. The concurrence between these two transport coefficients in CF_4 is equivalent to the concurrence between $Q_L^{(f)}$ and $D_L^{(f)}$, which is already discussed in this paper. This concurrence is absent in the field region between approximately 100 Td and 170 Td. However, $Q_T^{(f)}$ is negative up to around 140 Td. Thus, the field dependence of $Q_T^{(f)}$ is not related to the field dependence of diffusion in the field range where it is negative, and in the vicinity of the field where it becomes positive, similarly to $Q_L^{(f)}$.

The physical reasons for the observed concurrence between the third-order transport coefficients and diffusion coefficients have been discussed in our previous paper [69] for the example of atomic gases with considerably simpler sets of cross sections. The third-order transport coefficients represent a small asymmetric correction to diffusive motion, that is represented by the components of the diffusion tensor. As discussed previously [58], the rise of the reduced electric field leads to an increase of the directional component of electron velocity (in the absence of NDC) and to an increase of

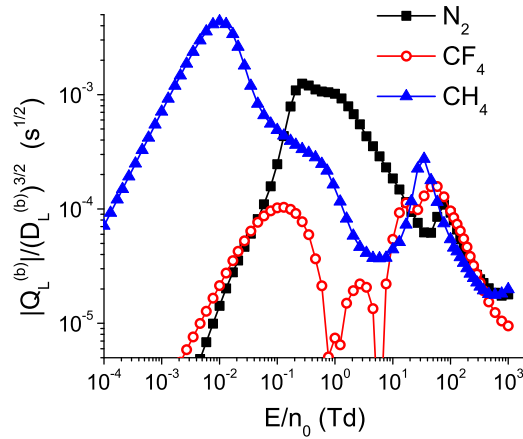


Figure 15. The values of the ratio $|Q_L^{(b)}|/(D_L^{(b)})^{3/2}$ for electrons in N_2 , CF_4 and CH_4 as functions of E/n_0 . For $E/n_0 \leq 100$ Td, where the differences between the bulk and flux values are negligible, the results are obtained from numerical multi-term solutions of the Boltzmann equation, while for higher values of E/n_0 the results are obtained in MC simulations.

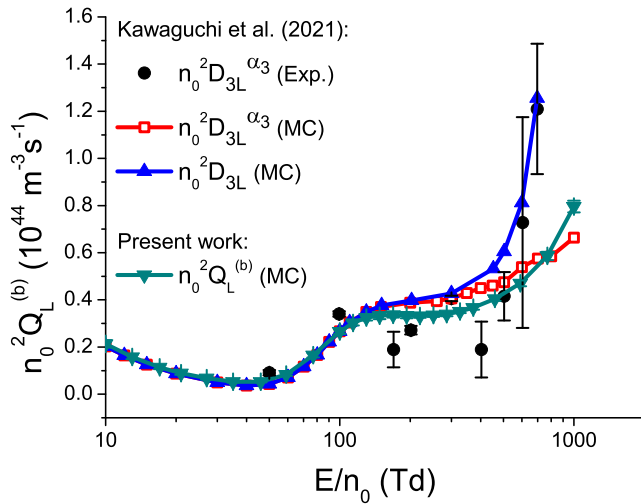


Figure 16. Comparison of the values of $n_0^2 Q_L^{(b)}$, that are determined in this work, with the results of Kawaguchi *et al* [59]. In this figure $n_0^2 D_{3L}^{\alpha_3}$ represents simulation results from the reference [59] that are determined from equation (24) by employing MC simulations, while $n_0^2 D_{3L}^{\alpha_3}$ represents $n_0^2 Q_L^{(b)}$ that are determined in reference [59] from alpha parameters, after neglecting alpha parameters of fourth and higher order. Experimental results of Kawaguchi *et al* are represented by black circles, while results that are obtained from MC simulations are represented by a combination of symbols and continuous lines.

the electron energy. These two effects favour the increase of the third-order transport coefficients if the frequency of electron collisions with atoms/molecules of the background gas is not rising with increasing energy. However, if the collision frequency is rising steeply enough with increasing electron energy, this leads to a reduction of the third-order transport coefficients. The same holds for the components of the diffusion tensor, which are also quenched by elastic and inelastic collisions. Comparing these two sets of transport coefficients, third-order transport coefficients represent a form of motion

that ‘carries’ a smaller amount of energy and momentum, and as such they are much more sensitive to collisions with the background gas, than the components of the diffusion tensor. This suggests that for a sufficiently high E/n_0 , the third-order transport coefficients are reduced with increasing E/n_0 , if the diffusion is being reduced, and even if the slope of diffusion in the log–log scale decreases with increasing E/n_0 . However, this concurrence is absent at the lowest fields and under conditions in which third-order transport coefficients are negative, due to reasons that are already discussed in this manuscript.

In figure 15 we show the values of the ratio $|Q_L^{(b)}|/(D_L^{(b)})^{3/2}$ for electrons in N_2 , CF_4 and CH_4 , as functions of E/n_0 . Calculations are performed assuming the concentration of background molecules $n_0 = 3.54 \times 10^{22} \text{ m}^{-3}$. This ratio determines the contribution of the longitudinal component of the third-order transport tensor to the spatial profile of the swarm, as can be seen from equation (6). From this figure, we observe that the contribution of $Q_L^{(b)}$ to the spatial profile of the swarm is larger in CH_4 than in the remaining two gases for E/n_0 lower than 0.1 Td and for E/n_0 between 21 Td and 46 Td. For E/n_0 between 0.13 Td and 17 Td the quantity $|Q_L^{(b)}|/(D_L^{(b)})^{3/2}$ is larger in N_2 than in CH_4 and CF_4 . For E/n_0 between 70 Td and 300 Td this ratio is slightly lower in CH_4 than in the remaining two gases. For E/n_0 between 400 Td and 1000 Td this ratio is lower in CF_4 than in N_2 and CH_4 . It is interesting to note that differences between the values of $|Q_L^{(b)}|/(D_L^{(b)})^{3/2}$ in N_2 , CH_4 and CF_4 do not exceed the factor of three in the field range between 50 Td and 700 Td. In most of this region, these differences do not exceed the factor of two. Moreover, the values of this ratio are very close to each other for electrons in these three gases in the field range between 200 Td and 450 Td. This indicates that $n_0^2 Q_L^{(b)}$ can be measured in CH_4 and CF_4 , in the field range between 50 Td and 700 Td, under similar experimental conditions that were applied for measurements in N_2 . Recently Kawaguchi and co-workers using a MC simulation technique have shown that $n_0^2 Q_L^{(b)}$ can be measured in CH_4 and SF_6 in the arrival time spectra experiment [71].

In figure 16 we show the comparison of the longitudinal component of the third-order transport tensor $n_0^2 Q_L^{(b)}$ for electrons in N_2 with the corresponding values that are determined by Kawaguchi *et al* [59]. In this figure, $n_0^2 D_{3L}$ is determined from MC simulations by using equation (24), while $n_0^2 D_{3L}^{\alpha_3}$ is evaluated from the alpha parameters based on equation (25) from reference [59] by neglecting the alpha parameters of fourth and higher order. Kawaguchi and co-workers determined alpha parameters from the arrival time spectra experiment and the MC simulations. All results are in an excellent agreement up to about 130 Td, while differences between these sets of results become noticeable at higher values of E/n_0 . Our calculated values of $n_0^2 Q_L^{(b)}$ are somewhat lower than the theoretical results of Kawaguchi *et al* for E/n_0 between 130 Td and 460 Td. For higher values of E/n_0 our results are significantly lower than $n_0^2 D_{3L}$ and somewhat below $n_0^2 D_{3L}^{\alpha_3}$ until approximately 770 Td. At around 1000 Td the value of $n_0^2 Q_L^{(b)}$ in the present calculations, is somewhat above the theoretical values of $n_0^2 D_{3L}^{\alpha_3}$ that are determined by Kawaguchi *et al*. The difference between our calculations of $n_0^2 Q_L^{(b)}$ and those of Kawaguchi and co-workers for $n_0^2 D_{3L}$ is a clear

indication of different sets of cross sections used as input data in MC simulations. The sensitivity of the third-order transport coefficients to the cross sections used in the transport calculations was demonstrated by Kawaguchi and co-workers [63]. The deviation of $n_0^2 D_{3L}^{\alpha_3}$ from $n_0^2 D_{3L}$ for higher values of E/n_0 can be attributed to neglecting alpha parameters of fourth and higher order in equation from which the values of $n_0^2 D_{3L}^{\alpha_3}$ are determined, as discussed by Kawaguchi *et al* [59]. Our calculations of $n_0^2 Q_L^{(b)}$ and experimental values of $n_0^2 D_{3L}^{\alpha_3}$ agree very well up to about 600 Td. If we take a careful look, we observe that our calculations are somewhat below experimental values up to about 100 Td and somewhat above experimental results until approximately 500 Td. For higher values of E/n_0 , however, our results are significantly below experimental points. For $E/n_0 = 600$ Td our calculations of $n_0^2 Q_L^{(b)}$ are within the experimental error, while at 700 Td they are significantly below the lower boundary of experimental results at 700 Td. Strictly speaking, $n_0^2 Q_L^{(b)}$ and $n_0^2 D_{3L}^{\alpha_3}$ cannot be directly equated, because $n_0^2 D_{3L}^{\alpha_3}$ represents an approximation of $n_0^2 Q_L^{(b)}$ when the fourth and higher order alpha parameters are negligible. Strict comparison with experimental results obtained by Kawaguchi and co-workers [59] would be possible if $n_0^2 D_{3L}^{\alpha_3}$ was determined using measured or calculated alpha parameters.

5. Conclusion

In this paper, we have investigated the behaviour of the third-order transport coefficients for electrons in N_2 and CF_4 . Calculations have been performed using a multi-term theory for solving the Boltzmann equation and MC simulation technique. The initial MC code has been extended to allow the calculations of third-order transport coefficients in the presence of non-conservative collisions. We found that the moment method for solving the Boltzmann equation works very well for the third-order transport coefficients, and is particularly fast and accurate for model gases.

One of the most striking phenomena observed in the present work is the occurrence of negative values in the E/n_0 -profiles of $n_0^2 Q_{xx}^{(f)}$ and $n_0^2 Q_{zz}^{(f)}$ for electrons in CF_4 . After the relaxation of the swarm to the steady-state, transport coefficients of the third-order attain negative values over the range of electron energies where the most energetic electrons may undergo many collisions leading to the vibrational excitation of CF_4 molecule. We have also noticed that the occurrence of negative values in the E/n_0 -profiles of $n_0^2 Q_{xx}^{(f)}$ and $n_0^2 Q_{zz}^{(f)}$ in CF_4 takes place in the energy region where the cross sections for vibrational excitations exceed the cross section for momentum transfer in elastic collisions. Likewise, we have also observed that $n_0^2 Q_T^{(f)}$ has negative values in the field region between the end of the occurrence of NDC and the field where the drift velocity reaches 90% of its initial value before the onset of NDC. Based on the results presented in this work, it may be assumed that there is a slight concurrence between $n_0^2 Q_T^{(f)}$ and drift velocity. This concurrence refers to the occurrence of negative values of $n_0^2 Q_T^{(f)}$ that are essentially controlled by the collision processes, which promote the development of NDC.

As the two-term approximation has become a commonplace in the calculation of electron transport properties in gases and as it forms the foundations of many publicly available codes for solving the Boltzmann equations, we have been motivated to investigate its limitations in the context of the present research. Comparisons between the two-term and multi-term calculations were performed for E/n_0 less than 300 Td. For electrons in N_2 , the accuracy of the two-term approximation is sufficient to investigate the behaviour of the third-order transport coefficients in the presence of the electric field. In contrast, for electrons in CF_4 the two-term approximation produces large errors and it is not even qualitatively correct, particularly over the range of electron energies where the cross section for transfer of momentum in elastic collisions is at minimum, while the cross sections of vibrational excitations become significant. This favours a large asymmetry in the distribution function in the velocity space which in turn renders the two-term approximation quite inappropriate for the analysis of third-order transport coefficients.

In the present work, we have studied the implicit and explicit effects of non-conservative collisions on the third-order transport coefficients. While implicit effects of non-conservative collisions are induced by direct population and depopulation of the distribution function in velocity space, the explicit effects are caused by the combined effects of the energy dependence of non-conservative collisions and spatial variation of the average energy along the swarm. Using the modified Ness–Robson model with the attachment heating, we have observed that the bulk values of $n_0^2 Q_L$ and $n_0^2 Q_T$ are larger than the corresponding flux values at low electric fields. At intermediate fields the opposite situation holds: the flux values are larger than the corresponding bulk values. This behaviour and relationship between the bulk and flux values of both $n_0^2 Q_L$ and $n_0^2 Q_T$, are inverted for the attachment cooling model.

The effects of electron-impact ionisation on the third-order transport coefficients are analysed for electrons in the ionisation model of Lucas and Saelee, N_2 and CF_4 . For all gases we considered, bulk values of $n_0^2 Q_L$ and $n_0^2 Q_T$ are larger than the corresponding flux values for the higher electric fields. In particular, comparing the explicit influence of ionisation on $n_0^2 Q_L^{(b)}$ and $n_0^2 Q_T^{(b)}$ in the ionisation model of Lucas and Saelee, effects are more pronounced for $n_0^2 Q_T^{(b)}$.

In this work the concurrence between $n_0^2 Q_L^{(f)}$ and $n_0 D_L^{(f)}$ is analysed. For electrons in N_2 the concurrence is effective over the entire range of the considered E/n_0 . This concurrence is also present for electrons in CF_4 over the range of E/n_0 where $n_0^2 Q_L^{(f)}$ is positive. However, in the field region where $n_0^2 Q_L^{(f)}$ is negative, there is a range of E/n_0 values, where $n_0^2 Q_L^{(f)}$ is rising although $n_0 D_L^{(f)}$ is being reduced. This effect is analysed using the physical interpretation of the negative values of $n_0^2 Q_L^{(f)}$. The concurrence between $n_0^2 Q_T^{(f)}$ and the components of the diffusion tensor is also investigated. In particular, for electrons in CF_4 we found that the E/n_0 profile of $n_0^2 Q_T^{(f)}$ is more related to the corresponding profile of $n_0 D_T^{(f)}$ than to the corresponding profile of $n_0 D_L^{(f)}$.

Contribution of the longitudinal component of the third-order transport tensor to the spatial profile of the swarm was

studied for electrons in N_2 , CF_4 and CH_4 . This contribution is proportional to the ratio $|Q_L^{(b)}|/(D_L^{(b)})^{3/2}$. Between 50 Td to 700 Td differences between the values of this ratio for electrons in N_2 , CF_4 and CH_4 do not exceed the factor of 3. More precisely, we have observed that these differences do not differ from each other by a factor of 2 over the majority of E/n_0 values in the above-mentioned field region. Even though this result of the study seems modest, it is very important because it shows that the existing experimental infrastructure used to measure third-order transport coefficients in N_2 can be used equally successfully for measurements of these quantities in other gases.

The present calculations of $n_0 Q_L^{(b)}$ for electrons in N_2 are compared with the arrival time spectra measurements and MC simulations of Kawaguchi and co-workers [59]. The present calculations and results of Kawaguchi and co-workers agree very well up to approximately 500 Td. For higher values of E/n_0 , the discrepancy between our calculations and those obtained by Kawaguchi and co-workers in MC simulations, may be directly attributed to the details of the cross sections for electron scattering in N_2 used as input data in numerical codes.

It is hoped that the present study will provide an incentive for further theoretical and experimental studies of the third-order transport coefficients for electrons in gases. Particular attention has recently been focussed on extracting cross-sections from swarm data [90, 91]. The inclusion of these sensitive higher order transport coefficients, may result in improved cross-section sets, particularly given the new machine learning algorithms implemented [92–94]. Our plans for future research include the study of third-order transport coefficients in the presence of pressure dependent effects and third-order transport coefficients for positrons in gases of interest for further development and optimization of positron traps.

Acknowledgments

The authors acknowledge the support of the Institute of Physics Belgrade and the Ministry of Education, Science and Technological Development of the Republic of Serbia. Z Lj Petrović is grateful to the SASA F155 project for support. R D White acknowledges the financial support from the Australian Research Council scheme.

Data availability statement

All data that support the findings of this study are included within the article (and any supplementary files).

ORCID iDs

I Simonović  <https://orcid.org/0000-0001-6704-9042>
 D Bošnjaković  <https://orcid.org/0000-0002-2725-5287>
 Z Lj Petrović  <https://orcid.org/0000-0001-6569-9447>
 R D White  <https://orcid.org/0000-0001-5353-7440>
 S Dujko  <https://orcid.org/0000-0002-4544-9106>

References

- [1] Lieberman M A and Lichtenberg A J 2005 *Principles of Plasma Discharges and Materials Processing* (New York: Interscience (Wiley-Interscience))
- [2] Makabe T and Petrović Z Lj 2014 *Plasma Electronics: Applications in Microelectronic Device Fabrication* (Boca Raton, FL: CRC Press)
- [3] Rudenko K V 2009 *High Energy Chem.* **43** 196
- [4] Shustin E G 2017 *J. Commun. Technol. Electron.* **62** 454
- [5] Shamiryan D, Paraschiv V, Boullart W and Baklanov M R 2009 *High Energy Chem.* **43** 204
- [6] Donnelly V M and Kornblit A 2013 *J. Vac. Sci. Technol. A* **31** 050825
- [7] Shahidi S and Ghoranneviss M 2015 *Cloth. Text. Res. J.* **34** 37
- [8] Xie L, Brault P, Bauchire J-M, Thomann A-L and Bedra L 2014 *J. Phys. D: Appl. Phys.* **47** 224004
- [9] Friedrich J F, Wettmarhausen S, Hanelt S, Mach R, Mix R, Zeynalov E B and Meyer-Plath A 2010 *Carbon* **48** 3884
- [10] Takai O 2008 *Pure Appl. Chem.* **80** 2003
- [11] Weltmann K-D and von Woedtk T 2017 *Plasma Phys. Control. Fusion* **59** 014031
- [12] Laroussi M 2018 *Plasma* **1** 47
- [13] Grisetti E, Kolosnjaj-Tabi J, Gibot L, Fourquaux I, Rols M-P, Yousfi M, Merbahi N and Golzio M 2019 *Sci. Rep.* **9** 7583
- [14] Alves L L, Bogaerts A, Guerra V and Turner M M 2018 *Plasma Sources Sci. Technol.* **27** 023002
- [15] Colonna G et al 2021 *Eur. Phys. J. D* **75** 183
- [16] Makabe T 2018 *Plasma Sources Sci. Technol.* **27** 033001
- [17] Madshaven I, Hestad O L and Åstrand P-O 2021 *Comput. Phys. Commun.* **265** 107987
- [18] Petrović Z Lj, Dujko S, Marić D, Malović G, Nikitović Ž, Šašić O, Jovanović J, Stojanović V and Radmilović-Radenović M 2009 *J. Phys. D: Appl. Phys.* **42** 194002
- [19] Ruiz-Vargas G, Yousfi M and de Urquijo J 2010 *J. Phys. D: Appl. Phys.* **43** 455201
- [20] Makabe T 2019 *Japan. J. Appl. Phys.* **58** 110101
- [21] Silva T, Grofulović M, Klarenaar B L M, Morillo-Candas A S, Guaitella O, Engeln R, Pintassilgo C D and Guerra V 2018 *Plasma Sources Sci. Technol.* **27** 015019
- [22] Minesi N, Mariotto P, Pannier E, Stancu G D and Laux C O 2021 *Plasma Sources Sci. Technol.* **30** 035008
- [23] Ribire M, Eichwald O and Yousfi M 2020 *J. Appl. Phys.* **128** 093304
- [24] Upadhyay R R, Suzuki K, Raja L L, Ventzek P L G and Ranjan A 2020 *J. Phys. D: Appl. Phys.* **53** 435209
- [25] Nijdam S, Teunissen J and Ebert U 2020 *Plasma Sources Sci. Technol.* **29** 103001
- [26] Arslanbekov R R and Kolobov V I 2021 *Plasma Sources Sci. Technol.* **30** 045013
- [27] Marinov D, Teixeira C and Guerra V 2017 *Plasma Process. Polym.* **14** 1600175
- [28] Derzsi A, Horváth B, Donkó Z and Schulze J 2020 *Plasma Sources Sci. Technol.* **29** 074001
- [29] Huxley L G H and Crompton R W 1974 *The Diffusion and Drift of Electrons in Gases* (New York: Wiley)
- [30] Dyatko N A, Kochetov I V and Ochkin V N 2020 *Plasma Sources Sci. Technol.* **29** 125007
- [31] Babaeva N Y and Naidis G V 2016 *Phys. Plasmas* **23** 083527
- [32] Babaeva N Y and Naidis G V 2018 *Plasma Sources Sci. Technol.* **27** 075018
- [33] Li X, Sun A, Zhang G and Teunissen J 2020 *Plasma Sources Sci. Technol.* **29** 065004
- [34] Bagheri B et al 2018 *Plasma Sources Sci. Technol.* **27** 095002
- [35] Arcese E, Rogier F and Boeuf J-P 2017 *Phys. Plasmas* **24** 113517
- [36] Dujko S, Markosyan A H, White R D and Ebert U 2013 *J. Phys. D: Appl. Phys.* **46** 475202

- [37] Taran M D, Dyatko N A, Kochetov I V, Napartovich A P and Akishev Y S 2018 *Plasma Sources Sci. Technol.* **27** 055004
- [38] Peng Y, Chen X, Lan L, Zhan H, Liu Y, He W and Wen X 2021 *Plasma Sci. Technol.* **23** 064013
- [39] Petrović Z Lj, Šuvakov M, Nikitović Ž, Dujko S, Šasić O, Jovanović J, Malović G and Stojanović V 2007 *Plasma Sources Sci. Technol.* **16** S1–S12
- [40] Pitchford L C et al 2013 *J. Phys. D: Appl. Phys.* **46** 334001
- [41] Rabie M, Haefliger P, Chachereau A and Franck C M 2015 *J. Phys. D: Appl. Phys.* **48** 075201
- [42] Grofulović M, Alves L L and Guerra V 2016 *J. Phys. D: Appl. Phys.* **49** 395207
- [43] Li C, Brok W J M, Ebert U and van der Mullen J J A M 2007 *J. Appl. Phys.* **101** 123305
- [44] Li C, Teunissen J, Nool M, Hundsdorfer W and Ebert U 2012 *Plasma Sources Sci. Technol.* **21** 055019
- [45] Higginson D P, Holod I and Link A 2020 *J. Comput. Phys.* **413** 109450
- [46] Wilczek S et al 2016 *Phys. Plasmas* **23** 063514
- [47] Hartmann P et al 2020 *Plasma Sources Sci. Technol.* **29** 075014
- [48] Takahashi H and Sugawara H 2020 *Japan. J. Appl. Phys.* **59** 036001
- [49] Nakashima K, Takahashi H and Sugawara H 2019 *Japan. J. Appl. Phys.* **58** 116001
- [50] Pitchford L C et al 2017 *Plasma Process. Polym.* **14** 1600098
- [51] Lovaas T H, Skullerud H R, Kristensen O-H and Linhjell D 1987 *J. Phys. D: Appl. Phys.* **20** 1465
- [52] Koutselos A D 2001 *Chem. Phys.* **270** 165
- [53] Viehland L A and Johnsen R 2019 *J. Geophys. Res. Atmos.* **124** 13593–600
- [54] Viehland L A 2018 *Gaseous Ion Mobility, Diffusion, and Reaction* (Berlin: Springer)
- [55] Viehland L A, Ducasse E, Cordier M, Trout A and Dashdorj J 2021 *J. Chem. Phys.* **155** 204301
- [56] Vrhovac S B, Petrović Z Lj, Viehland L A and Santhanam T S 1999 *J. Chem. Phys.* **110** 2423
- [57] Sugawara H and Sakai Y 2006 *Japan. J. Appl. Phys.* **45** 5189
- [58] Simonović I, Bošnjaković D, Petrović Z Lj, Stokes P, White R D and Dujko S 2020 *Phys. Rev. E* **101** 023203
- [59] Kawaguchi S, Nakata N, Satoh K, Takahashi K and Satoh K 2021 *Plasma Sources Sci. Technol.* **30** 035006
- [60] Dujko S, White R D and Petrović Z Lj 2008 *J. Phys. D: Appl. Phys.* **41** 245205
- [61] Penetrante B M and Bardsley J N 1990 *Non-Equilibrium Effects in Ion and Electron Transport* ed J W Gallagher, D F Hudson, E E Kunhardt and R J Van Brunt (New York: Plenum) p 49
- [62] Petrović Z Lj, Simonović I, Marjanović S, Bošnjaković D, Marić D, Malović G and Dujko S 2017 *Plasma Phys. Control. Fusion* **59** 014026
- [63] Kawaguchi S, Takahashi K and Satoh K 2021 *Plasma Sources Sci. Technol.* **30** 035010
- [64] Stojanovic V D and Petrovic Z L 1998 *J. Phys. D: Appl. Phys.* **31** 834
- [65] Whealton J H and Mason E A 1974 *Ann. Phys., NY* **84** 8
- [66] Koutselos A D 1996 *J. Chem. Phys.* **104** 8442
- [67] Koutselos A D 1997 *J. Chem. Phys.* **106** 7117
- [68] Koutselos A D 2001 *Chem. Phys.* **315** 193
- [69] Simonović I, Bošnjaković D, Petrović Z Lj, White R D and Dujko S 2020 *Eur. Phys. J. D* **74** 63
- [70] Stokes P W, Simonović I, Philippa B, Cocks D, Dujko S and White R D 2018 *Sci. Rep.* **8** 2226
- [71] Kawaguchi S, Takahashi K and Satoh K 2018 *Plasma Sources Sci. Technol.* **27** 085006
- [72] Kumar K, Skullerud H and Robson R 1980 *Aust. J. Phys.* **33** 343
- [73] Nolan A M, Brennan M J, Ness K F and Wedding A B 1997 *J. Phys. D: Appl. Phys.* **30** 2865
- [74] Franceschini C and Loperfido N 2019 *Symmetry* **11** 970
- [75] Dujko S, White R D, Petrović Z Lj and Robson R E 2010 *Phys. Rev. E* **81** 046403
- [76] Robson R E and Ness K F 1986 *Phys. Rev. A* **33** 2068
- [77] White R D, Ness K F, Robson R E and Li B 1999 *Phys. Rev. E* **60** 2231
- [78] White R D, Robson R E, Dujko S, Nicoletopoulos P and Li B 2009 *J. Phys. D: Appl. Phys.* **42** 194001
- [79] Dujko S, White R D, Petrović Z Lj and Robson R E 2011 *Plasma Sources Sci. Technol.* **20** 024013
- [80] Ness K F and Robson R E 1986 *Phys. Rev. A* **34** 2185
- [81] Raspopovic Z M, Sakadzic S, Bzenic S A and Petrovic Z Lj 1999 *IEEE Trans. Plasma Sci.* **27** 1241
- [82] Petrović Z Lj, Raspopović Z M, Dujko S and Makabe T 2002 *Appl. Surf. Sci.* **192** 1–25
- [83] Dujko S, Raspopović Z M and Petrović Z Lj 2005 *J. Phys. D: Appl. Phys.* **38** 2952
- [84] Lucas J and Salee H T 1975 *J. Phys. D: Appl. Phys.* **8** 64
- [85] Kurihara M, Petrovic Z Lj and Makabe T 2000 *J. Phys. D: Appl. Phys.* **33** 2146
- [86] Sasic O, Malovic G, Strinic A, Nikitovic Z and Petrovic Z L 2004 *New J. Phys.* **6** 74
- [87] Petrovic Z Lj, Crompton R and Haddad G 1984 *Aust. J. Phys.* **37** 23
- [88] Vrhovac S B and Petrović Z Lj 1996 *Phys. Rev. E* **53** 4012
- [89] Mirić J, Bošnjaković D, Simonović I, Petrović Z Lj and Dujko S 2016 *Plasma Sources Sci. Technol.* **25** 065010
- [90] White R D et al 2018 *Plasma Sources Sci. Technol.* **27** 053001
- [91] Casey M J E, de Urquijo J, Serkovic Loli L N, Cocks D G, Boyle G J, Jones D B, Brunger M J and White R D 2017 *J. Chem. Phys.* **147** 195103
- [92] Stokes P W, Cocks D G, Brunger M J and White R D 2020 *Plasma Sources Sci. Technol.* **29** 055009
- [93] Stokes P W, Casey M J E, Cocks D G, de Urquijo J, Garcia G, Brunger M J and White R D 2020 *Plasma Sources Sci. Technol.* **29** 105008
- [94] Stokes P W, Foster S P, Casey M J E, Cocks D G, González-Magaña O, de Urquijo J, Garcia G, Brunger M J and White R D 2021 *J. Chem. Phys.* **154** 084306

PAPER

Axisymmetric fluid streamer model in the AMReX library

To cite this article: I Simonović *et al* 2024 *Plasma Sources Sci. Technol.* **33** 085012

View the [article online](#) for updates and enhancements.

You may also like

- [pynucastro: A Python Library for Nuclear Astrophysics](#)
Alexander I. Smith, Eric T. Johnson, Zhi Chen et al.
- [Meeting the Challenges of Modeling Astrophysical Thermonuclear Explosions: Castro, Maestro, and the AMReX Astrophysics Suite](#)
M. Zingale, A. S. Almgren, M. G. Barrios Sazo et al.
- [PICSAR-QED: a Monte Carlo module to simulate strong-field quantum electrodynamics in particle-in-cell codes for exascale architectures](#)
Luca Fedeli, Neïl Zaïm, Antonin Sainte-Marie et al.



Analysis Solutions for your **Plasma Research**

For Surface Science

- ▶ Surface Analysis
- ▶ SIMS
- ▶ 3D depth Profiling
- ▶ Nanometre depth resolution





For Plasma Diagnostics

- ▶ Plasma characterisation
- ▶ Customised systems to suit plasma Configuration
- ▶ Mass and energy analysis of plasma ions
- ▶ Characterisation of neutrals and radicals



[Click to view our product catalogue](#)

■ Knowledge
■ Experience ■ Expertise

Contact Hiden Analytical for further details:
 www.HidenAnalytical.com
 info@hiden.co.uk

Axisymmetric fluid streamer model in the AMReX library

I Simonović¹ , D Bošnjaković¹ , J Teunissen²  and S Dujko^{1,*} 

¹ Institute of Physics Belgrade, University of Belgrade, Pregrevica 118, 11080 Belgrade, Serbia

² Centrum Wiskunde and Informatica (CWI), Amsterdam, The Netherlands

E-mail: sasha@ipb.ac.rs

Received 30 March 2024, revised 31 July 2024

Accepted for publication 15 August 2024

Published 29 August 2024



Abstract

We have implemented an axisymmetric fluid model of streamers in the AMReX open-source library. Our implementation is based on the first-order fluid model with a local field approximation. Photoionization is implemented by employing the Zhelenznyak's model using the Helmholtz approach. We have verified our code in standard conditions by comparing our results for positive streamers in air with the existing benchmarks from the literature. To verify the performance of our code in strongly attaching gases, we compare the properties of negative streamers with those obtained from the Afivo-streamer open-source code. Calculations have been performed in mixtures of carbon dioxide and perfluoro-nitrile with a background number density of electrons and positive ions of 10^{13} m^{-3} . We found an excellent agreement between the two sets of results, which indicates the numerical integrity of our code.

Keywords: streamer discharge, axisymmetric fluid model, AMReX library, air, CO_2 - $\text{C}_4\text{F}_7\text{N}$ mixtures

1. Introduction

1.1. Streamers in nature and technology

Streamers are thin channels of weakly-ionized nonstationary plasma produced by an ionization front that moves through non-ionized matter [1–7]. They appear in nature as sprite discharges in the upper planetary atmospheres [8–10], and as precursors of lightning [11–14]. Streamers have numerous applications in technology. They are the ignition mechanism in high-intensity discharge lamps [15]. Streamers are used for purification of water from harmful organic pollutants [16]. In plasma medicine, streamers are used for sterilization [17] and wound healing [18]. Streamers are the main mechanism of breakdown in circuit breakers [19] and gas-insulated switchgear [20]. They occur in parallel plate and spark chambers, as well as in resistive plate chambers that are commonly used in high-energy physics [21, 22]. Further development and optimization of these applications requires a thorough understanding of streamer physics. Such understanding is best developed by

joint efforts of experimental investigation of streamers and their modeling in computer simulations.

1.2. Modeling of streamers in computer simulations

Simulating streamers is a challenging numerical task, due to the steep gradients of the number densities of charged particles at the streamer front, and the coupling of the dynamics of these particles to the electric field that they generate, as well as the non-local nature of photoionization [23]. Most computer codes, that are designed for studying streamers, implement fluid models of plasma [23]. In these models, the number densities of charged particles are represented by continuous functions [24, 25]. These functions are determined by solving a set of differential balance equations, that are coupled to the Poisson equation for the electrostatic potential [24, 25]. These balance equations require transport and reaction coefficients as input data, and these coefficients can be obtained either by solving the Boltzmann equation or through a Monte Carlo simulation [24, 25].

In the computer codes that implement the fluid models of streamers, numerical solutions of fluid equations are

* Author to whom any correspondence should be addressed.

often determined on rectangular grids by employing the finite volume method [26], although finite difference method has also been used [27, 28]. The finite volume method is advantageous for simulating streamers because it is inherently conservative [26]. However, in this method additional care must be taken to ensure that the numerical solution is stable [26]. The numerical stability of the solution is often ensured by using the flux/slope limiters including the total variation diminishing scheme with the Koren flux limiter [29–31] and the monotonic upwind-centered scheme for conservation-law (MUSCL scheme) [26, 32, 33]. Weighted essentially non-oscillatory methods (WENO scheme) have also been used for streamer simulations [27].

Models that utilize the finite element method have been developed due to the simpler implementation of complex geometries [28, 34–36]. The comparison of a code which uses the finite-element method with flux-corrected transport technique and a code that employs the finite-volume method with MUSCL scheme has been performed by Ducasse *et al* in case of a positive streamer in point-to-plane geometry [37]. It has been observed that both codes accurately describe the streamer dynamics and morphology, although the computational cost is higher for the finite element code [37].

Besides the fluid models, particle-in-cell Monte Carlo (PIC-MCC) simulations of streamers have also been carried out [38–40]. In these simulations, the dynamics of individual particles are followed, which makes these simulations very computationally intensive. Hybrid models, which are more computationally efficient than PIC-MCC models, alleviate this problem, but they are more challenging to implement [41–43].

1.3. Open source libraries for scientific computing

The development of computer codes for scientific computing is greatly simplified by open-source libraries. Much of the functionality that is needed by scientific computing application codes has already been implemented in these open-source computing platforms. This functionality includes data structures for storing grid and particle data, algorithms for processing this data, and the existing infrastructure for saving data to output files. These libraries can also include the implementation of parallelization, multigrid method for efficiently solving the elliptic differential equations and adaptive mesh refinement. Some open-source libraries have been used for simulating streamers and non-equilibrium plasma, and the open-source codes that were derived from these libraries are outlined below.

Afivo is an open-source library which implements a tree-based adaptive mesh refinement (AMR) [44]. This library uses OpenMP parallelization and has an inbuilt implementation of the geometric multigrid method. The Afivo library has been the basis for the development of two open-source codes for simulating streamer discharges: Afivo-streamer, which employs the first-order fluid model [30], and Afivo-pic, which employs a PIC-MCC simulation [45].

Chombo is an open-source library that uses finite difference and finite volume methods to solve partial differential equations [46, 47]. This library implements block-structured adaptive mesh refinement. The Chombo library has been

used to simulate streamers in point-to-plane geometry by employing a 3D fluid model [48, 49]. It has also been utilized to develop a new open-source code with parallelization and block-structured adaptive mesh refinement, known as Chombo-discharge [50]. Chombo-discharge is developed to investigate non-equilibrium gas discharges in complex geometries.

FEniCS is an open-source computing platform for solving partial differential equations by employing the finite element method [51, 52]. The FEniCS library has been the basis for the development of the open-source code for simulating electrical discharges FEDM [53]. FEDM extends the FEniCS library with features that enable the implementation and solution of an arbitrary number of particle balance equations that are coupled to the Poisson equation in an automated manner [53].

Finally, a three-dimensional fluid model of streamers has been implemented by Niknezhad *et al* in Ansys Fluent software platform in order to study the influence of unsteady air-flow on electric discharges [54].

1.4. Benefits of using the AMReX library

AMReX is an open-source C++ library for massively parallel block-structured adaptive mesh refinement applications [55, 56]. Despite being implemented in C++, AMReX has Fortran and Python interfaces. The inbuilt implementation for adaptive mesh refinement in the AMReX library is very user friendly and it includes automatic refining and coarsening different parts of the grid, according to user defined refinement criteria, initialization of data on newly created fine regions from the interpolated data from the next coarser level, and updating coarse grid values by averaging over the next finer grid. AMReX also automatically handles generation and filling of ghost cells at the domain boundary, at the coarse/fine interface, and at the boundary between parts of the domain which belong to different parallel processes. The AMReX library has an built-in implementation for parallelization. This includes MPI and OpenMP for parallelization on central processing units (CPUs), as well as parallelization on graphic processing units (GPUs). AMReX uses the native programming languages for GPUs: CUDA, HIP, and SYCL for NVIDIA, AMD, and Intel GPUs, respectively. The AMReX library has built-in multigrid solvers for both the Poisson equation and the Helmholtz equation. These solvers can be easily applied across a hierarchy of adaptive mesh refinement levels. AMReX has inbuilt data structures for implementing both grid and particle data and algorithms for processing this data. This includes inbuilt procedures for mapping of particle data to grid data, which can be quite useful for particle-in-cell codes, and hybrid plasma models. AMReX has an inbuilt implementation of embedded boundaries, which enables modelling of complex geometries [57–59]. It also includes inbuilt functions for writing data to output files for plotting and for generation checkpoint files, from which simulations can be easily resumed. Finally, AMReX has the possibility to use machine learning models, which are trained in the PyTorch library, directly in AMReX codes. This feature is useful for the data-driven developments in plasma processing [60]. Most of the functionality outlined in this subsection is handled by the AMReX built-in functions

automatically, and it is largely hidden from the application codes.

AMReX has been employed for developing an exascale computing platform for beam-plasma simulations, Warp-X [61–63], and a compressible astrophysics simulation code, CASTRO [64], an adaptive mesh refinement solver for compressible reacting flows PeleC [65], and a fluid dynamic code HyBurn [66]. Among its many applications, AMReX has been employed for plasma-assisted oxidation of hydrocarbon fuels using nanosecond pulsed discharges [67, 68]. AMReX has also been used for studying the relationship between volcanic eruption parameters and radio-frequency emission [69].

1.5. The present work

In this work we implement an axisymmetric fluid streamer model in the AMReX library. We have decided to develop our own code in which we could straightforwardly include curvilinear electrodes, various models for the implementation of chemical reactions and treatment of nonconservative collisions, as well as machine learning methods for determining the electrical potential and photoionization terms. This code needs to be flexible enough to simulate a wide range of systems. These systems include streamers in strongly attaching gases, that are relevant for gaseous insulation in high voltage technology, electrical discharges and the formation of transient plasma in the planetary atmospheres, electrical discharges in liquids, and gaseous detectors in high-energy physics.

Our model is based on the first-order fluid model with local field approximation. We give a detailed description of the implementation of our code in this paper, so that it can be easily replicated by other researchers. In order to demonstrate the validity of our code under standard conditions we compare its results with the existing benchmarks from the literature for the case of a positive streamer in air [23]. The preliminary results of the testing were shown elsewhere [70, 71]. To test the validity of our code in case of strongly attaching gases, we perform simulations of negative streamers in the mixtures of carbon dioxide (CO₂) and perfluoronitrile (C₄F₇N) and we compare our results to those of the Afivo-streamer code. The mixtures of CO₂ and C₄F₇N are chosen as the background gas for two reasons. The first reason is the importance of these mixtures for insulation in high-voltage technology as a potential replacement of sulfur hexafluoride (SF₆). Due to its excellent physical and chemical properties, high dielectric strength, and arc performance, SF₆ is the most important gaseous dielectric in high-voltage technology [72–74]. For this reason, SF₆ is widely used in gas circuit breakers, transformers, high voltage transmission lines and gas-insulated switchgear [72–74]. However, SF₆ is one of the most potent industrial greenhouse gases [72, 73]. As anthropogenic global warming is one of the most pressing concerns [75, 76], there is an urgent need to replace SF₆ with more sustainable alternatives [72, 73]. C₄F₇N is one of the most promising candidates because it has a low global warming potential and a shorter atmospheric lifetime compared to SF₆ and at least twice the dielectric strength of SF₆ [73, 77, 78]. C₄F₇N is often mixed with CO₂ or N₂ due to its high liquefaction temperature [73, 77, 78]. As streamers present one of

the main breakdown mechanisms in electric insulation technology, the study of streamer propagation in the mixtures of CO₂ and C₄F₇N is important for investigating the applicability of these mixtures as a replacement for SF₆ in circuit breakers and gas-insulated switchgear.

The second reason for choosing the mixtures of CO₂ and C₄F₇N is the desire to make a qualitative comparison of our results with those of Guo and co-workers who have investigated the propagation of positive and negative streamers in these mixtures by employing 3D PIC-MCC simulations [73]. This is done to investigate if the axisymmetric fluid model of streamer discharges, that is implemented in this code and the Afivo-streamer code, produces a similar qualitative behavior as fully 3D PIC-MCC simulations in strongly attaching gases that are of interest for electric insulation technology.

1.6. Structure of the paper

In section 2 we outlay the first-order fluid model, that is being employed in our code. In section 3 we describe the implementation of our code. In section 3.1, we describe spatial discretization. In section 3.2, we cover temporal discretization and time step restrictions. The procedure for adaptive mesh refinement is described in section 3.3. The AMReX inbuilt geometric multigrid solvers we have employed are discussed in section 3.4. In section 4 we present our results. section 4.1 details the test cases we utilized. In section 4.2, we show the electron swarm transport coefficients that are being used as input in our model. In sections 4.3–4.5 we consider the following three test cases: (i) propagation of a positive streamer in air with a high background ionization, (ii) propagation of a positive streamer in air with photoionization, and (iii) propagation of negative streamers in the mixtures of CO₂ and C₄F₇N. The concluding remarks are given in section 5.

2. Theory

In this work we implement the first-order fluid model [24, 79–82]. In this model, the time evolution of the number density of electrons is represented by the drift-diffusion-reaction equation:

$$\frac{\partial n_e(\mathbf{r}, t)}{\partial t} = \nabla \cdot (n_e(\mathbf{r}, t) \mu_e(\mathbf{r}, t) \mathbf{E}(\mathbf{r}, t) + D_e(\mathbf{r}, t) \nabla n_e(\mathbf{r}, t)) + (\alpha(\mathbf{r}, t) - \eta(\mathbf{r}, t)) \mu_e(\mathbf{r}, t) |\mathbf{E}(\mathbf{r}, t)| n_e(\mathbf{r}, t) + S_{ph}(\mathbf{r}, t), \quad (1)$$

where $n_e(\mathbf{r}, t)$ is the number density of electrons, $\mathbf{E}(\mathbf{r}, t)$, $\mu_e(\mathbf{r}, t)$, $D_e(\mathbf{r}, t)$, $\alpha(\mathbf{r}, t)$, $\eta(\mathbf{r}, t)$, and $S_{ph}(\mathbf{r}, t)$ are the resulting electric field, electron mobility, electron diffusion coefficient, ionization coefficient, attachment coefficient and non-local photoionization source term, respectively, while \mathbf{r} and t are the coordinate vector and time, respectively. In our model, the diffusion coefficient is approximated by the transverse component of the diffusion tensor. The influence of anisotropic diffusion on streamer simulations has been previously investigated [33]. As ion motion is neglected in our model, the time evolution of the number densities of positive and negative ions is

given by the reaction equations:

$$\frac{\partial n_p(\mathbf{r}, t)}{\partial t} = \alpha(\mathbf{r}, t) \mu_e(\mathbf{r}, t) |\mathbf{E}(\mathbf{r}, t)| n_e(\mathbf{r}, t) + S_{ph}(\mathbf{r}, t), \quad (2)$$

$$\frac{\partial n_n(\mathbf{r}, t)}{\partial t} = \eta(\mathbf{r}, t) \mu_e(\mathbf{r}, t) |\mathbf{E}(\mathbf{r}, t)| n_e(\mathbf{r}, t), \quad (3)$$

where $n_p(\mathbf{r}, t)$ and $n_n(\mathbf{r}, t)$ are the number densities of positive and negative ions, respectively. In our model, the spatial dependence of $\mu_e(\mathbf{r}, t)$, $D_e(\mathbf{r}, t)$, $\alpha(\mathbf{r}, t)$, and $\eta(\mathbf{r}, t)$ is represented by the local field approximation [24]. Thus, it is assumed that at every point in time the value of these quantities is determined solely by the local intensity of the resulting electric at that point in time. The resulting electric field is the vector sum of the applied electric field \mathbf{E}_{appl} , and the electric field due to space charges \mathbf{E}_{spch} . The electric field that is generated by the space charges is determined from the electrostatic potential of space charges ϕ_{spch} as

$$\mathbf{E}_{spch} = -\nabla \phi_{spch}. \quad (4)$$

The electrostatic potential of space charges is determined by solving the Poisson equation:

$$\Delta \phi_{spch} = -\frac{q_e (n_p(\mathbf{r}, t) - n_e(\mathbf{r}, t) - n_n(\mathbf{r}, t))}{\varepsilon_0}, \quad (5)$$

where q_e is the elementary charge, while ε_0 is the vacuum permittivity.

The photoionization source term $S_{ph}(\mathbf{r}, t)$ is inherently non-local, as it describes the production of free electrons and positive ions at the given point in the domain by the absorption of photons which are emitted in another part of the domain [23, 83, 84]. In air, excited nitrogen molecules emit photons which have a sufficient energy to ionize oxygen molecules. This is the main source of free electrons in air. As free electrons ahead of the streamer front are necessary for the propagation of positive streamers, photoionization is of a crucial importance for the dynamics of positive streamers in air. In our work we use the Zhelenznyak's model of photoionization [85]. In this model, the photoionization source term is represented by the following integral:

$$S_{ph}(\mathbf{r}) = \int d^3r' \frac{I(\mathbf{r}') f(|\mathbf{r} - \mathbf{r}'|)}{4\pi |\mathbf{r} - \mathbf{r}'|^2}, \quad (6)$$

where $I(\mathbf{r})$ is the photon production term and $f(|\mathbf{r} - \mathbf{r}'|)$ is the absorption function, and time dependence is suppressed for simplicity. We use the Bourdon three term parametrization in this work [84]. In this parametrization the photon production term is given by:

$$I(\mathbf{r}) = \frac{p_q}{p + p_q} \xi^B \frac{\nu_u}{\nu_i} S_i(\mathbf{r}), \quad (7)$$

where p is the pressure of the background gas, p_q is the quenching pressure, ν_u and ν_i are the electron impact excitation frequency for level u and the impact ionization rate,

Table 1. The parameters of three-term exponential fitting by Bourdon *et al* [84].

j	$A_j(\text{cm}^{-2}\text{Torr}^{-2})$	$\lambda_j(\text{cm}^{-1}\text{Torr}^{-1})$
1	1.986×10^{-4}	0.0553
2	0.0051	0.1460
3	0.4886	0.8900

respectively, ξ^B is the photoionization efficiency, while $S_i(\mathbf{r})$ is the ionization production rate. This rate is given by $S_i(\mathbf{r}) = \alpha(\mathbf{r}) \mu_e(\mathbf{r}) |\mathbf{E}(\mathbf{r})| n_e(\mathbf{r})$, where we have suppressed the temporal dependence for the sake of clarity. We use the quenching pressure of $p_q = 40$ mbar in this work. In this parametrization, the absorption function is approximated as:

$$f(|\mathbf{r} - \mathbf{r}'|) = p_{O_2}^2 |\mathbf{r} - \mathbf{r}'| \sum_{j=1}^3 A_j e^{-\lambda_j p_{O_2} |\mathbf{r} - \mathbf{r}'|}, \quad (8)$$

where p_{O_2} is the partial pressure of oxygen molecules, and A_j and λ_j are Bourdon's coefficients that are given in table 1. By inserting equations (7) and (8) into equation (6), the photoionization source term has the form:

$$S_{ph}(\mathbf{r}) = \frac{p_q}{p + p_q} \xi^B \frac{\nu_u}{\nu_i} \sum_{j=1}^3 p_{O_2}^2 A_j \int d^3r' \frac{S_i(\mathbf{r}') e^{-\lambda_j p_{O_2} |\mathbf{r} - \mathbf{r}'|}}{4\pi |\mathbf{r} - \mathbf{r}'|}. \quad (9)$$

Thus, the photoionization source term has a form of a linear combination of solutions of the Helmholtz equation [83, 84]. For this reason, $S_{ph}(\mathbf{r})$ can be determined by solving the corresponding set of Helmholtz differential equations [83, 84]:

$$\left(\nabla^2 - (p_{O_2} \lambda_j)^2 \right) S_{ph,j}(\mathbf{r}) = - \left(A_j p_{O_2}^2 \frac{p_q}{p + p_q} \xi^B \frac{\nu_u}{\nu_i} \right) S_i(\mathbf{r}), \quad (10)$$

$$S_{ph}(\mathbf{r}) = \sum_{j=1}^3 S_{ph,j}(\mathbf{r}). \quad (11)$$

In this work, we have used $\xi^B \frac{\nu_u}{\nu_i} = 0.075$, $p_{O_2} = 150$ Torr, and $p = 750$ Torr = 1 bar. The same values are used in the Bagheri *et al* paper [23]. The coefficients A_j and λ_j for the three term Bourdon parametrization are given in table 1.

3. Model implementation

3.1. Spatial discretization

3.1.1. Brief mention of AMReX data structures. In AMReX, grid data is defined on rectangular boxes. Boxes are represented by a range of indices, where different index values correspond to different cells of the individual box. The data can be defined at cell centers (cell-centered), cell faces (face-centered) or cell nodes (corner/nodal). This is determined by the index type of a given box. Boxes can be broken into

smaller boxes, that are owned by different parallel processes. *BoxArray* represents an array of such boxes.

The data that is defined on a *BoxArray* is stored in data structures defined in the *MultiFab* class and *IMultiFab* class in the case of double and integer values, respectively. The instances of these two classes store data on a single level of mesh refinement, while vectors of these class instances are used to store data across a hierarchy of adaptive mesh refinement levels. The instances of these classes are constructed on a *BoxArray* with a given *DistributionMapping*, number of components and number of ghost cells. *DistributionMapping* is a class that maps different boxes in the *BoxArray* to the individual parallel processes. Each *MultiFab* has a valid region and ghost cells. Valid region represents the part of the domain that is covered by this *MultiFab*. Ghost cells are used to represent the data that is stored at the boundaries of the valid region.

There are three basic types of boundaries in AMReX. The physical boundary corresponds to the boundaries of the computation domain. The coarse/fine boundary is the border between two levels of adaptive mesh refinement. The internal boundary is the boundary between different boxes in the same *BoxArray*. Ghost cells are required even for the internal boundaries as different boxes can belong to different parallel processes.

The filling of ghost cells in the case of internal and coarse/fine boundaries, as well as in the case of external boundaries for the homogeneous Neumann boundary conditions, are handled by the inbuilt AMReX functions automatically. In the case of external boundaries for the Dirichlet boundary conditions, the filling of ghost cells can be done by user defined functions.

3.1.2. Finite volume discretization and the Koren flux limiter.

For the spatial discretization of all quantities in our code, we employ the finite volume method. In this method, scalar variables are defined at cell centers, while vector variables are defined at cell faces. Thus, the number densities of electrons and ions, the electrostatic potential of space charges and the resulting electric field intensity, as well as the photoionization source terms, are defined at cell centers, while the electric field components and the electron fluxes are defined at cell faces.

The components of the electric field, that is generated by space charges, are calculated from the electrostatic potential of space charges by using the *getGradSolution* method of the AMReX's multilevel multigrid (*MLMG*) class. The resulting electric field is calculated as the vector sum of this electric field and the applied electric field. The components of the resulting electric field are interpolated from cell faces to cell centers to calculate the electric field intensity. This is done by employing linear interpolation:

$$E_{r,cc;i,j} = (E_{r,i+1/2,j} + E_{r,i-1/2,j}) / 2, \quad (12)$$

$$E_{z,cc;i,j} = (E_{z,i,j+1/2} + E_{z,i,j-1/2}) / 2. \quad (13)$$

It should be noted that indexing is integer and zero based in AMReX in the case of all index types. Thus, in the valid region of the domain, both cell centered and face centered arrays

start with index zero. For this reason, the i th value of the face centered array is between $(i - 1)$ th and i th cell centered value. However, in the equations in this paper this face centered value is indexed as $i - 1/2$ for the sake of clarity. The electric field intensity is then calculated as

$$E_{i,j} = \sqrt{E_{r,cc;i,j}^2 + E_{z,cc;i,j}^2}. \quad (14)$$

The interpolation of the number density of electrons from cell centers to cell faces to calculate the advective part of the electron flux is nontrivial. Linear interpolation (center differencing) leads to strong numeric oscillations [31], while the first-order upwind scheme creates too much numeric diffusion [31]. For this reason, flux limiters are used. In our code, we use the Koren flux limiter for the advective part of the electron flux. This limiter has been introduced in [29] and it is defined by the expression:

$$\psi(x) = \max(0, \min(1, (2+x)/6, x)). \quad (15)$$

The advective part of the electron flux along the radial direction is then discretized as [86]

$$f_{r,i+1/2,j}^{(a)} = v_{r,i+1/2,j} \left(n_{e,i+1,j} - \psi \left(\frac{n_{e,i+2,j} - n_{e,i+1,j}}{n_{e,i+1,j} - n_{e,i,j}} \right) \times (n_{e,i+1,j} - n_{e,i,j}) \right), \quad (16)$$

if $v_{r,i+1/2,j} < 0$ and as:

$$f_{r,i+1/2,j}^{(a)} = v_{r,i+1/2,j} \left(n_{e,i,j} + \psi \left(\frac{n_{e,i,j} - n_{e,i-1,j}}{n_{e,i+1,j} - n_{e,i,j}} \right) \times (n_{e,i+1,j} - n_{e,i,j}) \right), \quad (17)$$

if $v_{r,i+1/2,j} \geq 0$. The velocity at cell faces $v_{r,i+1/2,j}$ is calculated as [30, 86]

$$v_{r,i+1/2,j} = -E_{r,i+1/2,j} \mu(E^*), \quad (18)$$

where $E^* = (E_{i,j} + E_{i+1,j})/2$, and similarly for the flux along other direction. The discretization in equations (16) and (17) is third-order accurate in most of the domain, while the accuracy drops to first order near local extrema and in the presence of strong density gradients. It should be noted that in the equations (16) and (17) division by zero can occur. However, in our code we use the implementation of the Koren flux limiter from the Afivo-streamer code [30, 86] in which no explicit division is performed.

The diffusive part of the electron flux is calculated with the standard second-order central differences. The diffusive flux along the radial direction is given by [30, 31]:

$$f_{r,i+1/2,j}^{(d)} = \frac{D_e(E^*)}{\Delta r} (n_{e,i,j} - n_{e,i+1,j}), \quad (19)$$

where Δr is the cell size along the radial direction, while the diffusive flux along the axial direction is calculated in the equivalent way. The resulting flux is determined as the sum of the

advective and diffusive contributions $\mathbf{f} = \mathbf{f}^{(a)} + \mathbf{f}^{(d)}$. The discretized form of the update equations for the number density of electrons, positive ions and negative ions are given by

$$\begin{aligned} \frac{dn_{e;i,j}}{dt} = & \frac{1}{r_i \Delta r} (r_{i-1/2} f_{r;i-1/2,j} - r_{i+1/2} f_{r;i+1/2,j}) \\ & + \frac{1}{\Delta z} (f_{z;i,j-1/2} - f_{z;i,j+1/2}) \\ & + (S_{\text{ion};i,j} - S_{\text{att};i,j}) n_{e;i,j} + S_{\text{ph};i,j}, \end{aligned} \quad (20)$$

$$\frac{dn_{p;i,j}}{dt} = S_{\text{ion};i,j} n_{e;i,j} + S_{\text{ph};i,j}, \quad (21)$$

$$\frac{dn_{n;i,j}}{dt} = S_{\text{att};i,j} n_{e;i,j}, \quad (22)$$

where $S_{\text{ion};i,j}$ and $S_{\text{att};i,j}$ are rates for electron impact ionization and electron attachment, respectively, while $S_{\text{ph};i,j}$ is the photoionization term. The first two rates are calculated as $S_{\text{ion};i,j} = \alpha(E_{i,j}) \mu(E_{i,j}) E_{i,j}$ and $S_{\text{att};i,j} = \eta(E_{i,j}) \mu(E_{i,j}) E_{i,j}$. The photoionization source term is determined by solving a set of Helmholtz equations as discussed in the section 2.

3.2. Temporal discretization

The time stepping in our code is performed by employing the Heun's method (a variant of the second order Runge–Kutta method) [87]. For each of the charged particle species number densities, we define four vectors of *MultiFabs* which correspond to old values, new values, temporary values, and the change in a single Runge–Kutta substep. At the start of the time step, old values and temporary values are updated to new values from the previous time step. Then at each Runge–Kutta substep, the electrostatic potential of space charges, the resulting electric field, and its intensity, the electron fluxes, and the rates for nonconservative processes are calculated from the temporary values. For the first Runge–Kutta substep, the temporary values are equal to the old values. In the second Runge–Kutta substep, the temporary values are equal to the estimate of the new values that is obtained by using the explicit Euler method. Then the change in each Runge–Kutta substep is determined by using the equations (20–22) with fluxes and non-conservative source terms that are calculated from the temporary values for the current substep. The changes in these two substeps are used to calculate the new values of the number densities of charged particles:

$$\text{new_values} = \text{old_values} + \frac{1}{2} (\text{change}_1 + \text{change}_2). \quad (23)$$

While calculating photoionization source terms at each Runge–Kutta substep is the 'proper' way of doing time integration, it is quite computationally expensive and it is not necessary. It is sufficient to calculate photoionization source terms once per several time steps. In this work, we calculate

photoionization at every fourth step when photoionization is included.

We use three time step restriction criteria: the CFL condition, the dielectric relaxation time and the time step restriction due to rates of nonconservative processes. The CFL condition for the advection diffusion equation is given by

$$\Delta t \left(\sum_{i=1}^{\text{dim}} \frac{|v_i|}{\Delta x_i} + 2 \sum_{i=1}^{\text{dim}} \frac{D_e}{\Delta x_i^2} \right) < \text{CFL}, \quad (24)$$

where dim is the problem dimension, which is set to 2 in the axisymmetric model, v_i are velocity components, Δx_i is the grid spacing along the direction i , D_e is the diffusion coefficient, while CFL is the number chosen to ensure the stability of the time integration. In all simulations shown in this paper we have used the value of $\text{CFL} = 0.4$.

The dielectric relaxation time restriction is given by:

$$\Delta t < \frac{\epsilon_0}{q_e \mu_e n_e}. \quad (25)$$

The time step restriction due to rates of nonconservative processes, for a given charged particle species, is given by:

$$\Delta t_{\text{nc}} = \frac{\epsilon_{\text{nd}} + n_{\text{sp}}}{\epsilon_{\text{nd}} + |R_{\text{sp}}|}, \quad (26)$$

where n_{sp} is the number density of a given species, R_{sp} is the change rate of the species due to nonconservative processes per unit time, from equations (20)–(22), while ϵ_{nd} is a small number used to avoid both division by zero, and values of Δt_{nc} that are unnecessarily small. In our code, the value of this number is determined as $\epsilon_{\text{nd}} = 10^{-4} n_{\text{bg}}$, where n_{bg} is the initial background number density of electrons and positive ions. The time step restriction due to nonconservative processes can restrict the time step size to very low values at the beginning of the simulation, especially if the number density of a charged particle species (for instance negative ions) is initialized to zero. For this reason, one can use a higher value of ϵ_{nd} at the beginning of the simulation, or one can restrict the time step size to always be higher than a predefined minimum. However, none of these extra measures are currently used in our code, and the time step size rises to reasonable values after several time steps. The Δt_{nc} is determined for electrons, positive ions and negative ions, and the smallest of these three values is used as the third time step restriction criterion. It should be noted that the time step restriction in the equation (26) is quite stringent, as it controls both the relative increase and the relative decrease of the number densities of charged particles. For this reason, a more relaxed criterion is currently used in the Afivo-streamer code [30, 44]. However, we currently use the time step restriction from the equation (26), as it is conceptually the most straightforward.

3.3. Adaptive mesh refinement

AMReX employs block-structured adaptive mesh refinement. Coarser levels of mesh refinement are covered by finer levels,

where necessary. At the beginning of the simulation, the initial distribution of electrons and ions, at each level of refinement, is determined from the initial conditions, while the number of refinement levels is determined by the refinement criteria that are used. In accordance with the refinement criteria, a new refinement level can be generated during the regrid procedure at later stages of the simulation. The values of all quantities at the new level of refinement are determined by interpolating the corresponding values from the next coarser level. Every existing level of mesh refinement is recreated during the regrid procedure, as different parts of the domain need to be refined at different times during the simulation. If the refinement criteria no longer require it, an existing level of mesh refinement can be removed during the regrid procedure. The entire regrid procedure including the creation of new levels, the initialization of data on these levels, the remaking of the existing levels, as well as the removal of old levels, that are no longer necessary, is handled by the AMReX infrastructure automatically, and it is largely hidden from the application codes. The user can define an arbitrary set of conditions for refining and derefining the existing grid using user-defined functions. In our code, we use the same three refinement criteria as the Afivo-streamer code.

The first criterion is the ionization rate criterion, which is defined as:

$$\Delta x \bar{\alpha} (c_1 E) < c_0, \quad (27)$$

where $\bar{\alpha} = \alpha - \eta$, while c_0 and c_1 are constants. This criterion creates a fine mesh in front of the streamer, where the electric field enhancement occurs.

The second criterion is the potential curvature criterion, which is given by:

$$\frac{\Delta x^2 |\rho_{\text{sph}}|}{\varepsilon_0} < c_2, \quad (28)$$

where $\rho_{\text{sph}} = n_p - n_e - n_n$ is the number density of space charges, ε_0 is the vacuum permittivity, while c_2 is a constant. This criterion creates a fine mesh at the streamer front where the charge separation occurs. It should be noted that the criterion from the equation (28) is not used in the Afivo-streamer code by default, although it can optionally be used [30, 44]. However, we have observed that the use of this criterion prevents numerical instabilities from occurring in the early stages of the simulation. These instabilities can occur if the mesh around the initial condition is not sufficiently refined.

The third criterion is the initial condition criterion, which is given by

$$\Delta x < \Omega \xi, \quad (29)$$

where ξ is the width of the initial seed, while Ω is a constant. This condition is used only in the subset of the domain where the following condition is satisfied

$$(\omega - \xi) < 2\Delta x, \quad (30)$$

where ω is the distance of the grid location from the initial seed. In all simulations shown in this paper we have used the

value $\Omega = 0.25$, and this condition is used only during the first nanosecond. This criterion creates a fine mesh around the initial condition, to capture the initial stages of the simulation with sufficient accuracy. The fourth refinement criterion, which can optionally be used, creates a constant refinement in a predefined subset of the domain. This is computationally expensive but can be desirable in case of very strong gradients. The same refinement criterion can be used in the Afivo-streamer code. In the refinement procedure, AMReX also allows the use of buffer cells, which are automatically refined around every cell that is refined due to the employed refinement criteria. The buffer cells are needed as the accuracy of numerical schemes drops near the coarse/fine boundary. The number of the buffer cells that are used is determined by the *amr.n_error_buf* parameter, which can be set in the input file. In calculations presented here we have set this parameter to 16. If the value of this parameter is too small, the numeric diffusion at the streamer front is too high, which can lead to a reduction of the number density of electrons at the streamer front, and the reduction of the enhancement of the longitudinal electric field, which ultimately leads to an unphysical branching of the streamer in the transverse direction.

In our code we also use a derefinement criterion, which reduces mesh refinement in the streamer channel, where high precision is no longer needed. The derefinement criterion, that is used in our code, is given by

$$\Delta x < \Delta x_{\text{deref}}, \bar{\alpha} (c_1 E) \Delta x < c_{0;\text{deref}}, \frac{\Delta x^2 |\rho_{\text{sph}}|}{\varepsilon_0} < c_{2;\text{deref}}, \quad (31)$$

where Δx_{deref} , $c_{0;\text{deref}}$ and $c_{2;\text{deref}}$ are constants that are set in the input file at the start of the simulation. The derefinement of the grid is performed only if all three conditions from the expression above are satisfied. To avoid any confusion regarding the ‘<’ sign in the refinement and the derefinement criteria, the following should be noted: In the refinement criteria the grid is further refined until all refinement criteria are satisfied for the finest grid at the given point in the domain. However, in the derefinement criterion the grid is derefined when the derefinement criterion is satisfied. During the time integration of the simulation, at each Runge–Kutta substep, first coarser levels are updated in time. Then finer levels are updated, and the coarser levels provide boundary values for the finer levels. At the end of each Runge–Kutta substep the values of the coarser levels are recalculated by using the values from the next finer level.

3.4. Multigrid solvers for elliptic equations

In streamer simulations, the Poisson equation for the electric potential of space charges needs to be solved at each Runge–Kutta substep. When photoionization is included, the Helmholtz equation for the photoionization terms also needs to be solved. Both of these equations are elliptic equations. The solution of elliptic equations is very computationally expensive, as the solution in each part of the domain depends

on the right-hand side in the entire domain. The geometric multigrid method is a very efficient method for solving elliptic equations. It consists of applying a simple iterative procedure (like Jacobi or Gauss Seidel) across a hierarchy of grids with reducing resolution [88]. In this method, short wavelength errors are efficiently resolved at fine grids, while long wavelength errors are efficiently resolved at coarse grids [88]. In AMReX, the geometric multigrid solver is already implemented in the *Multi-Level Multi-Grid (MLMG)* class. The constructor of this class takes the reference to an instance of the *MLLinOp* class, which is an abstract base class of various linear operator classes. These linear operator classes determine the type of equation that is to be solved. The *MLPoisson* class is used for solving the Poisson equation, while the *MLABecLaplacian* class can be used for solving the Helmholtz equation. The parameters, which determine the solution procedure, including targeted relative and absolute error tolerances, and the number of V cycles can then be set. The boundary conditions for the solution of the elliptic equation have to be set before the solution procedure can be initiated. In our code, the electrostatic potential of space charges is determined by solving the Poisson equation, as the boundary conditions for ϕ_{spch} are simpler than the boundary conditions for the resulting ϕ , for which inhomogeneous Dirichlet boundary conditions have to be used. We use the zero Dirichlet boundary conditions for the ϕ_{spch} at boundaries which are perpendicular to the applied field, and zero Neumann boundary conditions at the other boundaries. We use the same boundary conditions for the photoionization terms. These boundary conditions for photoionization terms are also used in the Afivo-streamer code, and they are a good approximation when the streamer head is not too close to the domain boundaries [23]. The correct implementation of the boundary conditions for photoionization terms is shown in [84].

The solution procedure in the multigrid method requires the initial guess of the solution. In our code, as the initial guess of the solution for the multigrid method we choose the current value of the corresponding vector of *MultiFabs*. Specifically, we choose the current value of the electric potential of space charges as the initial guess for solving the Poisson equation, and the current values of the photoionization source terms as the initial guess for the set of Helmholtz equations. All of these values are initialized to zero at the start of the simulation.

4. Results

4.1. Test cases

In this work we employ three test cases. The first two test cases consider the propagation of a positive streamer in dry air at 1 bar and 300 K. In these test cases, we use the same simulation conditions including the domain size, boundary conditions, background electric field, the initial conditions, and transport data as those used in cases 1 and 3 from the Bagheri *et al* [23]. We have chosen these simulation conditions to compare our results to those in the supplementary data that is provided for that paper. In the Bagheri *et al* paper, six groups compare the results of their simulation codes in

order to verify the numerical integrity of these codes [23]. These groups include the CWI group from The Netherlands which uses the Afivo-streamer open-source code [30], the ES group from Spain which uses the ARCoS code [89], the FR group from France which uses the code that is implemented in [33], the CN group from China which uses a streamer model that is implemented in COMSOL Multiphysics 5.3 with the plasma module [90], the TUE group from The Netherlands which uses the drift-diffusion module of the plasma simulation software PLASIMO [91], the DE group from Germany which uses INP, a MATLAB-COMSOL toolbox [92, 93]. The first two test cases in the present work are employed to test the validity of our code under conditions that are usually encountered in streamer simulations. The third test case considers the propagation of negative streamers in three mixtures of CO₂ and C₄F₇N. For this test case, the results of our code are compared to the results of the Afivo-streamer code. This test case is included to test the validity of our code in strongly attaching gases.

4.2. Transport data

In the first two test cases we consider streamer discharges in dry air consisting of 80% nitrogen (N₂) and 20% oxygen (O₂), at the pressure of 1 bar and the absolute temperature of 300 K. We use the same analytical approximations for the transport coefficients that are used in Bagheri *et al* [23]. For the temperature and pressure used in this study, the electron swarm transport properties are given by the following expressions

$$\begin{aligned}\mu_e &= 2.3987E^{-0.26}, \\ D_e &= 4.3628 \times 10^{-3} E^{0.22}, \\ \alpha &= (1.1944 \times 10^6 + 4.3666 \times 10^{26}/E^3) e^{-2.73 \times 10^7/E}, \\ \eta &= 340.75, \\ \bar{\alpha} &= \alpha - \eta,\end{aligned}$$

where all quantities are given in SI units. For example, E is the electric field strength in Vm⁻¹, μ_e is the electron mobility in m²V⁻¹s⁻¹, etc. It should be noted that for these transport coefficients the critical field is about 24 kVcm⁻¹, while the typical value for air is about 30 kVcm⁻¹ [23]. For a more detailed presentation of these transport coefficients, the user is referred to Bagheri *et al* [23].

We have studied the propagation of negative streamers in 90% CO₂ – 10% C₄F₇N, 85% CO₂ – 15% C₄F₇N, and 80% CO₂ – 20% C₄F₇N mixtures. In figure 1 we show the bulk drift velocity $W^{(b)}$, bulk transverse diffusion multiplied by the neutral gas density $n_0 D_T^{(b)}$, attachment rate coefficient k_{att}/n_0 , and ionization rate coefficient k_{ion}/n_0 as functions of the reduced electric field E/n_0 , for electrons in the studied mixtures. From these transport coefficients we have calculated electron mobility $\mu_e = W^{(b)}/E$, electron diffusion coefficient $D_e = D_T^{(b)}$, ionization coefficient $\alpha = k_{\text{ion}}/W^{(b)}$ and attachment coefficient $\eta = k_{\text{att}}/W^{(b)}$, which are used as input data in our code and the Afivo-streamer code. The transport coefficients from figure 1 have been determined by employing the multi term method for solving the Boltzmann equation and Monte Carlo simulations

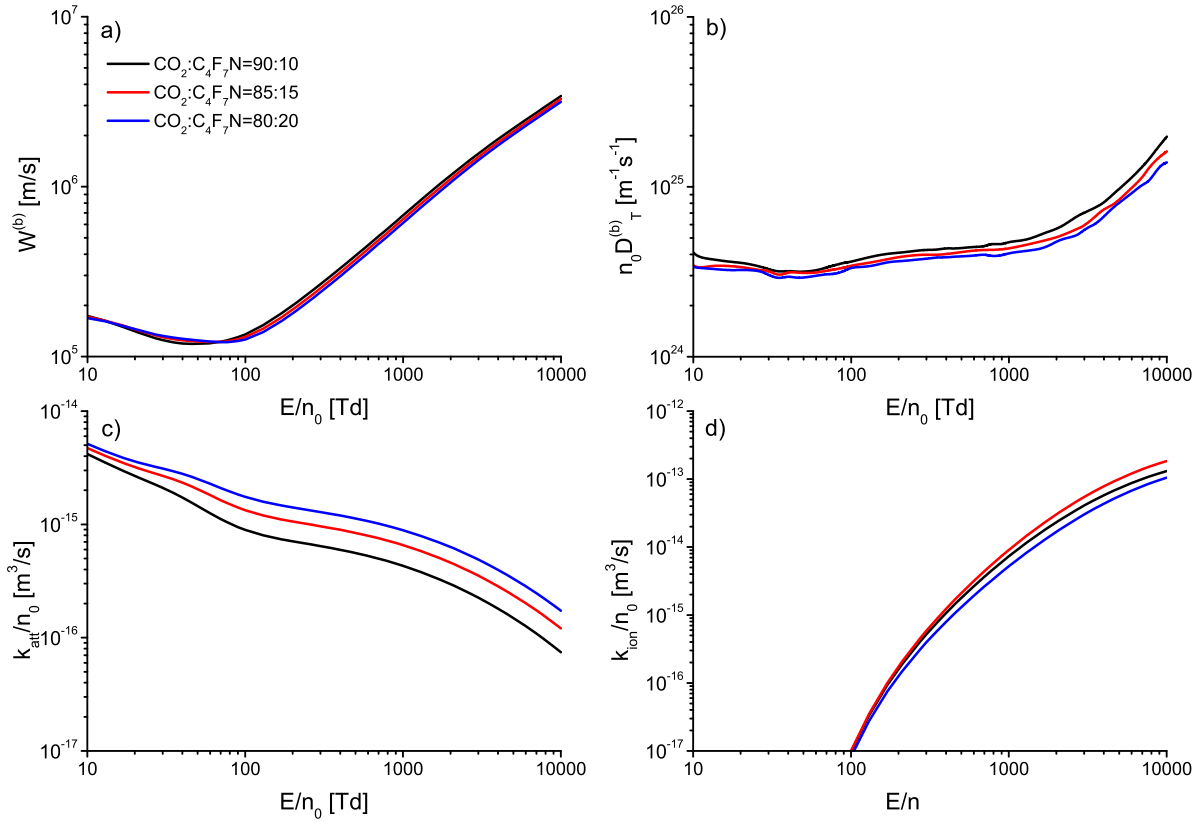


Figure 1. Transport data of an electron swarm in the mixtures of CO_2 and $\text{C}_4\text{F}_7\text{N}$ as functions of the reduced electric field E/n_0 : (a) bulk drift velocity, (b) bulk transverse diffusion, (c) attachment rate coefficient and (d) ionization rate coefficient. The reduced electric field is given in the units of Td, where $1\text{Td} = 10^{-21}\text{Vm}^{-2}$.

[94, 95]. We have used electron-neutral collision cross sections for $\text{C}_4\text{F}_7\text{N}$ and CO_2 from the XJTUAETLab database [96, 97] and the Biagi database [98], respectively.

4.3. Test case 1: positive streamer in air with high background electron density and no photoionization

The domain size is 1.25 cm along both radial and axial coordinate in this test case. In the entire domain, the homogeneous background electric field of -15 kVcm^{-1} is applied along the axial coordinate. A Gaussian of positive ions is chosen for the initial seed to create the local field enhancement that enables the formation of a positive streamer. The initial condition is given by the following equations

$$\begin{aligned} n_e(r, z) &= n_{\text{bg}}, \\ n_p(r, z) &= n_{\text{bg}} + N_0 \exp\left(-\frac{r^2 + (z - z_0)^2}{\sigma^2}\right), \\ n_n(r, z) &= 0, \end{aligned}$$

where $n_{\text{bg}} = 10^{13}\text{ m}^{-3}$, $\sigma = 0.4\text{ mm}$, $z_0 = 1\text{ cm}$, $N_0 = 5 \times 10^{18}\text{ m}^{-3}$. In this test case, photoionization is not included. Instead, a high value of the homogeneous background electron density n_{bg} is used.

For the grid refinement procedure, we have used the following parameter values: $c_0 = 0.8$, $c_1 = 1.2$, $c_2 = 1.0\text{ V}$, $c_{0\text{deref}} =$

0.1 , $c_{2\text{deref}} = 1.0\text{ V}$, $\Delta x_{\text{deref}} = 10^{-4}\text{ m}$. The simulation was performed on 4 cores and 8 virtual threads of Intel i9-10900KF processor running at 3.70 GHz. The simulation took 12 h. However, the part of the simulation until the positive streamer comes very close to the lower boundary took only 6 h.

In figure 2(a) we show the comparison of the streamer length as a function of time $L(t)$ for our results and the results of the six groups which are presented in the Bagheri *et al* paper [23]. In cases 1 and 2 the streamer length is defined as $L(t) = 1.25\text{ cm} - z_{\text{max}}$, where z_{max} is the position of the maximum of the electric field intensity along z axis. The agreement between all groups is very good in the first half of the time range, while small differences are apparent in the second half of this range. To observe these differences more clearly, we show $L(t) - vt$ in figure 2(b), where $v = 0.05\text{ cmns}^{-1}$. For CWI, FR and DE groups we show the results with the smallest grid spacing. It can be seen in figure 2(b) that our values of $L(t) - vt$ are in the best agreement with the CWI and FR groups.

In figure 3(a) we show the maximum of the electric field intensity as a function of the streamer length. For CWI, FR and DE groups we show the results with the smallest grid spacing. The agreement between all groups is generally good. Again, our results are in very good agreement with CWI and FR groups over the entire range. However, in the range between 0.85 cm and 1.1 cm our results are in the best agreement with those of ES group.

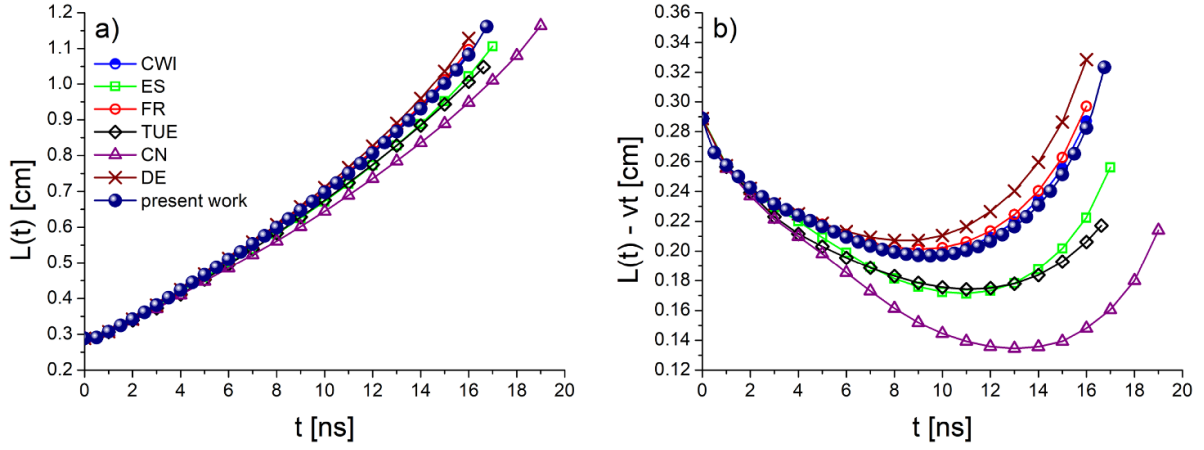


Figure 2. Test case 1: (a) the streamer length $L(t)$ versus time. (b) $L(t) - vt$, where $v = 0.05 \text{ cm ns}^{-1}$.

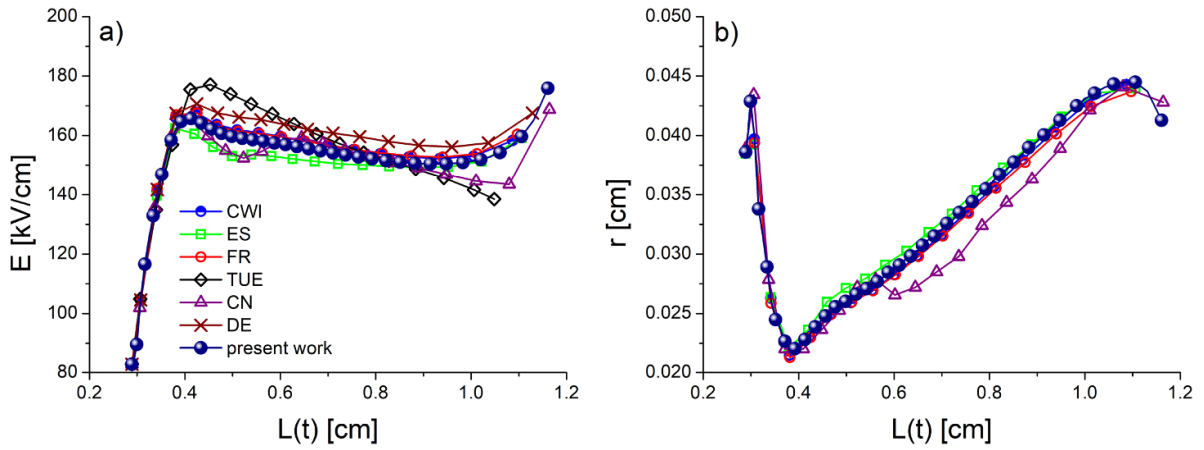


Figure 3. Test case 1: (a) maximal electric field intensity, (b) streamer radius.

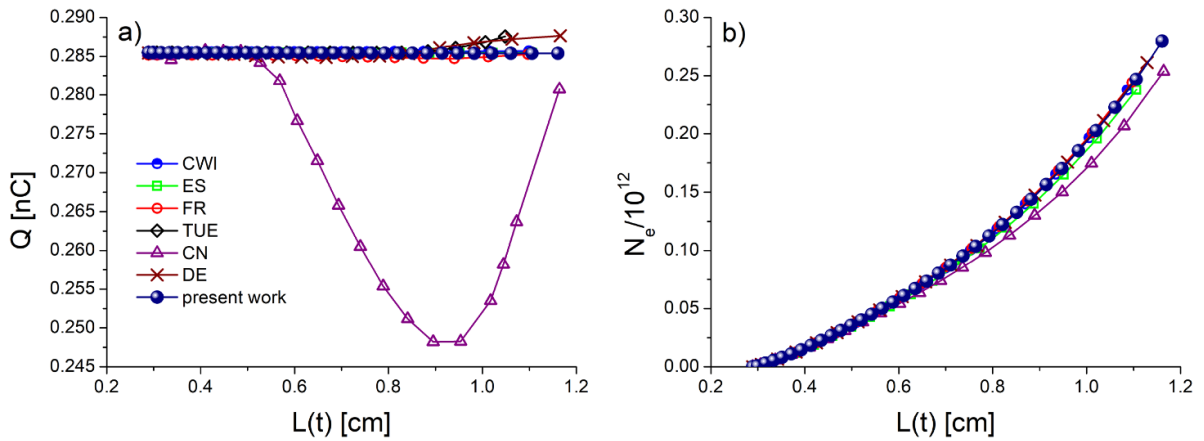


Figure 4. Test case 1: (a) total charge in the system, (b) total number of electrons.

In figure 3(b) we show the streamer radius as a function of the streamer length. It should be noted that for case 1 the streamer radius was not shown in Bagheri *et al* paper [23]. However, the corresponding values are present in the supplementary data for this paper. Our results for the streamer radius

are in very good agreement with the results of CWI, FR and ES groups.

In figure 4(a) we show the total electric charge as a function of the streamer length. In principle, charge is conserved, and its value should remain constant throughout the duration of

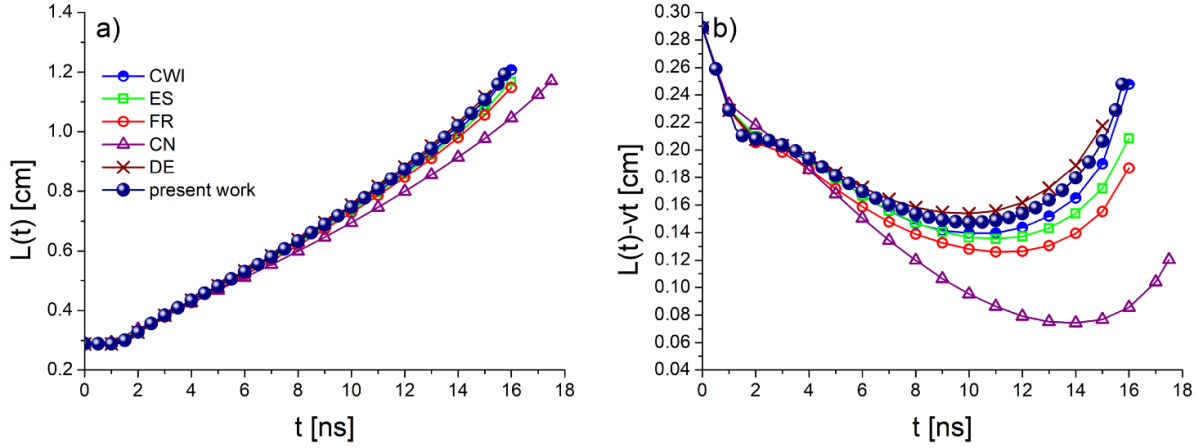


Figure 5. Test case 2: (a) the streamer length $L(t)$ versus time, (b) $L(t) - vt$, where $v = 0.06 \text{ cm ns}^{-1}$.

the simulation. However, the charge conservation is violated in simulations to some degree due to various reasons. Some of these reasons are the nonconservative interpolation procedure in the adaptive mesh refinement technique, roundoff errors, and possible systematic errors in different simulation codes. We observe that the violation of the charge conservation is very low in our code.

In figure 4(b) we show the total number of electrons as the function of the streamer length. Our values are in very good agreement with the corresponding values of most other simulation groups.

4.4. Test case 2: positive streamer in air with photoionization

For this test case, the domain size and the applied electric field are the same as in test case 1. Again, a Gaussian of positive ions is chosen as the initial seed to create the local field enhancement that enables the formation of a positive streamer. The initial condition in this test case differs from the initial condition in the previous test case only in the value of the background electron density, n_{bg} . For this test case n_{bg} is set to 10^9 m^{-3} . The main difference between these two test cases is the inclusion of photoionization in this test case. This provides a more accurate representation of the streamer dynamics in air, where photoionization plays a very significant role in the propagation of positive streamers [84].

For the grid refinement procedure, we have used the following parameter values: $c_0 = 1.0$, $c_1 = 1.0$, $c_2 = 5.0 \text{ V}$. Thus, we have used less strict refinement criteria in this case than in the previous case, due to photoionization which greatly reduces electron density gradients in streamer simulations. We have not used the explicit derefinement procedure in this case, as the simulation time is low enough without using this procedure. The exclusion of explicit derefinement is easily achieved in our code by setting the Δx_{deref} to a negative value. The simulation was performed on 4 cores and 8 virtual threads of Intel i9-10900KF processor running at 3.70 GHz, and it took 3 h. However, the part of the simulation until the streamer comes

close enough to the lower domain boundary, that additional field enhancement due to image charges occurs, took only 1.5 h.

In figure 5(a) we show the comparison of the streamer length as a function of time $L(t)$ for our results and the results of the five groups which are presented in the Bagheri *et al* [23]. Again, the differences between the results of different groups are small and they become more clearly visible near the end of the time range. For this reason, we show $L(t) - vt$ in figure 5(b). It can be seen from figure 5(b) that our values of $L(t) - vt$ are somewhat below the corresponding values of the DE group, and somewhat above the corresponding values of the CWI group.

In figure 6(a) we show the maximum of the electric field intensity as a function of the streamer length. Our values of the electric field intensity maximum are very close to those of CWI and DE groups in most of the domain. However, our results are somewhat below those of the CWI group near the end of the domain, while our results are in excellent agreement with those of DE group for the highest values of the streamer length.

In figure 6(b) we show the streamer radius as a function of the streamer length. The results of all groups are in good agreement in most of the streamer length range. Our results are in the best agreement with those of the ES group.

In figure 7(a) we show the total electric charge as a function of the streamer length. In this test case the violation of charge conservation in our simulation is more pronounced than in the first test case. We have observed that the use of refinement criteria that are less strict, as in this case, leads to a more pronounced violation of charge conservation. This implies that this violation can be attributed to the nonconservative interpolation procedure in the adaptive mesh refinement technique. However, the violation of charge conservation in our simulation for this test case is still less than 0.2% of the initial total charge in the system.

In figure 7(b) we show the total number of electrons as the function of the streamer length. The differences between the

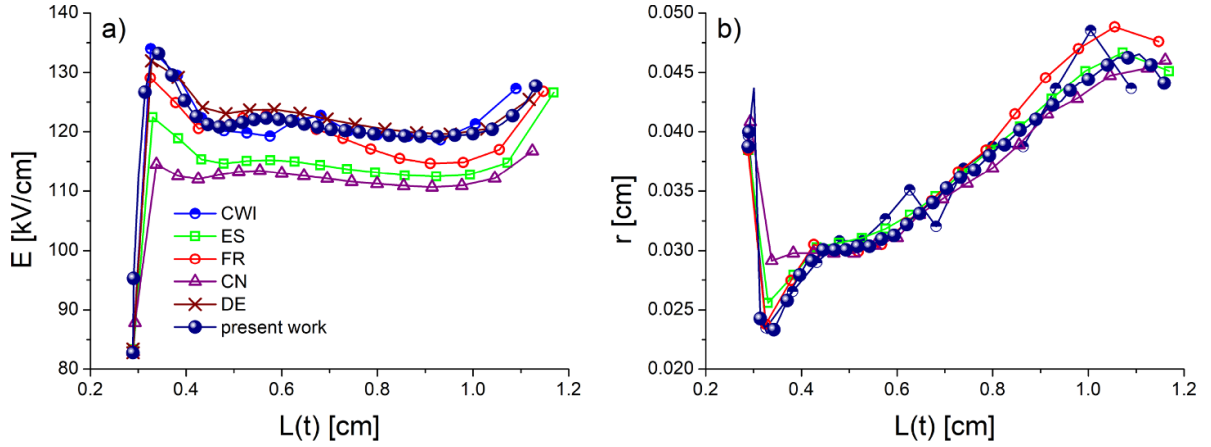


Figure 6. Test case 2: (a) maximal electric field intensity, (b) streamer radius.

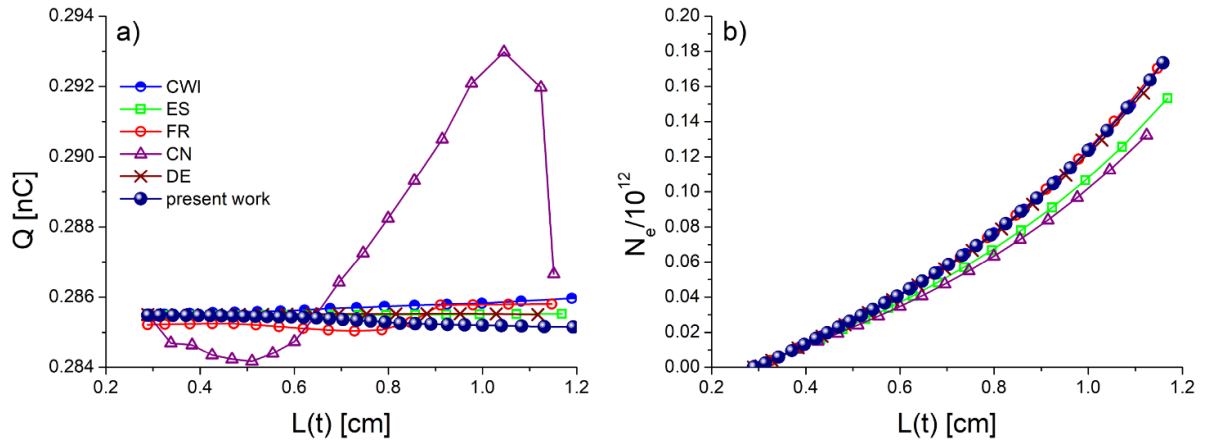


Figure 7. Test case 2: (a) total charge in the system, (b) total number of electrons.

results of different groups become apparent in the second half of the streamer length range. Our results are in the best agreement with those of CWI, FR and DE groups.

In figures 8 and 9 we show the time evolution of the resulting electric field intensity and the number density of electrons, respectively, up to 14 ns. This upper limit is chosen as the streamer is fully formed, while the streamer tip is still far from the domain boundaries. For this reason, the boundary conditions that are used for the photoionization terms are still a good approximation at 14 ns.

4.5. Test case 3: negative streamers in CO_2 - $\text{C}_4\text{F}_7\text{N}$ mixtures

This test case is not intended to analyze realistic experimental conditions. It is only intended to analyze the applicability of our code to simulate the inception and propagation of streamers in strongly attaching gases. Performing simulations in realistic experimental conditions is intended for future publications.

In this test case, the domain size is 16 mm along both axes. The initial condition is a line segment of electrons extending from 48% to 52% of the domain along z axis, with a smooth-step falloff and a width of 0.2 mm between the center and the lateral edges. We have chosen a line segment of electrons for

the initial condition as it allows a quick formation of a negative streamer, while it can be easily replicated in other simulation codes. The initial condition is shown in figure 10. The initial background density of electrons and positive ions is set to 10^{13} m^{-3} . The minimum number density of electrons is set to 10^7 m^{-3} to prevent number densities of electrons, which are too low to be physically realistic, from occurring in the simulation. If the number density of electrons in any part of the domain becomes lower than this value, the number densities of electrons and positive ions are increased by the same amount to restore the number density of electrons to values above the allowed minimum. This artificial process of charge generation is included for purely conceptual reasons, as there are additional sources of free electrons that are not included explicitly in our model, although they generate free electrons even in parts of the domain in which electron impact ionization is not significant. The possible sources of free electrons in these mixtures, that are not explicitly included in our model, are photoionization, electron detachment from negative ions, cosmic radiation, and the background radioactivity. Due to large uncertainties regarding these processes, the value of the minimum number density of electrons is chosen somewhat arbitrarily in this work, and it is 100 times lower than the number density of charged particles in air at the atmospheric pressure.

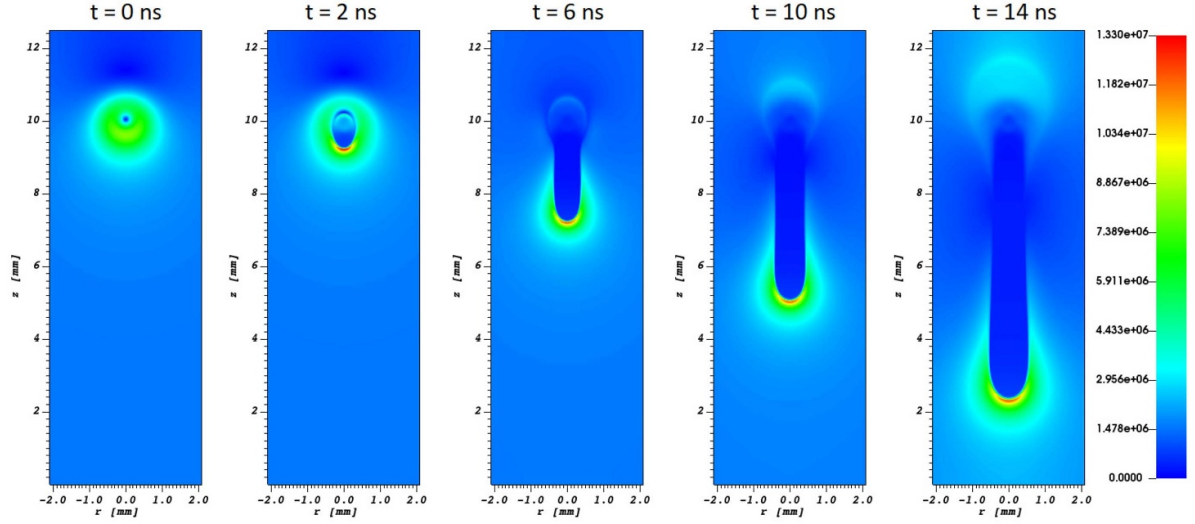


Figure 8. Test case 2: The time evolution of the electric field intensity. The electric field intensity is given in V m^{-1} .

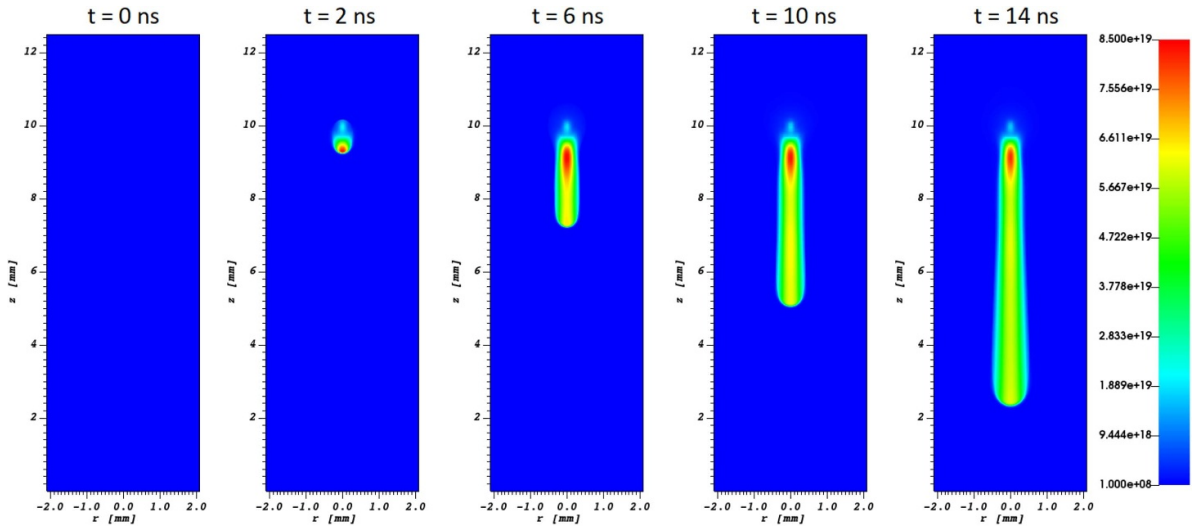


Figure 9. Test case 2: The time evolution of the number density of electrons. The number density of electrons is given in m^{-3} .

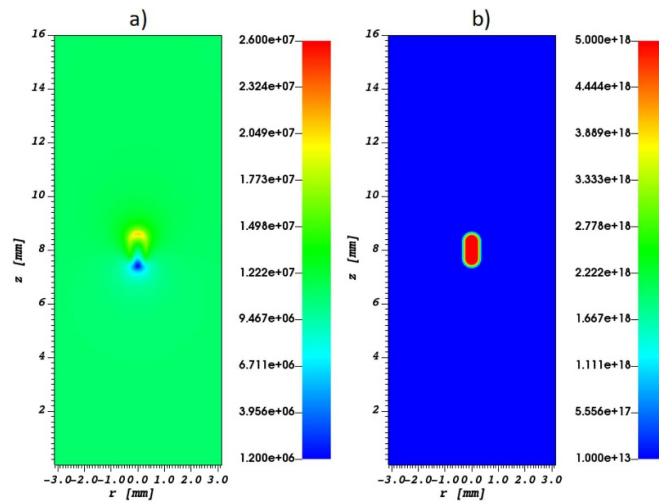


Figure 10. Test case 3, the initial condition: (a) the initial intensity of the resulting electric field in V m^{-1} , (b) the initial number density of electrons in m^{-3} .

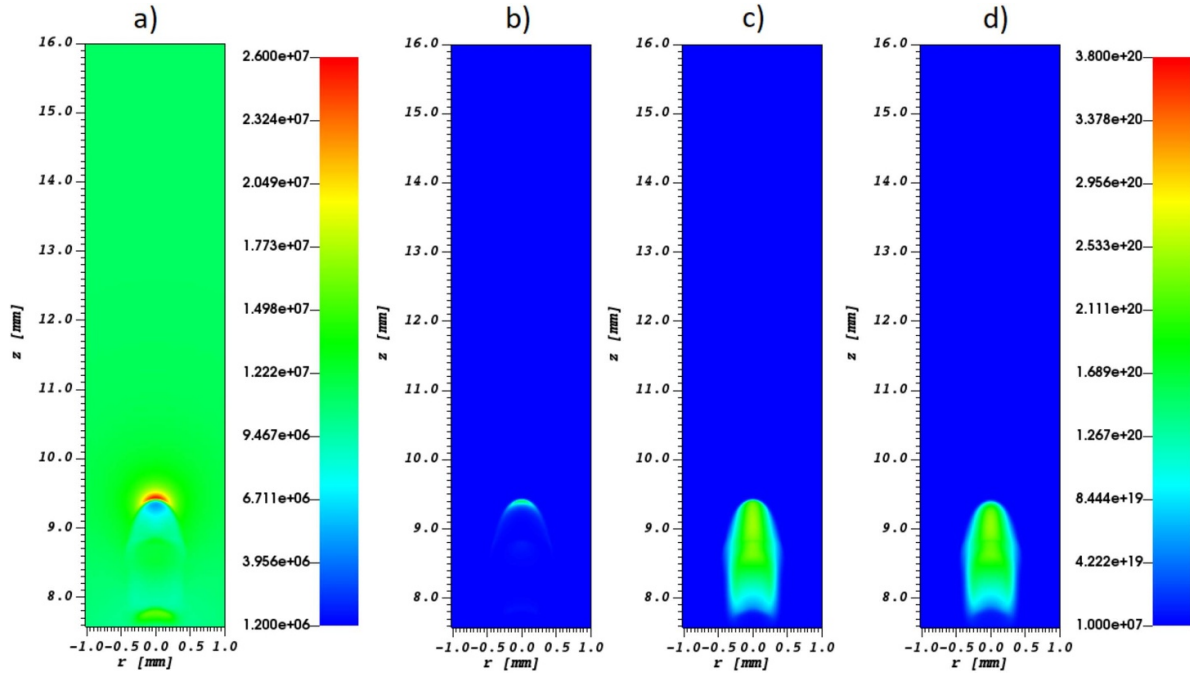


Figure 11. Test case 3, the 80% CO_2 – 20% $\text{C}_4\text{F}_7\text{N}$ mixture: (a) the electric field intensity in V m^{-1} , (b) the number density of electrons in m^{-3} , (c) the number density of positive ions in m^{-3} , (d) the number density of negative ions in m^{-3} , at 0.5 ns.

However, we have verified that this value produces simulation results that are practically the same as those obtained when using zero for this value. Specifically, when running our simulations without this artificial process of charge generation, we obtain exactly the same dynamic of the streamer front including the electric field enhancement, the number density of electrons and ions, as well as the streamer velocity. The only difference, when this additional process is not included, is that the number density of electrons in the streamer channel falls to values that are very close to zero, which we consider to be unrealistic. Photoionization is not explicitly included in this test case, due to the absence of data regarding photoionization in these mixtures in the literature. Moreover, it is expected that photoionization will be significantly weaker in these mixtures than in the N_2 – O_2 mixtures [73]. We show only the upper half of the domain in the remaining figures with 2D profiles for this test case, to make the relevant part of the domain more clearly visible.

In this test case, we have chosen the applied electric field that is about 90% of the critical field for the given mixture. The same choice of the applied electric field is employed by Guo and co-workers in their recent paper [73], as the field enhancement of negative streamers in these mixtures is not too high. The applied electric field is about $-7.57 \times 10^6 \text{ V m}^{-1}$, $-8.32 \times 10^6 \text{ V m}^{-1}$ and $-1.10 \times 10^7 \text{ V m}^{-1}$ for the 90% CO_2 – 10% $\text{C}_4\text{F}_7\text{N}$, 85% CO_2 – 15% $\text{C}_4\text{F}_7\text{N}$, and 80% CO_2 – 20% $\text{C}_4\text{F}_7\text{N}$ mixtures, respectively.

For the grid refinement procedure, we have used the following parameter values: $c_0 = 0.8$, $c_1 = 1.2$, $c_2 = 1.0 \text{ V}$. We have not used the explicit derefinement procedure in this case, as we wanted to obtain ion distributions with a higher resolution.

These simulations took around 6 h on 2 cores and 4 virtual threads of Intel i9-10900KF processor running at 3.70 GHz.

In figures 11(a)–(d) we show the number densities of electrons, positive ions, and negative ions, and the resulting electric field, respectively, for a negative streamer in the mixture with 80% CO_2 and 20 % $\text{C}_4\text{F}_7\text{N}$ at 0.5 ns. The corresponding profiles at 2.0 ns are shown in figures 12(a)–(d), respectively, while the corresponding profiles at 3.0 ns are shown in figures 13(a)–(d), respectively. The qualitative behavior of negative streamers in the remaining two mixtures is the same as the one observed in the 80% CO_2 – 20% $\text{C}_4\text{F}_7\text{N}$ mixture. This qualitative behavior is very similar to the one that is observed by Guo *et al* in their 3D PIC simulations in the point to plane geometry [73].

In both cases, negative streamers quickly form. Due to strong electron attachment, electron number density in the streamer channel falls to very low values, and the resulting electric field in the channel is restored to values that are very close to the applied electric field. The streamer head becomes practically isolated as it propagates. During this propagation, the maximum electric field at the streamer front and the maximum electron density are being reduced in time. Streamer velocity and streamer radius are also being reduced. The propagation of an isolated streamer head has been observed by Guo *et al*, and Francisco *et al* [73, 99]. The reduction of streamer velocity and radius in strongly attaching gases has been observed by Francisco *et al* [99]. In our simulations, the streamer disappears before crossing the gap between the initial condition and the domain boundary. For instance, at about 3.5 ns the electric field enhancement at the streamer front becomes lower than the electric field enhancement near the

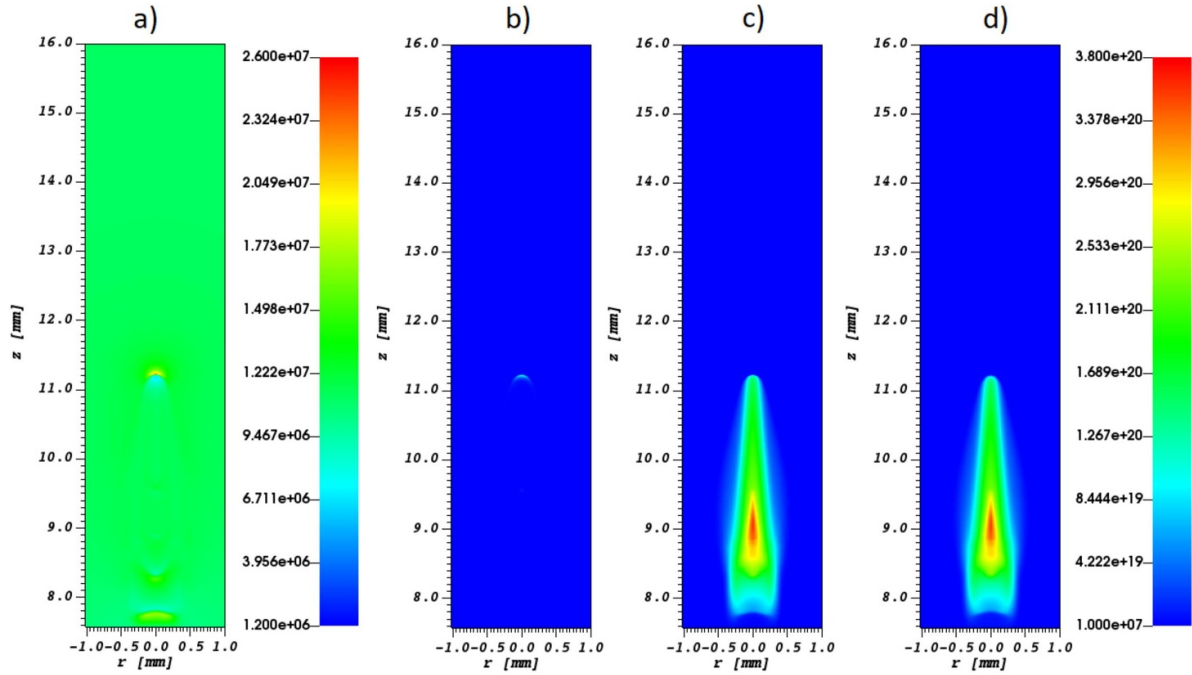


Figure 12. Test case 3, the 80% CO₂ – 20% C₄F₇N mixture: (a) the electric field intensity in V m⁻¹, (b) the number density of electrons in m⁻³, (c) the number density of positive ions in m⁻³, (d) the number density of negative ions in m⁻³, at 2.0 ns.

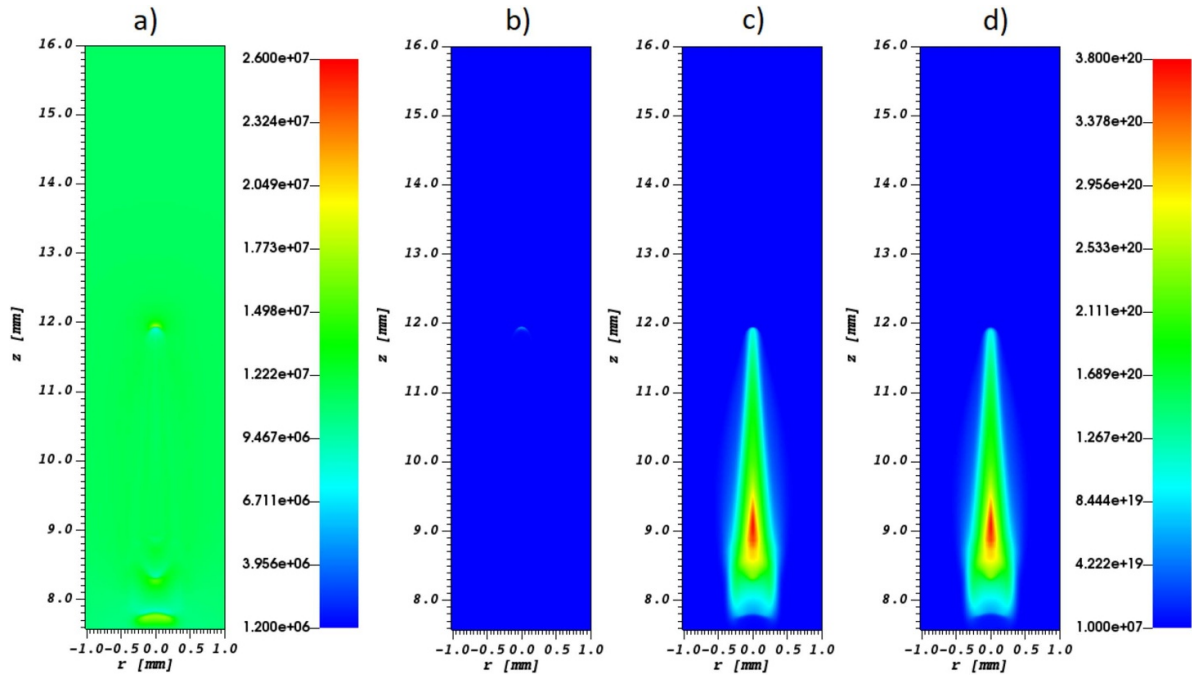


Figure 13. Test case 3, the 80% CO₂ – 20% C₄F₇N mixture: (a) the electric field intensity in V m⁻¹, (b) the number density of electrons in m⁻³, (c) the number density of positive ions in m⁻³, (d) the number density of negative ions in m⁻³, at 3.0 ns.

ion distribution around the initial condition. Then the maximum electric field remains constant at about 170 kV cm⁻¹ throughout the rest of the simulation. At 3.5 ns the maximum of the number density of electrons at the streamer front is about $4.36 \times 10^{19} \text{ m}^{-3}$. At 11 ns, the maximum of the number density of electrons in the entire domain is about $2.45 \times 10^{11} \text{ m}^{-3}$, which is much lower than the background density of electrons

and positive ions at the start of the simulation. It should be noted that the local maximum of the number density of electrons, which is a remnant of the streamer front, has not yet reached the upper domain boundary at this time. Interestingly, the value of this maximum is about 10^{20} m^{-3} during the first two nanoseconds of the simulation, which corresponds to the maximal electron density in the simulations performed by Guo

et al [73]. The same phenomenon of a reduction of the electric field enhancement at the streamer front with time and the reduction of the corresponding electron number density has been observed by Guo et al [73]. In their study as well, this reduction leads to disappearing of a negative streamer before it crosses the gap at the applied electric field that is about 90% of the critical field for the given mixture. Thus, the qualitative behavior of negative streamers in our axisymmetric fluid model is the same as the one in the 3D PIC simulations of Guo et al [73]. It should be noted, however, that streamer branching that was observed by Guo et al [73], cannot be replicated in an axisymmetric streamer model.

In figure 14 we show $L(t) - vt$ for all three mixtures on the left y axis. The relative difference between the sets of results that are obtained by using the Afivo-streamer code and our code is shown on the right y axis of the same figure. The relative difference is denoted as *rel diff*. It is calculated as the difference between the results of our AMReX based code and the results of the Afivo-streamer code, that is divided by the results of the Afivo-streamer code. In the test case 3, the streamer length is defined as $L(t) = z_{\max} - 0.8$ cm, where z_{\max} is the position of the maximum of the resulting electric field along the z axis. It can be seen from figure 14 that the agreement between the results of our code and the Afivo-streamer code is good. These results are shown only up to about 4.5 ns for the 90% CO₂ – 10% C₄F₇N mixture and only up to around 3.5 ns for the remaining two mixtures. This is done for the following reason. The streamer length in both codes is determined from the position of the electric field maximum. However, in these gases the number density of electrons at the streamer front and the corresponding electric field enhancement are quickly being reduced due to a very high rate for the electron attachment. The electric field enhancement at the streamer front becomes lower than the corresponding field enhancement near the ion distribution around the position of the initial condition at about 4.5 ns for the 90% CO₂ – 10% C₄F₇N mixture and at around 3.5 ns for the remaining two mixtures. Thus, at later times the streamer length cannot be determined in the standard way in any of the two codes.

In figure 15 we show the maximum electric field as a function of the streamer length for all three mixtures on the left y axis. The relative difference between the sets of results that are obtained by using the Afivo-streamer code and our code is shown on the right y axis of the same figure. The relative difference is denoted as *rel diff*, and it is calculated in the equivalent way as in the previous figure. The agreement between these two sets of values, that are obtained by the two simulation codes, is very good. In all three mixtures, the electric field quickly rises to the maximal value, and then it rapidly decreases as the streamer propagates.

In figure 16 we show the streamer velocity as a function of the streamer length in all three mixtures. The streamer velocity is calculated at every 0.025 ns by dividing the change of position of the electric field maximum along the z -axis by this time interval. The agreement between the values of the streamer velocity that are obtained by employing these two

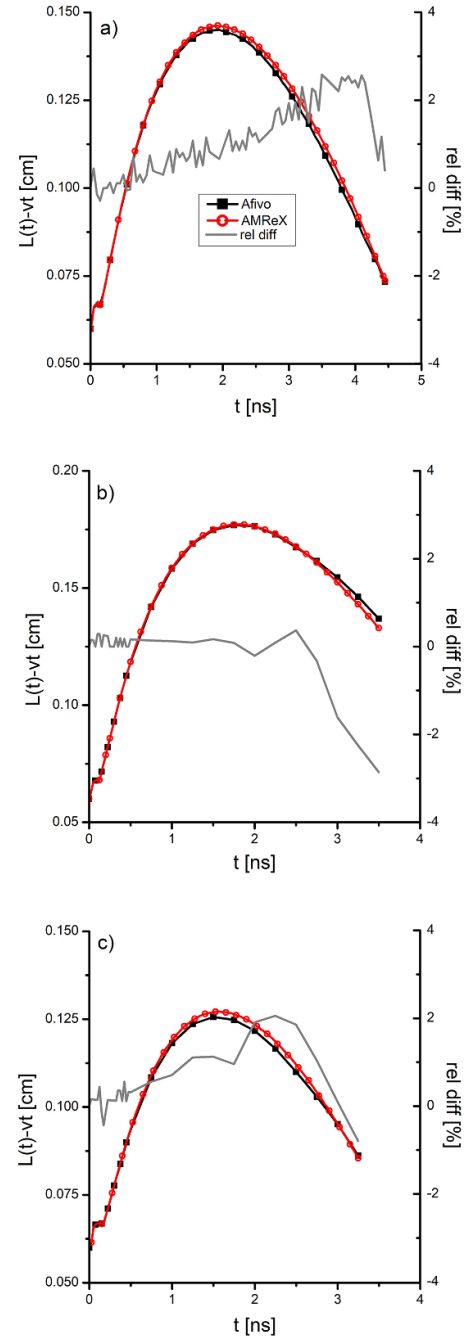


Figure 14. Test case 3: Left y axis: $L(t) - vt$ as a function of time for a negative streamer in (a) 90% CO₂ – 10% C₄F₇N, (b) 85% CO₂ – 15% C₄F₇N and (c) 80% CO₂ – 20% C₄F₇N. Where $v = 10^6 \text{ m s}^{-1}$. Right y axis: the relative difference between the results that are obtained by employing the two compared simulation codes.

simulation codes is good. In all three mixtures the streamer velocity quickly reaches a global maximum, and then rapidly decreases reaching a local minimum. After reaching a local minimum, it quickly rises again, reaching a local maximum. For higher values of the streamer length, the streamer velocity gradually decreases as the streamer propagates.

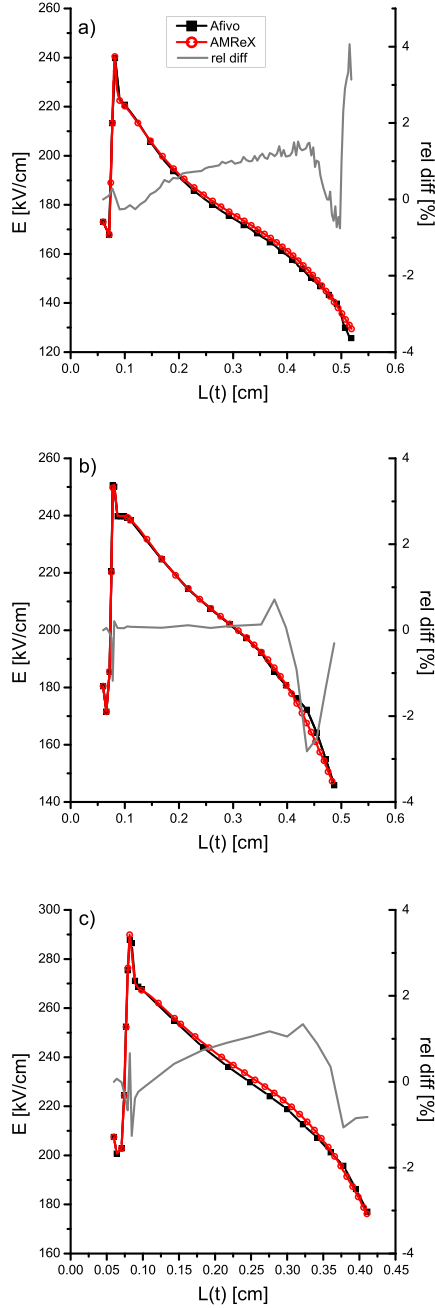


Figure 15. Test case 3: Left y axis: electric field maximum as a function of $L(t)$ for a negative streamer in (a) 90% CO_2 – 10% $\text{C}_4\text{F}_7\text{N}$, (b) 85% CO_2 – 15% $\text{C}_4\text{F}_7\text{N}$ and (c) 80% CO_2 – 20% $\text{C}_4\text{F}_7\text{N}$. Right y axis: the relative difference between the results that are obtained by employing the two compared simulation codes.

5. Conclusion

We have implemented an axisymmetric streamer model in the AMReX open-source library. Our model is based on the first-order fluid model. The spatial dependence of the transport coefficients is represented by the local field approximation. Photoionization is implemented by employing the Zhelenznyi's model. The Zhelenznyi's photoionization integral is approximated by using the Helmholtz approach. We have used the three term Bourdon parametrization of the

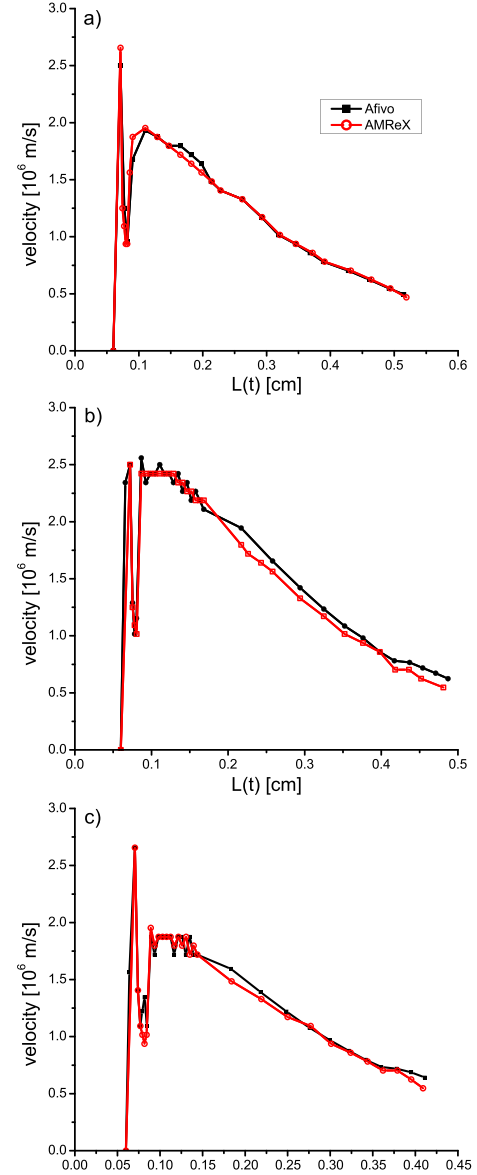


Figure 16. Test case 3: streamer velocity as a function of $L(t)$ for a negative streamer in (a) 90% CO_2 – 10% $\text{C}_4\text{F}_7\text{N}$, (b) 85% CO_2 – 15% $\text{C}_4\text{F}_7\text{N}$ and (c) 80% CO_2 – 20% $\text{C}_4\text{F}_7\text{N}$.

absorption function in the photoionization integral. In this paper, we give a detailed description of the implementation of our code which can be easily replicated by other researchers. We have verified our code in the standard simulation conditions by comparing our results for positive streamers in air to those from the Bagheri *et al* benchmarks [23]. Our results are in a very good agreement with those of other groups. In the test case 1, our results for all the calculated quantities are in the best agreement with those from the CWI and FR groups. In the test case 2, our results for $L(t) - vt$ are between those of the DE group and those of the CWI group. Our values of the streamer radius in this test case are in the best agreement with the ES group. For all the other quantities in this test case, our results are in the best agreement with those from CWI and DE groups.

The performance of our code in strongly attaching gases is verified by comparing our results for negative streamers in the mixtures of CO₂ and C₄F₇N with those simulated by the Afivo-streamer code. Our results for negative streamers in these mixtures are in an excellent agreement with those of the Afivo streamer code for $L(t) - vt$, maximal electric field and the streamer velocity. The qualitative behavior of negative streamers, that is observed in our simulations, is very similar to the one previously observed in these mixtures by employing fully 3D particle-in-cell simulations. In both cases, the number density of electrons in the streamer channel falls to very low values, leaving an isolated streamer head which propagates forward, while the resulting electric field intensity behind the streamer head returns to values that are very close to the applied electric field. The streamer head becomes narrower as it propagates and the number density of electrons in the streamer head is being reduced. This ultimately leads to the streamer disappearing before it crosses the gap between the two domain boundaries.

Data availability statement

All data that support the findings of this study are included within the article (and any supplementary files).

Acknowledgements

This work is supported by the Institute of Physics Belgrade and the Science Fund of the Republic of Serbia, Grant No. 7749560, Exploring ultra-low global warming potential gases for insulation in high-voltage technology: Experiments and modelling (EGWIn). IS is deeply grateful to Miloš Blagojević for his support and many useful discussions.

Author contribution statement

IS, DB, and SD have been involved in the research and in the preparation of the manuscript. JT read and commented on the manuscript, helped to diagnose discrepancies between the codes, and wrote the Afivo-streamer source code that served as inspiration for the present code. All the authors have read and approved the final manuscript.

ORCID iDs

I Simonović  <https://orcid.org/0000-0001-6704-9042>
 D Bošnjaković  <https://orcid.org/0000-0002-2725-5287>
 J Teunissen  <https://orcid.org/0000-0003-0811-5091>
 S Dujko  <https://orcid.org/0000-0002-4544-9106>

References

- [1] Ebert U, Montijn C, Briels T M P, Hundsdorfer W, Meulenbroek B, Rocco A and van Veldhuizen E M 2006 *Plasma Sources Sci. Technol.* **15** S118
- [2] Naidis G V 2009 *Phys. Rev. E* **79** 057401
- [3] Nijdam S, Teunissen J and Ebert U 2020 *Plasma Sources Sci. Technol.* **29** 103001
- [4] Babaeva N Y and Naidis G V 2021 *J. Phys. D: Appl. Phys.* **54** 223002
- [5] Babaeva N Y and Naidis G V 2001 *J. Electrostat.* **53** 123
- [6] Luque A, Ratushnaya V and Ebert U 2008 *J. Phys. D: Appl. Phys.* **41** 234005
- [7] Qin J and Pasko V P 2014 *J. Phys. D: Appl. Phys.* **47** 435202
- [8] Qin J, Celestin S and Pasko V P 2012 *Geophys. Res. Lett.* **39** L22803
- [9] Luque A and Ebert U 2009 *Nat. Geosci.* **2** 757
- [10] Pasko V P, Qin J and Celestin S 2013 *Surv. Geophys.* **34** 797
- [11] Morrow R and Blackburn T R 2002 *J. Phys. D: Appl. Phys.* **35** L69
- [12] Ebert U and Sentman D D 2008 *J. Phys. D: Appl. Phys.* **41** 230301
- [13] Sadighi S, Liu N, Dwyer J R and Rassoul H K 2015 *J. Geophys. Res. D* **120** 3660
- [14] Köhn C, Heumesser M, Chanrion O, Nishikawa K, Reglero V and Neubert T 2020 *Geophys. Res. Lett.* **47** 2020GL089749
- [15] Czichy M, Hartmann T, Mentel J and Awakowicz P 2008 *J. Phys. D: Appl. Phys.* **41** 144027
- [16] Foster J E 2017 *Phys. Plasmas* **24** 055501
- [17] Fudamoto T, Namihira T, Katsuki S, Akiyama H, Imakubo T and Majima T 2008 *Electr. Eng. Japan* **164** 1
- [18] Babaeva N Y, Ning N, Graves D B and Kushner M J 2012 *J. Phys. D: Appl. Phys.* **45** 115203
- [19] Gandhi R, Chandrasekar S and Nagarajan C 2018 *J. Electr. Eng. Technol.* **13** 1663
- [20] Faizol Z, Zubir F, Saman N M, Ahmad M H, Rahim M K A, Ayop O, Jusoh M, Majid H A and Yusoff Z 2023 *Appl. Sci.* **13** 9605
- [21] Fonte P 1996 *IEEE Trans. Nucl. Sci.* **43** 2135
- [22] Bošnjaković D, Petrović Z L and Dujko S 2016 *J. Phys. D: Appl. Phys.* **49** 405201
- [23] Bagheri B et al 2018 *Plasma Sources Sci. Technol.* **27** 095002
- [24] Dujko S, Markosyan A H, White R D and Ebert U 2013 *J. Phys. D: Appl. Phys.* **46** 475202
- [25] Markosyan A H, Dujko S and Ebert U 2013 *J. Phys. D: Appl. Phys.* **46** 475203
- [26] Ducasse O, Eichwald O and Yousfi M 2012 Finite volume method for streamer and gas dynamics modelling in air discharges at atmospheric pressure *Finite Volume Method: Powerful Means of Engineering Design* p 283
- [27] Zhuang C, Zeng R, Zhang B and He J 2014 *IEEE Trans. Magn.* **50** 325
- [28] Georgioud G E, Morrow R and Metaxas A C 1999 *J. Phys. D: Appl. Phys.* **32** 1370
- [29] Koren B 1993 *A Robust Upwind Discretization Method for Advection, Diffusion and Source Terms* vol 45 (Centrum voor Wiskunde en Informatica) pp 117–38
- [30] Teunissen J and Ebert U 2017 *J. Phys. D: Appl. Phys.* **50** 474001
- [31] Montijn C, Hundsdorfer W and Ebert U 2006 *J. Comput. Phys.* **219** 801
- [32] Ducasse O, Eichwald O and Yousfi M 2010 *Adv. Appl. Fluid Mech.* **8** 1 (available at: <https://www.pphmj.com/abstract/5245.htm>)
- [33] Eichwald O, Bensaad H, Ducasse O and Yousfi M 2012 *J. Phys. D: Appl. Phys.* **45** 385203
- [34] Min W-G, Kim H-S, Lee S-H and Hahn S-Y 2000 *IEEE Trans. Magn.* **36** 1280
- [35] Velasco J, Frascella R, Albarracín R, Burgos J C, Dong M, Ren M and Yang L 2018 *Energies* **11** 361
- [36] Bhatt M and Bhatt P 2022 *Int. J. Eng. Technol. Innovat.* **12** 29
- [37] Ducasse O, Papageorgiou L, Eichwald O, Spyrou N and Yousfi M 2007 *IEEE Trans. Plasma Sci.* **35** 1287

- [38] Levko D, Pachuiilo M and Raja L L 2017 *J. Phys. D: Appl. Phys.* **50** 354004
- [39] Rose D V, Welch D R, Clark R E, Thoma C, Zimmerman W R, Bruner N, Rambo P K and Atherton B W 2011 *Phys. Plasmas* **18** 093501
- [40] Wang D, Wang L and Zheng Y 2018 *J. Appl. Phys.* **124** 203301
- [41] Li C, Ebert U and Hundsdorfer W 2009 *J. Phys. D: Appl. Phys.* **42** 202003
- [42] Li C, Ebert U and Hundsdorfer W 2012 *J. Comput. Phys.* **231** 1020
- [43] Li C, Teunissen J, Nool M, Hundsdorfer W and Ebert U 2012 *Plasma Sources Sci. Technol.* **21** 055019
- [44] (Available at: <https://github.com/MD-CWI/afivo-streamer>)
- [45] Teunissen J and Ebert U 2016 *Plasma Sources Sci. Technol.* **25** 044005
- [46] (Available at: <https://commons.lbl.gov/display/chombo/Chombo++Software+for+Adaptive+Solutions+of+Partial+Differential+Equations>)
- [47] Colella P, Graves D T, Ligocki T J, Miller G H, Modiano D, Schwartz P O, Van Straalen B, Pillod J, Trebotich D, and Barad M 2000 EBChombo software package for cartesian grid, embedded boundary applications *Technical Report LBNL-6615E* (Lawrence Berkeley National Laboratory)
- [48] Marskar R 2019 *J. Comput. Phys.* **388** 624
- [49] Marskar R 2020 *Plasma Sources Sci. Technol.* **29** 055007
- [50] Marskar R 2023 chombo-discharge: An AMR code for gas discharge simulations in complex geometries *J. Open Source Softw.* **8** 5335
- [51] FEniCS project team 2019 FEniCS project (available at: <https://fenicsproject.org>)
- [52] Logg A, Mardal K A and Wells G 2012 *Automated Solution of Differential Equations by the Finite Element Method: The Fenics Book* (Springer)
- [53] Jovanović A P, Loffhagen D and Becker M M 2023 *Plasma Sources Sci. Technol.* **32** 044003
- [54] Niknezhad M, Chanrion O, Köhn C, Holbøll J and Neubert T 2021 *Plasma Sour. Sci. Technol.* **30** 045012
- [55] (Available at: <https://github.com/AMReX-Codes/amrex>)
- [56] Zhang W et al 2019 *J. Open Source Softw.* **4** 1370
- [57] Sverdrup K, Almgren A and Nikiforakis N 2019 *Phys. Fluids* **31** 093102
- [58] Giuliani A, Almgren A S, Bell J B, Berger M J, de Frahan M T H and Rangarajan D 2022 *J. Comput. Phys.* **464** 111305
- [59] Natarajan M, Grout R, Zhang W and Day M 2022 *J. Comput. Phys.* **465** 111315
- [60] Kambara M, Kawaguchi S, Lee H J, Ikuse K, Hamaguchi S, Ohmori T and Ishikawa K 2023 *Jpn. J. Appl. Phys.* **62** SA0803
- [61] Vay J-L et al 2018 *Nucl. Instrum. Methods Phys. Res. A* **909** 476
- [62] Myers A et al 2021 *Parallel Comput.* **108** 102833
- [63] Vay J-L et al 2021 *Phys. Plasmas* **28** 023105
- [64] Almgren A, Sazo M B, Bell J, Harpole A, Katz M, Sexton J, Willcox D, Zhang W and Zingale M 2020 *J. Open Source Softw.* **5** 2513
- [65] Henry de Frahan M T et al 2023 *Int. J. High Perform. Comput. Appl.* **37** 115
- [66] von der Linden J et al 2021 *Commun. Earth Environ.* **2** 195
- [67] Deak N E, Duarte A J, Esclapez L, Day M and Bisetti F 2023 *AIAA SCITECH Forum* p 2385
- [68] Duarte A J, Bisetti F, Deak N, Esclapez L and Day M 2024 *AIAA SCITECH Forum* p 1820
- [69] von der Linden J, Cimarelli C, Gaudin D, Sears J, Kuhl A, Grote D, Converse M, Kueny C and Poole B 2019 Investigating the relationship between volcanic eruption parameters and radio-frequency emission with a multiphysics simulation *Geophysical Research Abstracts* vol 21 (Copernicus Publications)
- [70] Simonović I, Bošnjaković D and Dujko S 2023 *Book of Abstracts, ICPiG: 35th Int. Conf. on Phenomena in Ionized Gases* (Egmond aan Zee, The Netherlands, 9–15 July) p 235
- [71] Simonović I, Bošnjaković D and Dujko S 2023 *Book of Abstracts and Contributed Papers, V Meeting on Astrophysical Spectroscopy - A&M DATA - Astronomy & Earth Observations* (Palić, Serbia, 12–15 September) p 29
- [72] Tian S, Zhang X, Cressault Y, Hu J, Wang B, Xiao S, Li Y and Kabbaj N 2020 *AIP Adv.* **10** 050702
- [73] Guo B, Ebert U and Teunissen J 2023 *Plasma Sources Sci. Technol.* **32** 115001
- [74] Xiao D 2016 *Gas Discharge and Gas Insulation* (Shanghai Jiao Tong University Press and Springer)
- [75] Earle S 2021 *A Brief History of the Earth's Climate: Everyone's Guide to the Science of Climate Change* (New Society Publishers)
- [76] Alfred A K 2021 *How to Avoid a Climate Disaster: the Solutions we Have and the Breakthroughs we Need* (Vintage)
- [77] Li Y, Zhang X, Xiao S, Chen Q, Tang J, Chen D and Wang D 2018 *Ind. Eng. Chem. Res.* **57** 5173
- [78] Chachereau A, Hösl A and Franck C M 2018 *J. Phys. D: Appl. Phys.* **51** 495201
- [79] Kulikovskiy A A 1997 *J. Phys. D: Appl. Phys.* **30** 441
- [80] Bourdon A, Bonaventura Z and Celestin S 2010 *Plasma Sources Sci. Technol.* **19** 034012
- [81] Celestin S, Bonaventura Z, Zeghondy B, Bourdon A and Ségur P 2009 *J. Phys. D: Appl. Phys.* **42** 065203
- [82] Celestin S, Bonaventura Z, Guaitella O, Rousseau A and Bourdon A 2009 *Eur. Phys. J. Appl. Phys.* **47** 22810
- [83] Luque A, Ebert U, Montijn C and Hundsdorfer W 2007 *Appl. Phys. Lett.* **90** 081501
- [84] Bourdon A, Pasko V P, Liu N Y, Célestin S, Ségur P and Marode E 2007 *Plasma Sources Sci. Technol.* **16** 656
- [85] Zhelezniak M, Mnatsakanian A and Szykh S 1982 *High Temp.* **20** 357 (available at: <https://ui.adsabs.harvard.edu/abs/1982HTemS..20..357Z/abstract>)
- [86] Teunissen J 2015 3D simulations and analysis of pulsed discharges PhD Thesis Technische Universiteit Eindhoven (available at: <http://repository.tue.nl/801516>)
- [87] Butcher J C and Wanner G 1996 *Appl. Numer. Math.* **22** 113
- [88] Wesseling P and Oosterlee C W 2001 *J. Comput. Appl. Math.* **128** 311
- [89] Luque A and Ebert U 2012 *J. Comput. Phys.* **231** 904
- [90] The plasma module user's guide, Comsol Multiphysics, p 207
- [91] van Dijk J, Peerenboom K, Jimenez M, Mihailova D and van der Mullen J 2009 *J. Phys. D: Appl. Phys.* **42** 194012
- [92] Becker M M, Kählert H, Sun A, Bonitz M and Loffhagen D 2017 *Plasma Sources Sci. Technol.* **26** 044001
- [93] Becker M M, Hoder T, Brandenburg R and Loffhagen D 2013 *J. Phys. D: Appl. Phys.* **46** 355203
- [94] Dujko S, White R D, Petrović Z L and Robson R E 2010 *Phys. Rev. E* **81** 046403
- [95] Mirić J, Bošnjaković D, Simonović I, Petrović Z L and Dujko S 2016 *Plasma Sources Sci. Technol.* **25** 065010
- [96] Zhang B, Hao M, Yao Y, Xiong J, Li X, Murphy A B, Sinha N, Antony B and Ambalampitiya H B 2023 *J. Appl. Phys.* **56** 134001
- [97] XJTUAETLab database (C₄F₇N) (available at: www.lxcat.net)
- [98] Biagi database (CO₂) (available at: www.lxcat.net)
- [99] Francisco H, Bagheri B and Ebert U 2021 *Plasma Sources Sci. Technol.* **30** 025006



**31st Summer School and
International Symposium on
the Physics of Ionized Gases**

Belgrade, Serbia,
September 5 - 9, 2022

CONTRIBUTED PAPERS
&
**ABSTRACTS of INVITED LECTURES,
TOPICAL INVITED LECTURES and PROGRESS REPORTS**

Editors:
Dragana Ilić, Vladimir Srećković,
Bratislav Obradović and Jovan Cvetic



**БЕОГРАД
2022**

**31st Summer School and
International Symposium on
the Physics of Ionized Gases**



September 5 – 9, 2022, Belgrade, Serbia

S P I G 2022

CONTRIBUTED PAPERS

&

ABSTRACTS OF INVITED LECTURES,
TOPICAL INVITED LECTURES AND
PROGRESS REPORTS

Editors

Dragana Ilić, Vladimir Srećković,
Bratislav Obradović and Jovan Cvetić

University of Belgrade –
School of Electrical
Engineering

University of Belgrade –
Faculty of Physics
Serbian Academy of
Sciences and Arts

Belgrade, 2022

PUBLICATIONS OF THE ASTRONOMICAL OBSERVATORY OF BELGRADE

FOUNDED IN 1947

EDITORIAL BOARD:

Dr. Srdjan SAMUROVIĆ, Editor-in-Chief (Astronomical Observatory, Belgrade)

Dr. Rade PAVLOVIĆ (Astronomical Observatory, Belgrade)

Dr. Miroslav MIČIĆ (Astronomical Observatory, Belgrade)

Dr. Branislav VUKOTIĆ (Astronomical Observatory, Belgrade)

All papers in this Publication are peer reviewed.

Published and copyright © by Astronomical Observatory, Volgina 7, 11060 Belgrade 38, Serbia

Director of the Astronomical Observatory: Dr. Gojko Djurašević

Typesetting: Tatjana Milovanov

Internet address <http://www.aob.rs>

ISSN 0373-3742

ISBN 978-86-82296-02-7

Number of copies / tiraž : 200

Production: Skripta Internacional, Mike Alasa 54, Beograd

CIP - Каталогизација у публикацији - Народна библиотека Србије, Београд

537.56(082)

539.186.2(082)

539.121.7(082)

533.9(082)

SUMMER School and International Symposium on the Physics of Ionized Gases (31 ; 2022 ; Belgrade)

Contributed papers & abstracts of invited lectures, topical invited lectures and progress reports / 31st Summer School and International Symposium on the Physics of Ionized Gases - SPIG 2022, September 5-9, 2022, Belgrade, Serbia ; editors Dragana Ilić ... [et al.]. - Belgrade : Astronomical Observatory, 2022 (Beograd : Skripta Internacional). - 302 str. : ilustr. ; 24 cm. - (Publications of the Astronomical Observatory of Belgrade, ISSN 0373-3742)

Na nasl. str.: University of Belgrade, School of Electrical Engineering; University of Belgrade, Faculty of Physics; Serbian Academy of Sciences and Arts. - Tiraž 200. - Str. 17-18: Preface / editors Dragana Ilić ... [et al.]. - Bibliografija uz svaki rad. - Registar.

ISBN 978-86-82296-02-7

1. Ilić, Dragana, 1978- [urednik] [аутор додатног текста]

а) Јонизовани гасови – Зборници б) Атоми – Интеракција – Зборници в) Плазма – Зборници

COBISS.SR-ID 72751881

SPIG 2022

SCIENTIFIC COMMITTEE

D. Ilić (Co-chair), Serbia
V. Srećković (Co-chair), Serbia

A. Antoniou, Greece
D. Borka, Serbia
J. Burgdörfer, Austria
J. Cvetić, Serbia
V. Guerra, Portugal
M. Ivković, Serbia
K. Kutasi, Hungary
I. Mančev, Serbia
D. Marić, Serbia
N. J. Mason, UK
A. Milosavljević, France
V. Milosavljević, Serbia
K. Mima, Japan
Z. Mišković, Canada
L. Nahon, France
B. Obradović, Serbia
G. Poparić, Serbia
P. Roncin, France
I. Savić, Serbia
Y. Serruys, France
N. Simonović, Serbia
M. Škorić, Japan
M. Trtica, Serbia
S. Tošić, Serbia
R. White, Australia

ADVISORY COMMITTEE

D. Belić
N. Bibić
M. S. Dimitrijević
S. Đurović
N. Konjević
M. M. Kuraica
J. Labat
G. Malović
B. P. Marinković
Z. Mijatović
M. Milosavljević
Z. Lj. Petrović
L. Č. Popović
J. Purić
B. Stanić

ORGANIZING COMMITTEE

J. Cvetić (Co-chair)
B. Obradović (Co-chair)

M. Ignjatović (Co-secretary)
L. Gavanski (Co-secretary)

N. Konjević
N. Cvetanović
T. Gajo
I. Krstić
N. Sakan

FORMATION AND PROPAGATION OF STREAMERS IN $\text{CF}_3\text{I-SF}_6$ GAS MIXTURES

J. ATIĆ¹, D. BOŠNJAKOVIĆ¹, I. SIMONOVIĆ¹,
Z. Lj. PETROVIĆ² and S. DUJKO¹

¹*Institute of Physics Belgrade, University of Belgrade, Pregrevica 118,
11080 Belgrade, Serbia*

E-mail sasa.dujko@ipb.ac.rs

²*Serbian Academy of Science and Arts, Knez Mihailova 35, 11000 Belgrade, Serbia*

Abstract. The formation and propagation of streamers in $\text{CF}_3\text{I-SF}_6$ mixtures are studied by the classical fluid model in 1D and 1.5D configurations. We calculate the electron density, electric field, and velocity of streamers as a function of the applied reduced electric fields for various $\text{CF}_3\text{I-SF}_6$ mixtures. We found that the transition of an electron avalanche into a negative streamer occurs more slowly with an increasing fraction of CF_3I in the mixture.

1. INTRODUCTION

In high voltage technology, strong electronegative gases are used to prevent the electrical breakdown in power transmission and distribution systems. SF_6 is widely used in these applications because of its extraordinary dielectric characteristics (primarily, high critical electric field and low boiling point). However, SF_6 is a very powerful greenhouse gas with an extremely high global warming potential (22800 on a 100-year horizon) and a very long atmospheric lifetime (3200 years). Research on alternative gases is therefore one of the main activities of researchers worldwide.

The first step in this effort involves reducing the SF_6 concentration using gas mixtures. CF_3I , one of the most promising candidates for replacement of SF_6 , is also a strong electronegative gas. Its critical electric field is higher than that of SF_6 and it has a very short atmospheric lifetime (shorter than 2 days), as well as negligible global warming potential (lower than the referent gas CO_2). However, in comparison with SF_6 , its boiling point is not sufficiently low. Using these CF_3I characteristics as motivation factors, we investigated the formation and propagation of negative streamers in $\text{CF}_3\text{I-SF}_6$ mixtures.

2. METHODS OF CALCULATIONS

The transition from an avalanche to a streamer, and the propagation of streamers were considered by a numerical model based on fluid equations. We use the classical fluid model where the equation of continuity is combined with the drift-diffusion approximation. The resulting equation is coupled to the Poisson equation for space charge electric field calculations. The corresponding system of partial differential equations is solved numerically assuming the local field approximation (Bošnjaković et al. 2016). The calculations are carried out in the 1D and 1.5D configurations where the fixed value of the streamer radius is incorporated into the axial symmetrical model. The streamer velocities are calculated from the modeling performed in 1D and by using the analytical expression (Li et al. 2007) which requires knowledge of electron mobility, longitudinal diffusion coefficient and ionization coefficient as a function of the reduced electric field. The cross-section sets for electron scattering in CF_3I and SF_6 were developed in our laboratory (Mirić et al. 2016), and by Itoh and co-workers (Itoh et al. 1993) respectively.

3. RESULTS AND DISCUSSION

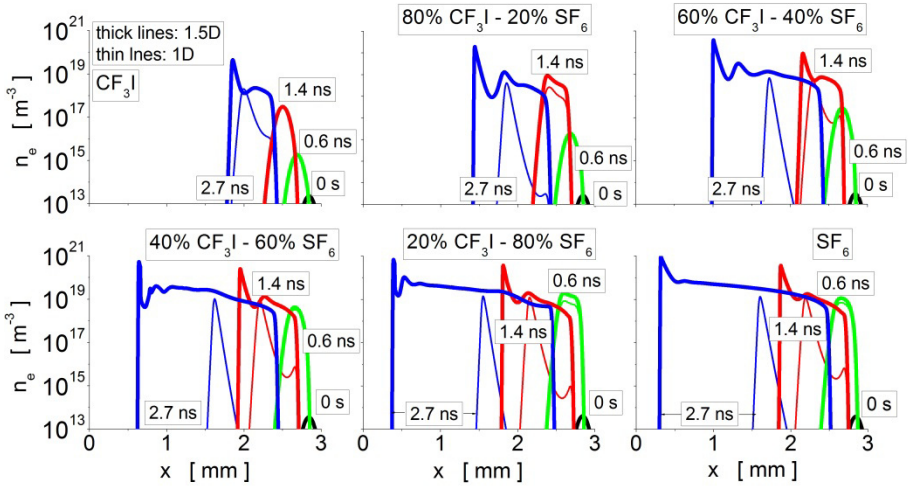


Figure 1: Electron density during streamer formation and propagation in CF_3I - SF_6 mixtures for $E_0/n_0 = 480 \text{ Td}$.

Figure 1 shows the electron density during streamer formation and propagation in CF_3I - SF_6 mixtures. The results are obtained from the classical 1D and 1.5D fluid models in which the input data are electron bulk transport coefficients calculated by Monte Carlo simulations. The external electric field is 480 Td, which is larger than the critical electrical fields of the two gases. This requirement permits the development of streamers. Comparing the results in two different configurations

for the fixed mixture shows that the electron density is higher in the 1.5D model. The results in the same configuration show that the development of streamers is slower with the decrease of SF₆ in mixture. This behavior is expected based on a greater critical electric field of CF₃I (437 Td) than SF₆ (361 Td). This is one of the indicators that CF₃I is better dielectric than SF₆ because of its capacity to prevent the development of streamers at higher electric fields.

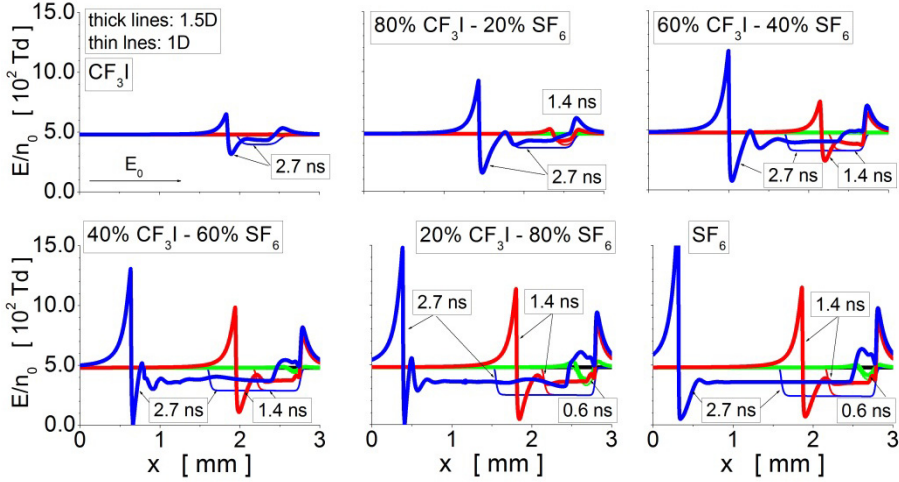


Figure 2: Electric field during streamer formation and propagation in CF₃I-SF₆ mixtures for $E_0/n_0 = 480$ Td. The calculation is performed using the 1.5D and 1D setups and balk transport coefficients as input to the classical fluid model.

Figure 2 shows the temporal development of the electrical field of the streamers in the CF₃I-SF₆ mixtures according to the same conditions as in Figure 1. The results of the 1.5D configuration show that the electric field in the streamer channel is equal to the critical electric field of the studied gas mixture. Field amplification in the region ahead of the streamer front starts from 40 % (pure CF₃I) up to 200 % (pure SF₆). By comparing the 1D and 1.5D configurations, we observe that the electrical field in the streamer channel descends to the lower level in the 1.5D configuration. In the 1D configuration, the electrical field in the region ahead of the streamer front is equal to the external field, independently of the gas mixture.

Figure 3 shows the streamer velocity and drift velocity of the electrons for various CF₃I-SF₆ mixtures. As the development of streamers is possible in electrical fields above the critical electrical field, the streamer velocity of gas mixtures can be calculated by the fluid model (left panel) starting from different electrical fields. The increase in streamer velocity with increasing concentration of SF₆ is a consequence of the evolution of streamers (Figures 1 and 2). Although it seems unexpected, the streamer velocity in the pure SF₆ is lower than that in the mixture 20% CF₃I - 80% SF₆ because of the behavior of the drift velocity of

electrons (right panel). The comparison of these two sets of results shows that the streamer velocity is higher than the drift velocity of electrons regardless of the gas mixture and the electric field. This follows from the fact that the streamer velocity is a combination of the electron drift velocity, the velocity induced by the strong diffusive flux at the streamer front and the creation of the electrons by electron-impact ionization. A comparison of the streamer velocities computed from the fluid model (left panel) and the analytical expression (middle panel) shows that these two sets of results differ from each other. This figure clearly illustrates the limits of the analytical formula that is often used for calculating streamer velocity.

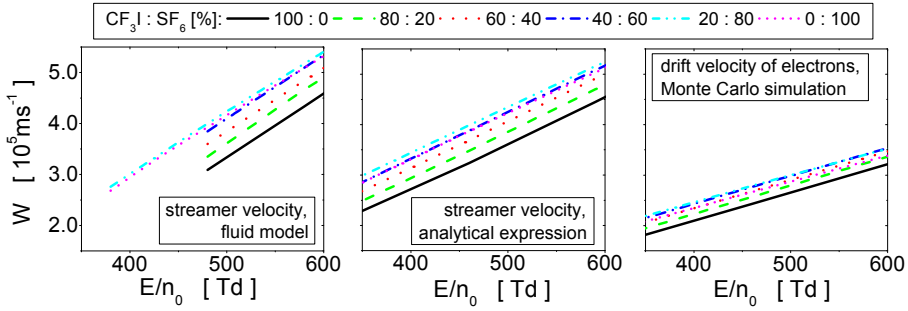


Figure 3: Streamer velocity calculated by the fluid model (left panel) and analytical expression (middle panel) and the drift velocity of electrons (right panel). Results in the CF_3I - SF_6 mixtures are given as a function of the reduced electric field.

Acknowledgment

This research was supported by the Institute of Physics Belgrade, and the Science Fund of the Republic of Serbia [Grant No. 7749560, EGWIn].

References

- Bošnjaković, D., Petrović, Z.Lj., Dujko, S.: 2016, *J. Phys. D: Appl. Phys.* **49**, 405201.
- Li, C., Brok, W.J.M., Ebert, U., van der Mullen, J.J.A.M.J.: 2007, *Appl. Phys.* **101**, 123305.
- Mirić, J., Bošnjaković, D., Simonović, I., Petrović Z.Lj., Dujko, S.: 2016, *Plasma Source Sci. Technol.* **25**, 065010.
- Itoh, H., Matsumura, T., Satoh, K., Date, H., Nakano, Y., Tagashira, H.: 1993, *J. Phys. D: Appl. Phys.* **26**, 1975.

THIRD-ORDER TRANSPORT COEFFICIENTS FOR ELECTRONS IN C₃F₈

I. SIMONOVIĆ¹, D. BOŠNJAKOVIĆ¹, Z. LJ. PETROVIĆ², and S. DUJKO¹

¹*Institute of Physics Belgrade, Pregrevica 118, 11080 Belgrade, Serbia*

²*Serbian Academy of Sciences and Arts, Knez Mihailova 35, 11000 Belgrade, Serbia*

Abstract. Monte Carlo simulations and multi term method for solving the Boltzmann equation are used to calculate the third-order transport coefficients for electrons in C₃F₈. The influence of elastic, inelastic and non-conservative collisions of electrons with molecules of the background gas on the individual components of the third-order transport tensor is investigated. The differences between flux and bulk values of the third-order transport coefficients are analyzed. The concurrence of the third-order transport tensor with diffusion is observed and studied.

1. INTRODUCTION

The investigation of electron transport in gases under the influence of an electric field is important for many technological applications. These applications are often modelled assuming hydrodynamic conditions in which the flux of electrons is represented in terms of drift velocity and the diffusion tensor, as higher-order transport coefficients have been systematically ignored in the traditional interpretation of swarm experiments. However, the longitudinal third-order transport coefficient has been recently measured from the arrival-time spectra of an electron swarm by Kawaguchi et al. (see Kawaguchi et al. 2021). It has been shown by Kawaguchi and coworkers that third-order and higher-order transport coefficients should be considered to obtain the longitudinal diffusion coefficient properly in the arrival-time spectra experiment at moderate and high reduced electric fields. Third-order transport coefficients are also necessary for the conversion of the hydrodynamic transport coefficients into transport data that is measured in the steady-state Townsend experiment (see Dujko et al. 2008.). If third-order transport coefficients were both calculated and measured with a sufficient precision, they would be very useful in the swarm procedure for determining the complete sets of cross sections, due to the high sensitivity of these transport coefficients to the energy dependence of cross sections for individual scattering processes (Vrhovac et al. 1999). In this work we investigate the third-order transport coefficients for electrons in C₃F₈ by employing Monte Carlo simulations and the multi term method for solving the Boltzmann equation. In section 2 we give a brief description of the methodology that is used in this work. Results and discussion are presented in section 3.

2. THEORETICAL METHODS

In our Monte Carlo simulations, we follow a swarm of electrons moving in a homogeneous background gas. The interactions between electrons are neglected due to their small number density, and the dynamics of an individual electron is determined by the electric field and by collisions with the molecules of the background gas. In these simulations random numbers are extensively employed in order to determine the time and the type of the next collision as well as postcollisional velocity of an electron. Transport coefficients are calculated from polynomials of the components of the position and velocity vectors of individual electrons, which are averaged over the entire swarm. The details of our Monte Carlo code are given in previous papers (see Dujko et al. 2010.). The bulk values of the third-order transport coefficients are determined from

$$\mathbf{Q}^{(b)} = \frac{1}{3!} \frac{d}{dt} \langle \mathbf{r}^* \mathbf{r}^* \mathbf{r}^* \rangle, \quad (1)$$

while the flux third-order transport coefficients are calculated as:

$$\mathbf{Q}^{(f)} = \frac{1}{3!} \left\langle \frac{d}{dt} \left(\mathbf{r}^* \mathbf{r}^* \mathbf{r}^* \right) \right\rangle, \quad (2)$$

where $\mathbf{r}^* = \mathbf{r} - \langle \mathbf{r} \rangle$, and the brackets $\langle \rangle$ represent ensemble averages. As these expressions have pronounced statistical fluctuations, a large number of electrons (at least 10^7) are followed in our Monte Carlo simulations in order to determine the third-order transport coefficients.

In the second method that is used in this work we employ numerical solutions of the Boltzmann equation. The Boltzmann equation represents the equation of continuity in the phase space, and it can be written as:

$$\frac{\partial f(\mathbf{r}, \mathbf{c}, t)}{\partial t} + \mathbf{c} \cdot \frac{\partial f(\mathbf{r}, \mathbf{c}, t)}{\partial \mathbf{r}} + \frac{q}{m} \mathbf{E} \cdot \frac{\partial f(\mathbf{r}, \mathbf{c}, t)}{\partial \mathbf{c}} = -J(f, f_0), \quad (3)$$

where q and m are electron charge and electron mass respectively, \mathbf{E} is electric field and J is collision operator. In the multi term method the phase space distribution function is expanded in terms of the spherical harmonics and Sonine polynomials in angular and radial parts of the velocity space, respectively. Under hydrodynamic conditions, the dependence of the phase space distribution function on the coordinates from the configuration space is expressed in terms of the density gradient series expansion. Then the Boltzmann equation is decomposed into a hierarchy of equations in terms of the coefficients in this expansion (the moments of the distribution function). Transport coefficients are then expressed in terms of these moments and this hierarchy of equations is truncated when the convergence of the transport coefficients is reached. The details of the multi term method, which is employed in this work, are given in previous papers (see Dujko et al. 2010.). Expressions for those components of the flux third-order transport tensor, which are independent in the electric field only configuration, are given by the following equations:

$$Q_{xxz}^{(f)} = \frac{1}{\sqrt{2}\alpha} [\text{Im}(F(011|221; \alpha)) - \text{Im}(F(01-1|221; \alpha))], \quad (4)$$

$$Q_{zxx}^{(f)} = -\frac{1}{\alpha} \left[\frac{1}{\sqrt{3}} \text{Im}(F(010|200; \alpha)) + \frac{1}{\sqrt{6}} \text{Im}(F(010|220; \alpha)) \right] + \frac{1}{\alpha} \text{Im}[F(010|222; \alpha)], \quad (5)$$

$$Q_{zzz}^{(f)} = \frac{1}{\alpha} \left[\sqrt{\frac{2}{3}} \text{Im}(F(010|220; \alpha)) - \frac{1}{\sqrt{3}} \text{Im}(F(010|200; \alpha)) \right], \quad (6)$$

where Im denotes imaginary parts of the moments of the phase space distribution function, and the z -axis is directed along the electric field.

3. RESULTS AND DISCUSSIONS

In this section we show the calculated values of the third-order transport coefficients, which are obtained by employing the methods described in the previous section. The calculation of the third-order transport coefficients by employing these two methods is described more thoroughly in our previous paper (see Simonović et al. 2022.). The cross section set for electron scattering on C₃F₈ molecules, that is used in these calculations, has been developed by Biagi (see Biagi).

In figure 1.a we show all three components of the skewness tensor for electrons in C₃F₈ that are independent in the electric field only configuration. These results are obtained by using the multi term method for solving the Boltzmann equation. The $n_0^2 Q_{zzz}$ component has two local maximums and one local minimum, $n_0^2 Q_{xxz}$ component has three local maximums and two local minimums, while the $n_0^2 Q_{zxx}$ component has two local maximums and two local minimums.

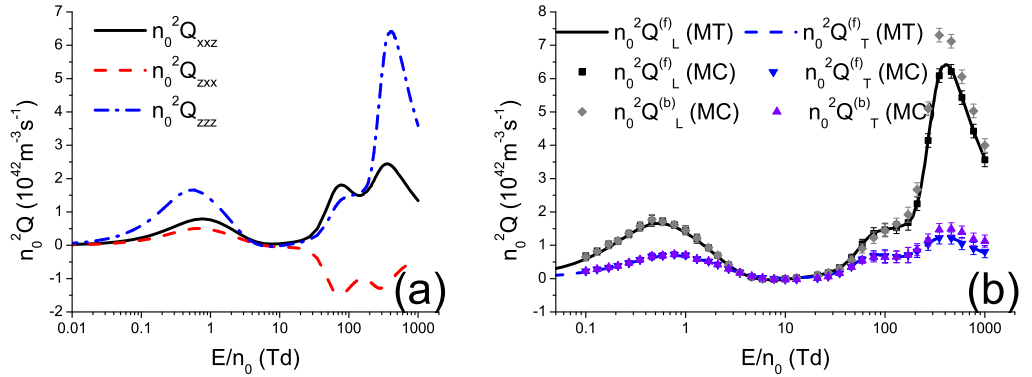


Figure 1: Independent components of the third-order transport tensor (a) and comparison of bulk and flux values of $n_0^2 Q_L$ and $n_0^2 Q_T$ (b) for electrons in C₃F₈.

In figure 1.b we show the comparison between bulk and flux values of $n_0^2 Q_L$ and $n_0^2 Q_T$. Bulk values are obtained by using Monte Carlo simulations, while flux values are determined by employing Monte Carlo simulations and the multi term method for solving the Boltzmann equation. Flux values that are obtained by using these two independent methods are generally in a good agreement, which verifies the validity of these two methods. At high electric fields bulk values are higher than the corresponding flux values, due to explicit effects of electron impact ionization.

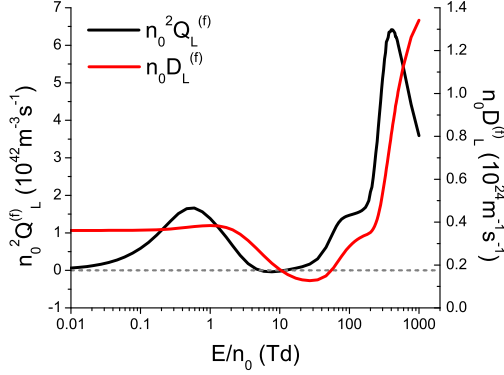


Figure 2: Concurrence between $n_0^2 Q_L^{(f)}$ and $n_0 D_L^{(f)}$ for electrons in C_3F_8 .

In figure 2 we show the concurrence between $n_0^2 Q_L^{(f)}$ and $n_0 D_L^{(f)}$. This concurrence implies that $n_0^2 Q_L^{(f)}$ is being reduced with increasing E/n_0 when $n_0 D_L^{(f)}$ is being reduced, or when it increases as a concave function of E/n_0 (see Simonović et al. 2022.). The observed concurrence can be attributed to the high sensitivity of the third-order transport coefficients to the elementary scattering processes, which quench diffusive motion. It can be seen in figure 2 that $n_0^2 Q_L^{(f)}$ has a local maximum and it starts to decrease at about 0.59 Td where $n_0 D_L^{(f)}$ becomes a concave function of E/n_0 . It can also be seen that $n_0^2 Q_L^{(f)}$ has a local minimum at about 8 Td, and it starts increasing at higher fields, although $n_0 D_L^{(f)}$ continues to decrease up to about 27 Td. However, $n_0^2 Q_L^{(f)}$ has negative values between approximately 5 Td, and 11 Td, and the concurrence with diffusion is violated in the vicinity of the field region where $n_0^2 Q_L^{(f)}$ is negative, as in the case of CF_4 (see Simonović et al. 2022.). Between approximately 70 Td and 170 Td, the rise of both functions slows down, while this rise becomes rapid again at higher fields. In the field region between approximately 400 Td and 1000 Td $n_0 D_L^{(f)}$ becomes a concave function of E/n_0 , while $n_0^2 Q_L^{(f)}$ is being reduced with increasing field.

Acknowledgment

This research was supported by the Institute of Physics Belgrade, and the Science Fund of the Republic of Serbia [Grant No. 7749560, EGWIn].

References

- Biagi, S.F., Magboltz code v11.11, <https://magboltz.web.cern.ch/magboltz/>
Dujko, S., White, R.D., and Petrović, Z.Lj.: 2008, *J. Phys. D: Appl. Phys.*, **41**, 245205.
Dujko, S., White, R.D., Petrović, Z.Lj., and Robson, R.E.: 2010, *Phys. Rev. E*, **81**, 046403.
Kawaguchi, S., Nakata, N., Satoh, K., Takahashi, K., and Satoh, K.: 2021 *Plasma Sources Sci. Technol.* **30**, 035006.
Simonović I., Bošnjaković D., Petrović Z. Lj., and Dujko S.: 2022 *Plasma Sources Sci. Technol.* **31**, 015003
Vrhovac, S.B., Petrović, Z.Lj., Viehland, L.A., Santhanam, T.S.: 1999 *J. Chem. Phys.* **110**, 2423

ICPIG XXXV Egmond aan Zee 2023



July 9th – 14th, 2023

Hotel Zuiderduin, Egmond aan Zee,
The Netherlands.

www.icpig2023.com

Version: July 12, 2023

TU/e

Contents

1	ICPIG — a forum for discussion	2
1.1	History and mission	2
1.2	Selection of talks	2
1.3	von Engel and Franklin prize	2
1.4	Information for Presenters	3
1.5	Conference Topics	3
1.6	Local Organizing Committee	4
1.7	International Scientific Committee	4
1.8	Sponsors	5
2	Practical information	6
2.1	Venue	6
2.2	International travel and local transport	6
2.2.1	Venue maps	7
3	Program	9
3.1	Program table	9
3.2	Detailed program including social program	10
3.3	Posters	20
3.3.1	Poster session P1, Mon, Jul 10, 14:00 - 16:00	20
3.3.2	Poster session P2, Tue, Jul 11, 14:00 - 16:00	24
3.3.3	Poster session P3, Thu, Jul 13, 13:45 - 15:45	29
3.3.4	Poster session P4, Thu, Jul 13, 17:00 - 19:00	33
4	Abstracts	38

Axisymmetric streamer model in the AMReX environment

I. Simonović¹, D. Bošnjaković¹ and S. Dujko¹

¹*Institute of Physics Belgrade, University of Belgrade, Pregrevica 118, 11080 Belgrade, Serbia*

In this work, we have developed an axisymmetric streamer code in the AMReX software framework. The model employed in this code is based on the first-order fluid model with bulk transport coefficients and local field approximation. This code is tested by comparison of its results with the results of the Afivo-streamer code.

Streamers are precursors of arcs and lightning leaders in nature and in plasma technologies [1]. Streamers are used for surface processing, and in plasma medicine for disinfection, and wound healing [1]. Further development of these applications would benefit from a better understanding of streamers through both experiment and modelling.

We have developed an axisymmetric streamer code that is based on the first-order fluid model with bulk transport coefficients. The code is implemented in the AMReX software framework [2]. AMReX is an open source library for numerical calculations with massively parallel, block-structured adaptive mesh refinement. AMReX enables both MPI and OpenMP parallelization, as well as parallelization on graphics processing units. In addition, AMReX comes with inbuilt multigrid solvers and functionality for saving both grid and particle data to checkpoints and to output files for plotting. Although AMReX is implemented in C++, it also has a Fortran interface and Python interface which is under development.

In our model, the time evolution of the number density of electrons is determined by employing the advection-diffusion-reaction equation, while the time evolution of the number densities of positive and negative ions is determined by the reaction equations. Ions are assumed to be stationary for the timescales of our simulations. The spatial dependence of transport coefficients (mobility, diffusion, and rate coefficients for electron impact ionization and attachment) is determined by employing the local field approximation. The total electric field is expressed as the sum of constant and homogeneous applied electric field and the electric field which is generated by space charge. The electric potential of space charge is determined by employing the AMReX inbuilt ge-

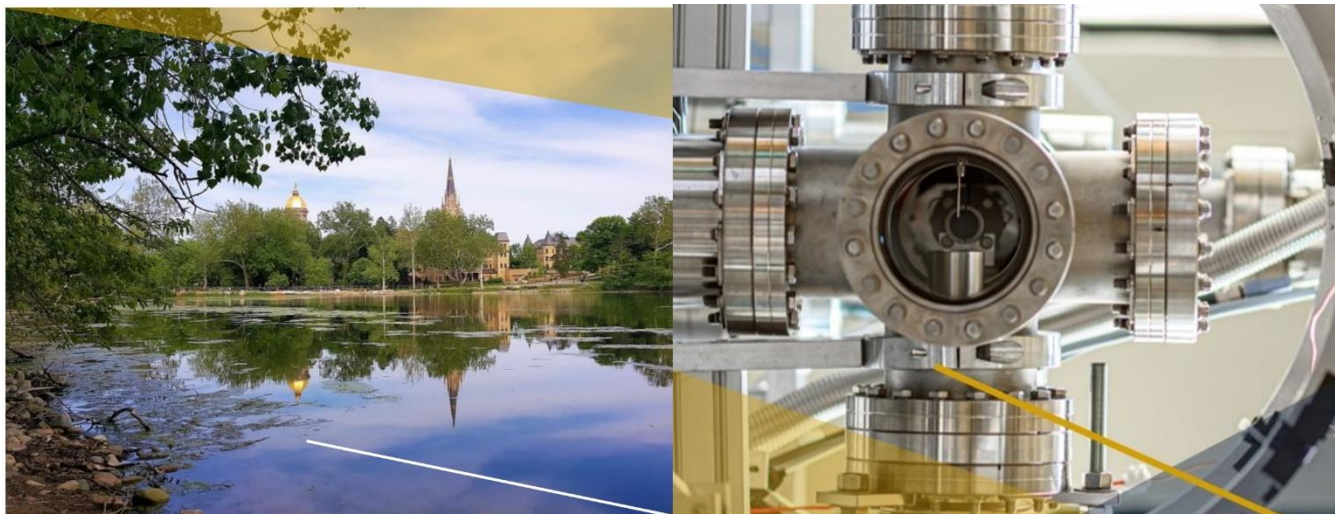
ometric multigrid solver for solving the Poisson equation. We employ zero Neumann boundary conditions for the number density of electrons at all boundaries. For the electric potential of space charge, we employ zero Neumann boundary conditions at boundaries that are perpendicular to the radial coordinate and zero Dirichlet boundary conditions at boundaries which are perpendicular to the axial coordinate.

We employ the finite volume method for the spatial discretization of the advection-diffusion-reaction equation. Electric field components and electron flux components are defined at cell faces, while the number densities of electrons and ions, the intensity of the total electric field, as well as transport coefficients, are defined at cell centers. We use the Runge-Kutta method for the time integration of this equation. In our code, both 2nd and 4th-order Runge-Kutta methods are supported. The validity of this code is tested by comparing its results to the results of the Afivo-streamer code [1] in a wide range of gases.

Acknowledgments: This work is supported by the Science Fund of the Republic of Serbia, Grant No. 7749560, Exploring ultra-low global warming potential gases for insulation in high-voltage technology: Experiments and modelling EGWI_n.

References

- [1] Teunissen, J. & Ebert, U. Simulating streamer discharges in 3D with the parallel adaptive Afivo framework. *Journal of Physics D: Applied Physics* **50**, 474001 (2017).
- [2] Zhang, W. *et al.* AMReX: a framework for block-structured adaptive mesh refinement. *Journal of Open Source Software* **4**, 1370 (2019).



POSMOL 2023

XXI International Workshop on Low-Energy Positron and Positronium Physics
&
XXIII International Symposium on
Electron-Molecule Collisions and
Swarms

August 3-6, 2023, University of Notre Dame, IN, USA

FOREWORD

Dear colleagues,

It is our pleasure to welcome you at POSMOL 2023.

The POSMOL will continue this year as a joint meeting of the International Workshop on Low-Energy Positron and Positronium Physics and the International Symposium on Electron-Molecule Collisions and Swarms, and as previously it is a satellite meeting of the International Conference on Photonic, Electronic, and Atomic Collisions (ICPEAC).

The POSMOL conference covers a wide range of research topics related to positron, electron, positronium, and antimatter interactions with particles, atoms, molecules, and complex systems, and related subjects. The meeting will continue the tradition of a scientific forum at which a diverse group of scholars from around the world will have an opportunity to share their theoretical and experimental findings, ideas, innovations, and methodologies through formal and informal discussions to advance scientific knowledge and understanding of the fundamental, collisional interactions.

We would like to express many thanks to both International Advisory Committees' members chaired by Prof. Dragana Maric and James Sullivan for their work and dedication on the scientific content of the conference and the Organizing Committee members, particularly Lisa Driver, for their assistance with logistics for this meeting. We also would like to thank our founders and sponsors for their generous contribution, which allowed us to keep the costs of registration down. Finally, we are grateful to all of the participants in this meeting who have contributed so much to the continued success of our scientific community.

Sylwia Ptasinska, Chair
University of Notre Dame

Daniel Slauchter, Co-Chair
Lawrence Berkeley National Laboratory

POSITRON INTERNATIONAL ADVISORY COMMITTEE

- James Sullivan (Australian National University, Australia) *Chair*
- Roberto S. Brusa (University of Trento, Italy)
- David Cassidy (University College London, United Kingdom)
- Michael Charlton (University Swansea, United Kingdom)
- Gustavo Garcia (Spanish National Research Council, Spain)
- Dermot Green (Queen's University Belfast, United Kingdom)
- Laszlo Liskay (Paris-Saclay University, France)
- Koji Michishio (National Institute of Advanced Industrial Science and Technology, Japan)
- Eve Stenson (Max Planck Institute for Plasma Physics, Germany)
- Marcio Varella (University of São Paulo, Brazil)

ELECTRON INTERNATIONAL ADVISORY COMMITTEE

- Dragana Maric (Institute of Physics Belgrade, Serbia) *Chair*
- Michael J. Brunger[†] (Flinders University, Australia)
- Roman Čurik (J. Heyrovsky Institute of Physical Chemistry, Czech Republic)
- Romarly da Costa (Federal University of ABC, Brazil)
- Jimena Gorfinkel (Open University, United Kingdom)
- Janina Kopyra (University of Siedlce, Poland)
- Paulo Limão-Vieira (Universidade NOVA de Lisboa, Portugal)
- Sylwia Ptasińska (University of Notre Dame, USA)
- Kohki Satoh (Muroran Institute of Technology, Japan)
- Ronald D. White (James Cook University, Australia)

AMReX based axisymmetric fluid model

Ilija Simonović¹, Danko Bošnjaković¹, and Saša Dujko¹

¹Institute of Physics Belgrade, University of Belgrade, Pregrevica 118, 11080 Belgrade, Serbia

sasa.dujko@ipb.ac.rs

We have developed an axisymmetric fluid model in the AMReX open source C++ library. In our model, the time evolution of the number density of electrons and ions is represented by the advection-diffusion-reaction equation and reaction equations, respectively. The time integration of these equations is performed by employing the 2nd order Runge-Kutta method. Our code is based on the local field approximation. Thus, transport properties of electrons are assumed to be functions of the local resulting electric field. The electric potential of space charges is determined by solving the Poisson equation. This equation is solved numerically by implementing the AMReX inbuilt geometric multigrid solver. Spatial discretization is performed by employing the finite volume method. As an illustrative example, in Fig. 1 we show the number density electrons of the positive streamer in the mixture with 20% N₂ and 80% of CH₄ (left), and 80% N₂ and 20% of CH₄ (right) at 7 ns. The applied electric field is set to $2 \cdot 10^6$ V/m in the entire domain.

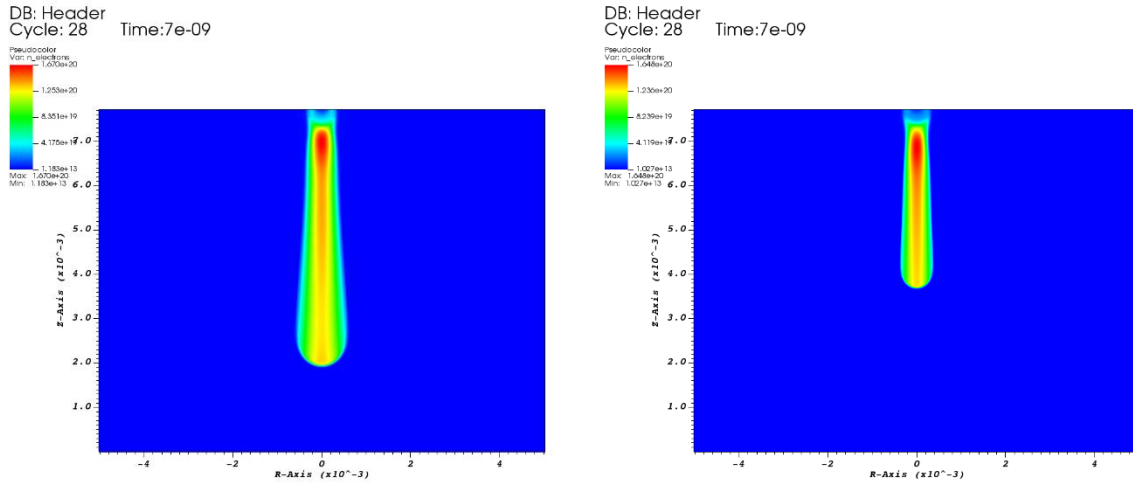


Fig. 1. The number density of electrons of the positive streamer in the mixture with 20% N₂ and 80% of CH₄ (left), and 80% N₂ and 20% of CH₄ (right) at 7 ns.

Acknowledgment. This work is supported by the Science Fund of the Republic of Serbia, Grant No. 7749560, Exploring ultra-low global warming potential gases for insulation in high-voltage technology: Experiments and modelling (EGWIn).

Simulations of streamers in C₃F₈ and its mixtures with N₂, CO₂ and SF₆

Saša Dujko¹, Ilija Simonović¹ and Danko Bošnjaković¹

¹Institute of Physics Belgrade, University of Belgrade, Pregrevica 118, 11080 Belgrade, Serbia

sasa.dujko@ipb.ac.rs

Using the classical fluid model, we study the inception and propagation of streamers in perfluoropropane (C₃F₈) and its mixtures with N₂, CO₂ and SF₆. The model is implemented within the AMReX, a C++ software framework that supports the development of block-structured adaptive mesh refinement algorithms for solving systems of partial differential equations with complex boundary conditions [1]. We simulate cylindrically symmetric positive (and negative) streamers in a volume spanned by radius r and axis z , with a certain level of background ionization. Electron swarm transport coefficients required as input to solve the system of fluid equations are calculated using a Monte Carlo simulation technique.

As an illustrative example, in Fig. 1 we show the resulting electric field of the positive streamer in the mixture with 95% N₂ and 5% of C₃F₈ (left), and 75% N₂ and 25% of C₃F₈ (right) at 2.25 ns. The applied electric field is set to $5 \cdot 10^6$ V/m in the entire domain.

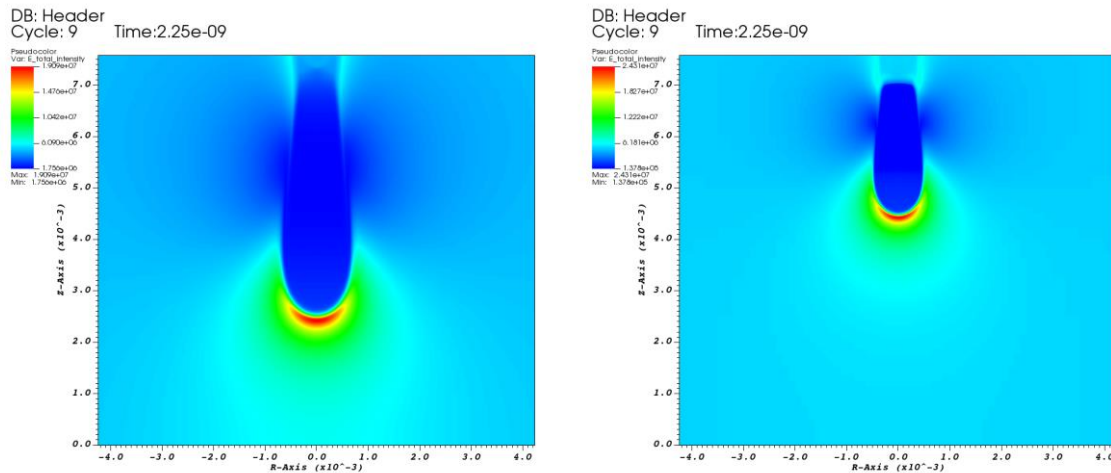


Fig. 1. The resulting electric field intensity of the positive streamer in the mixture with 95% N₂ and 5% of C₃F₈ (left), and 75% N₂ and 25% of C₃F₈ (right) at 2.25 ns.

Acknowledgment. This work is supported by the Science Fund of the Republic of Serbia, Grant No. 7749560, Exploring ultra-low global warming potential gases for insulation in high-voltage technology: Experiments and modelling (EGWIn).

References

[1] W. Zhang et al., J. Open Source Software **4** (2019) 1370.

**V Meeting on Astrophysical Spectroscopy -
A&M DATA - Astronomy & Earth Observations**

September 12 - 15, 2023, Palić, Serbia

**BOOK OF ABSTRACTS AND
CONTRIBUTED PAPERS**

**Edited by Vladimir A. Srećković, Milan S. Dimitrijević,
Aleksandra Kolarski, Zoran R. Mijić and Nikola B. Veselinović**

A&M DATA



UNIVERSITY OF BELGRADE
INSTITUTE OF PHYSICS | BELGRADE
NATIONAL INSTITUTE OF
THE REPUBLIC OF SERBIA

Belgrade 2023

Scientific Committee

Vladimir A. Srećković, **Co-Chairman**, Serbia
Milan S. Dimitrijević, **Co-Chairman**, Serbia

Nikolay Bezuglov, Russia
Nebil Ben Nessib, Saudi Arabia
Vesna Borka Jovanović, Serbia
Nikola Cvetanović, Serbia
Saša Dujko, Serbia
Stevica Đurović, Serbia
Zoran Grujić, Serbia
Rafik Hamdi, Tunisia
Magdalena D. Christova, Bulgaria
Dragana Ilić, Serbia
Milivoje Ivković, Serbia
Darko Jevremović, Serbia
Ognyan Kounchev, Bulgaria
Bratislav P. Marinković, Serbia
Zoran R. Mijić, Serbia
Aleksandar Milosavljević, France
Aleksandra Nina, Serbia
Bratislav M. Obradović, Serbia
Nicolina Pop, Romania
Luka Č. Popović, Serbia
Branko Predojević, Republic of Srpska, BiH
Sylvie Sahal-Bréchet, France
Igor Savić, Serbia
Sanja Tošić, Serbia
Nikola B. Veselinović, Serbia

Local Organizing Committee

Aleksandra Kolarski (Co-Chair), Institute of Physics Belgrade
Vladimir A. Srećković (Co-Chair), Institute of Physics Belgrade
Nikola B. Veselinović (Secretary), Institute of Physics Belgrade
Zoran R. Mijić, Institute of Physics Belgrade
Nenad M. Sakan, Institute of Physics Belgrade
Veljko Vujčić, Astronomical Observatory, Belgrade
Nikola Cvetanović, University of Belgrade, Faculty of Transport and Traffic Engineering

Simulations of positive and negative streamers in the AMReX environment

**Ilija B. Simonović, Danko V. Bošnjaković and
Saša Dujko**

*Institute of Physics, University of Belgrade, P.O. Box 68, 11080 Belgrade, Serbia
E-mail: isimonovic@ipb.ac.rs*

Streamers are thin channels of weakly-ionized nonstationary plasma produced by an ionization front that moves through non-ionized matter (Teunissen and Ebert 2017). They have applications in diverse areas of science and technology ranging from their role in creating lighting and sprite discharges in the upper planetary atmospheres to industrial applications such as the ignition of high-intensity discharge lamps and treatment of polluted gases and water. Further optimization and understanding of such applications are dependent on an accurate knowledge of streamer properties, electron transport and physical processes involved.

We have developed a computer code that implements an axisymmetric first order fluid model in the AMReX environment. AMReX is an open-source C++ library for numerical calculations with block structured adaptive mesh refinement (Zhang et al. 2019). It has inbuilt geometric multigrid solvers and it allows both MPI and OpenMP parallelization, as well as parallelization on graphic processing units. AMReX also has many inbuilt classes which enable a convenient implementation of both grid and particle data.

In our code the time evolution of the number density of electrons is represented by the drift-diffusion-reaction equation. The time evolution of the number densities of positive and negative ions are represented by the rate equations, as ions are assumed to be stationary for the timescales of our simulations. The time integration of these equations is performed by employing the second order Runge-Kutta method. The spatial dependence of transport coefficients in these equations is represented by the local field approximation. The electric potential due to space charges is determined by solving the Poisson equation, while photoionization is represented by solving a set of Helmholtz equations. These equations are solved by employing the AMReX inbuilt geometric multigrid solver. Bourdon three term parametrization (Bourdon et al. 2007) is employed for representing photoionization in the mixtures of nitrogen and oxygen.

Spatial discretization is implemented by using the finite volume method. Thus, scalar variables are defined at the cell centers, while vector variables are defined at the cell faces. For this reason, the number density of electrons needs to be

interpolated from cell centers to cell faces to calculate the electron flux. For this purpose, both TVD scheme with the Koren flux limiter (Koren 1993) and Munz implementation (Munz 1988) of the MUSCL scheme (Van Leer 1979) can be used. The validity of the code is tested by comparing its results to the results of the Afivo-streamer open-source fluid code (Teunissen 2017).

Acknowledgments

This work is supported by the Science Fund of the Republic of Serbia, Grant No. 7749560, Exploring ultra-low global warming potential gases for insulation in high-voltage technology: Experiments and modelling EGWin.

References

- Bourdon, A., Pasko, V. P., Liu, N. Y., Célestin, S., Ségur, P. and Marode, E., 2007, Plasma Sources Sci. Technol. 16, 656
Koren, B., 1993, In Numerical Methods for Advection-Diffusion Problems, pages 117–138. Braunschweig/Wiesbaden: Vieweg
Munz, C. D., 1988, J. Comput. Phys., 77, 18
Teunissen, J. and Ebert, U., 2017, Journal of Physics D: Applied Physics 50, 474001
Van Leer, B, 1979, Journal of computational Physics, 32, 101
Zhang, W. et al., 2019, Journal of Open Source Software, 4, 1370



**32nd Summer School and
International Symposium on
the Physics of Ionized Gases**

Belgrade, Serbia,
August 26 - 30, 2024

CONTRIBUTED PAPERS

&

**ABSTRACTS of INVITED LECTURES,
TOPICAL INVITED LECTURES and PROGRESS REPORTS**

Editors:

**Bratislav Obradović, Jovan Cvetić,
Miroslav Kuzmanović and Nikola Cvetanović**



**БЕОГРАД
2024**

**32nd Summer School and
International Symposium on
the Physics of Ionized Gases**



August 26 – 30, 2024, Belgrade, Serbia

S P I G 2024

CONTRIBUTED PAPERS

&

**ABSTRACTS OF INVITED LECTURES,
TOPICAL INVITED LECTURES AND
PROGRESS REPORTS**

Editors

**Bratislav Obradović, Jovan Cvetić,
Miroslav Kuzmanović and Nikola Cvetanović**

**University of Belgrade –
Faculty of Physical
Chemistry**

**Serbian Academy of
Sciences and Arts**

Belgrade, 2024

PUBLICATIONS OF THE ASTRONOMICAL OBSERVATORY OF BELGRADE

FOUNDED IN 1947

EDITORIAL BOARD:

Dr. Srdjan SAMUROVIĆ, Editor-in-Chief (Astronomical Observatory, Belgrade)

Dr. Rade PAVLOVIĆ (Institute of Physics, Belgrade)

Dr. Miroslav MIĆIĆ (Astronomical Observatory, Belgrade)

Dr. Branislav VUKOTIĆ (Astronomical Observatory, Belgrade)

All papers in this Publication are peer reviewed.

Published and copyright © by Astronomical Observatory, Volgina 7, 11060 Belgrade 38, Serbia

Director of the Astronomical Observatory: Dr. Luka Č. Popović

Typesetting: Tatjana Milovanov

Internet address <https://publications.aob.rs>

ISSN 0373-3742

ISBN 978-86-82296-08-9

Financially supported by the Ministry of Science, Technological Development and Innovation of the Republic of Serbia

CIP - Каталогизacija y publikaciji - Narodna biblioteka Srbije, Beograd

537.56(082)

539.186.2(082)

539.121.7(082)

533.9(082)

SUMMER School and International Symposium on the Physics of Ionized Gases (32 ; 2024 ; Beograd)

Contributed papers & abstracts of invited lectures, topical invited lectures and progress reports / 32nd Summer School and International Symposium on the Physics of Ionized Gases - SPIG 2024, August 26 – 30, 2024, Belgrade, Serbia ; editors Bratislav Obradović ... [et al.]. - Belgrade : Astronomical Observatory, 2024 (Beograd : Skripta Internacional). - 215 str. : ilustr. ; 24 cm. - (Publications of the Astronomical Observatory of Belgrade, ISSN 0373-3742)

Na nasl. str.: University of Belgrade, Faculty of Physical Chemistry; Serbian Academy of Sciences and Arts. - Tiraž 200. - Str. 17-18: Preface / editors Bratislav Obradović ... [et al.]. - Bibliografija uz svaki rad. - Registar.

ISBN 978-86-82296-08-9

1. Kuzmanović, Miroslav, 1967- [urednik] [autor dodatnog teksta]

a) Јонизовани гасови - Зборници b) Атоми - Интеракција - Зборници

v) Плазма - Зборници

COBISS.SR-ID 150439689

SPIG 2024

SCIENTIFIC COMMITTEE

J. Cvetić (Co-chair), Serbia
B. Obradović (Co-chair), Serbia

A. Antoniou, Greece
J. Burgdörfer, Austria
M. Čosić, Serbia
V. Guerra, Portugal
M. Ivković, Serbia
J. Kovačević-Dojčinović, Serbia
K. Kutasi, Hungary
I. Mančev, Serbia
D. Marić, Serbia
N. J. Mason, UK
A. Milosavljević, France
V. Milosavljević, Serbia
D. Milošević, BH
K. Mima, Japan
L. Nahon, France
G. Poparić, Serbia
I. Radović, Serbia
P. Ranitović, Serbia
P. Rousseau, France
I. Savić, Serbia
Y. Serruys, France
N. Simonović, Serbia
V. Srečković, Serbia
M. Škorić, Japan
S. Tošić, Serbia
M. Trtica, Serbia
R. White, Australia

ADVISORY COMMITTEE

D. Belić
N. Bibić
M. S. Dimitrijević
S. Đurović
D. Ilić
N. Konjević
M. M. Kuraica
J. Labat
G. Malović
B. P. Marinković
M. Milosavljević
Z. Mišković
Z. Lj. Petrović
L. Č. Popović
B. Stanić

ORGANIZING COMMITTEE

M. Kuzmanović (Chair)
M. Ristić (Co-secretary)
B. Stankov (Co-secretary)
N. Konjević
N. Cvetanović
D. Ranković
M. Milovanović
M. Marković
A. Šajić
I. Traparić

STUDIES ON STREAMER DISCHARGES IN ULTRA-LOW GWP GASES

DANKO BOŠNIAKOVIĆ , ILIJA SIMONOVIĆ  and SAŠA DUJKO 

Institute of Physics Belgrade, Pregrevica 118, 11080 Belgrade, Serbia

Abstract. In this work, we use a Particle-in-cell/Monte Carlo collision (PIC/MCC) model to investigate the inception and propagation of both positive and negative streamers in ultra-low GWP gases, including $C_3H_2F_4$ and C_3HF_5 . The modelling results can be used as a basis for assessing the performance of these gases in high-voltage insulation as eco-friendly alternatives to SF_6 .

The PIC/MCC model uses Velocity Verlet scheme to track individual electrons in 3D and a Monte Carlo null-collision technique to sample the electron-neutral collision parameters. The electric field is assumed to be axially symmetric and is computed on a 2D numerical grid coupled with a Poisson equation solver. The electric field solver is implemented using the iterative multigrid method provided by the AMReX software framework. AMReX is an open-source C++ library for massively parallel block structured adaptive mesh refinement applications. In addition to its in-built geometric multigrid solver, we use the programming abstractions that it provides to implement adaptive mesh refinement and to support MPI and OpenMP parallelization on multicore CPUs. We also employ a particle management technique in order to optimize the number of particles in a simulation and shorten the computation time. To study the propagation of positive streamers, we include a photoionization model and a stochastic background ionization as sources of free electrons.

Results of PIC/MCC simulations are presented as an evolution of electron and ion densities, electric field distribution, streamer radius and velocity, and are obtained as a function of the applied electric field strength. In addition to ultra-low GWP gases, calculations are also performed for artificial dry air so as to validate and compare our results with those from open source Afivo-pic code.

Acknowledgments: This work is supported by the Science Fund of the Republic of Serbia, Grant No. 7749560, Exploring ultra-low global warming potential gases for insulation in high-voltage technology: Experiments and modelling EGWin.

ELECTRON TRANSPORT IN RADIO-FREQUENCY ELECTRIC AND MAGNETIC FIELDS IN ULTRA-LOW GWP GASES

SAŠA DUJKO¹ , ILIJA SIMONOVIĆ¹ , DANKO BOŠNJAKOVIĆ¹ ,
JASMINA ATIĆ¹  and ZORAN LJ. PETROVIĆ² 

¹*Institute of Physics Belgrade, Pregrevica 118, 11080 Belgrade, Serbia*

²*Serbian Academy of Sciences and Arts, Knez Mihailova 35, 11001 Belgrade, Serbia*

Abstract. In this work, we study the transport of electrons in radio-frequency (RF) electric and magnetic fields in ultra-low global warming potential (GWP) gases. Calculations have been performed for electron swarms in $C_3H_2F_4$ and C_3HF_5 using a time-dependent multi-term technique to solve the Boltzmann equation and Monte Carlo simulation.

The progress and further improvements of plasma science require the most accurate modeling of charged particle transport under the influence of electric and magnetic fields in neutral gases. In this work, we study the transport of electrons in RF electric and magnetic fields in ultra-low GWP gases, including $C_3H_2F_4$ and C_3HF_5 . Electron swarm transport properties and distribution functions have been calculated using a unified time-dependent multi term theory to solve the Boltzmann equation and Monte Carlo simulation. The motivational factors for this study include the following: (1) understanding electron kinetics and electron heating mechanisms in inductively coupled plasmas, (2) understanding of the interaction between electromagnetic waves and ambient electrons inside gas-insulated switchgears used in electrical power transmission systems. We systematically investigate the explicit effects associated with the electric and magnetic fields including fields to density ratios, field frequency, field phases and field orientations. We also highlight the explicit modification of electron swarm transport coefficients by non-conservative collisions, including the electron attachment and ionization. We have observed a multitude of kinetic phenomena that are generally inexplicable with the conventional transport theory of electron swarms in direct-current (DC) fields. Phenomena of significant note include the increase of mean energy with increasing magnetic field, time-resolved negative differential conductivity, anomalous anisotropic diffusion, and transient negative diffusivity.

Acknowledgments: This work is supported by the Science Fund of the Republic of Serbia, Grant No. 7749560, Exploring ultra-low global warming potential gases for insulation in high-voltage technology: Experiments and modelling EGWIn.

STUDIES ON ELECTRON SWARMS AND STREAMER DISCHARGES IN ECO-FRIENDLY RPC GASES

SAŠA DUJKO¹ , ILIJA SIMONOVIĆ¹ , DANKO BOŠNJAKOVIĆ¹ ,
ZORAN LJ. PETROVIĆ²  and J. de URQUIJO³

¹*Institute of Physics Belgrade, Pregrevica 118, 11080 Belgrade, Serbia*

²*Serbian Academy of Sciences and Arts, Knez Mihailova 35, 11001 Belgrade, Serbia*

³*Instituto de Ciencias Físicas, Universidad Nacional Autónoma de México, 62251 Cuernavaca, Morelos, Mexico*

Abstract. In this work, we study the transport of electrons and the propagation of streamers in resistive plate chambers (RPC). We are considering the performance of new eco-friendly gas mixtures instead of the currently used $C_2H_2F_4$ and SF_6 .

Resistive plate chambers are gaseous particle detectors often used for timing and triggering purposes in high-energy physics experiments. At the Large Hadron Collider (LHC) at CERN, all key experiments, including ALICE, ATLAS, CMS and LHCb employ RPC detectors. RPCs in these experiments are operated with gas mixtures in which the main component is $C_2H_2F_4$. $C_2H_2F_4$ is mixed with $i-C_4H_{10}$ and SF_6 in various percentages, to control the amount of liberated charge and the occurrence of violent discharges. However, $C_2H_2F_4$ and SF_6 are characterized by high global warming potentials. In this work, we study the performance of new eco-friendly RPC gas mixtures. The $C_2H_2F_4$ is replaced with a proper mixture of $C_3H_2F_4$ and CO_2 , while CF_3I , C_4F_7N and $C_5F_{10}O$ were considered as alternatives to SF_6 . We approach the problem at three stages: (1) First, we propose complete and consistent sets of cross sections for $C_3H_2F_4$ and strongly attaching gases, including CF_3I , C_4F_7N and $C_5F_{10}O$, (2) Second, we investigate the transport of electrons in various eco-friendly gas mixtures, and (3) Third, we simulate the inception and propagation of streamers in LHC-like conditions. Swarm analysis was performed using pulsed-Townsend measurements of swarm data, numerical solutions of Boltzmann's equation, and Monte Carlo simulations. The inception and propagation of streamers were simulated using the classical fluid model, which involves the drift-diffusion approximation and local field approximation. The model is implemented in 3D setup within the AMReX environment.

Acknowledgments: This work is supported by the Science Fund of the Republic of Serbia, Grant No. 7749560, Exploring ultra-low global warming potential gases for insulation in high-voltage technology: Experiments and modelling EGWin.

THREE-DIMENSIONAL STREAMER MODEL IN THE AMREX ENVIRONMENT

ILIJA SIMONOVIĆ^{id}, DANKO BOŠNJAKOVIĆ^{id} and SAŠA DUJKO^{id}

Institute of Physics Belgrade, Pregrevica 118, 11080 Belgrade, Serbia

Abstract. Streamers appear in nature as sprite discharges in the upper-planetary atmospheres, and as precursors of lightning, see Teunissen and Ebert 2017. They have a wide variety of applications in technology including the ignition of high-intensity discharge lamps and the purification of gases and liquids from harmful organic pollutants. The further development of these applications requires a joint effort of experimental investigations and computer modelling of streamer discharges.

We have developed a 3D streamer model in the AMReX environment. AMReX is an open-source C++ library for massively parallel block structured adaptive mesh refinement applications, see Zhang et al. 2019. AMReX has inbuilt geometric multigrid solvers for solving elliptic differential equations, and it allows both MPI and OpenMP parallelization on CPUs as well as parallelization on GPUs. AMReX also has many inbuilt classes which enable a convenient implementation of both grid and particle data.

Our model is based on the first-order fluid model with local field approximation. The time integration in our code is performed by employing the second order Runge-Kutta method. The spatial discretization is performed by using the finite volume method. In our model, the non-local source term due to photoionization is represented by solving a set of Helmholtz equations, and we apply the Bourdon three term parametrization for representing the photon absorption function, see Bourdon et al. 2007. The verification of our code is performed by comparing its results to the results of the Afivo-streamer open-source code, see Teunissen and Ebert 2017.

Acknowledgments: This work is supported by the Science Fund of the Republic of Serbia, Grant No. 7749560, Exploring ultra-low global warming potential gases for insulation in high-voltage technology: Experiments and modelling EGWin.

References

- Bourdon A., Pasko V. P., Liu N. Y., Célestin S., Ségur P. and Marode E.: 2007, *Plasma Sources Sci. Technol.* **16**, 656
Teunissen, J. and Ebert, U.: 2017, *Journal of Physics D: Applied Physics* **50**, 474001
Zhang, W. et al.: 2019, *Journal of Open Source Software*, **4**, 1370

FLUID MODEL OF STREAMERS IN THE AMREX ENVIRONMENT

ILIJA SIMONOVIĆ^{id}, DANKO BOŠNJAKOVIĆ^{id} and SAŠA DUJKO^{id}

Institute of Physics Belgrade, Pregrevica 118, 11080 Belgrade, Serbia

Abstract. Streamers are thin filaments of weakly ionized non-stationary plasma, which appear in nature as precursors of lightning and as sprite discharges in the upper-planetary atmospheres, see Teunissen and Ebert 2017. Streamers are used for the ignition of high-intensity discharge lamps and for the purification of gases and liquids from harmful organic pollutants, and they are the main mechanism of breakdown in the high-voltage insulation technology.

We have developed a fluid model of streamer discharges in the AMReX library. Our model is implemented in both axisymmetric and 3D cases. AMReX is an open-source C++ library that is designed for massively parallel block structured adaptive mesh refinement applications, see Zhang et al. 2019. AMReX allows a straightforward use of both MPI and OpenMP parallelization on CPUs as well as parallelization on GPUs. This library also has inbuilt geometric multigrid solvers for solving elliptic differential equations, such as the Poisson equation and the Helmholtz equation.

Our code is based on the first-order fluid model with local field approximation. The time integration in our code is performed explicitly by employing the Heun's method. We employ the finite volume method for spatial discretization. The non-local source term due to photoionization is represented by employing the Zhelenznyak's model using the Helmholtz approximation, and the photon absorption function is represented by applying the Bourdon three term parametrization, see Bourdon et al. 2007. We have verified our code by comparing its results to the results of the Afivo-streamer open-source code, see Teunissen and Ebert 2017.

Acknowledgments: This work is supported by the Science Fund of the Republic of Serbia, Grant No. 7749560, Exploring ultra-low global warming potential gases for insulation in high-voltage technology: Experiments and modelling EGWin.

References

- Bourdon A., Pasko V. P., Liu N. Y., Célestin S., Ségur P. and Marode E.: 2007, *Plasma Sources Sci. Technol.* **16**, 656
Teunissen, J. and Ebert, U.: 2017, *Journal of Physics D: Applied Physics* **50**, 474001
Zhang, W. et al.: 2019, *Journal of Open Source Software*, **4**, 1370

**International Meeting on Data for Atomic and Molecular
Processes in Plasmas: Advances in Standards and Modelling**

November 12-15, 2024, Palić, Serbia

**BOOK OF ABSTRACTS AND
CONTRIBUTED PAPERS**

Edited by Vladimir A. Srećković, Aleksandra Kolarski,
Milica Langović, Filip Arnaut and Nikola Veselinović

Belgrade, 2024

Scientific Organizing Committee

Vladimir A. Srećković, Institute of Physics Belgrade, **Co-Chair**
Aleksandra Kolarski, Institute of Physics Belgrade, **Co-Chair**

Milan S. Dimitrijević, Serbia
Nikolai N. Bezuglov, Russia
Nebil Ben Nessib, Saudi Arabia
Vesna Borka Jovanović, Serbia
Nikola Cvetanović, Serbia
Saša Dujko, Serbia
Rafik Hamdi, Tunisia
Magdalena Hristova, Bulgaria
Ognyan Kounchev, Bulgaria
Bratislav Marinković, Serbia
Zoran Mijić, Serbia
Nicolina Pop, Romania
Luka Popović, Serbia
Branko Predojević, Republic of Srpska, BiH
Sylvie Sahal Brechot, France
Sanja Tošić, Serbia
Robert Beuc, Croatia
Felix Iacob, Romania

Local Organizing Committee

Aleksandra Kolarski (**Co-Chair**), Institute of Physics Belgrade
Vladimir A. Srećković (**Co-Chair**), Institute of Physics Belgrade
Filip Arnaut (**Secretary**), Institute of Physics Belgrade
Zoran Mijić, Institute of Physics Belgrade
Milica Langović, Institute of Physics Belgrade
Mihailo Savić, Institute of Physics Belgrade
Nikola Veselinović, Institute of Physics Belgrade
Veljko Vujčić, Astronomical Observatory, Belgrade
Nikola Cvetanović, University of Belgrade, Faculty of Transport and Traffic Eng.

Organizer

Institute of Physics Belgrade

ISBN 978-86-82441-69-4

Published and copyright by: Institute of Physics Belgrade

Printed by: Skripta Internacional, Mike Alasa 54, 11102, Beograd

Number of copies: 50

Fitting of the current signal of the Pulsed Townsend experiment with the gradient descent algorithm

Simonović, I.B.,¹  Bošnjaković, D.V.¹  and Dujko, S.¹ 

¹*Institute of Physics, University of Belgrade, P.O. Box 68, 11080 Belgrade, Serbia*
E-mail: sasa.dujko@ipb.ac.rs

The Pulsed Townsend experiment is used for determining the transport coefficients for a swarm of electrons in gases (see e.g., Casey 2021, De Urquijo 2007, Haeftiger 2018). These transport coefficients include drift velocity, longitudinal diffusion and the effective ionization coefficient. In general, these transport coefficients are determined by fitting an analytical expression, in which the current signal is expressed in terms of these transport coefficients, to the actual current signal that is measured in the experiment by a nonlinear curve fitting procedure. In the literature, different analytical expressions for the current signal are used by different authors, and the employed nonlinear curve fitting procedures are not always publicly available. For this reason, a systematic study of the fitting of the current signal of the Pulsed Townsend experiment is long overdue, and this work makes first steps in that direction.

In this contribution, we investigate the applicability of the gradient descent algorithm for the fitting of the current signal of the Pulsed Townsend experiment. The gradient descent algorithm is a method for unconstrained mathematical optimization, that is commonly used to train machine learning models including linear regression, logistic regression, neural networks, and support vector machines (see e.g. Bishop 2006). This algorithm minimizes the desired differentiable multivariate function by making repeated steps in the direction opposite to the gradient.

In this contribution, we investigate two different analytical expressions for the current signal from the Pulsed Townsend experiment. We have defined two machine learning models that implement these expressions in the `torch.nn.Module` class from the PyTorch library. PyTorch is an open-source library for machine learning, data science, and artificial intelligence, that has been originally developed by Meta AI (see e.g. Ketkar 2021). The transport coefficients, that are determined from the current signal of the Pulsed Townsend experiment, are included in these models as trainable parameters. The models are trained by employing the `torch.optim.Adam` class, which implements the Adam variant of the gradient descent algorithm (see e.g. Barakat 2021), and by using the data that is generated from the corresponding

analytical expressions, by employing NumPy and SciPy open-source libraries (see e.g. Bressert 2013). Three different learning rates are used for drift velocity, diffusion coefficient, and the effective ionization coefficient, to optimize the convergence of the training algorithm, as these three coefficients have different orders of magnitude. We have observed that excellent convergence is obtained for all four combinations of the two PyTorch models and the two current signals. However, it is important to first estimate the initial guess for the drift velocity from the time at which the current signal is being rapidly reduced, due to the absorption of the electron swarm at the anode.

Acknowledgments: This work is supported by the Science Fund of the Republic of Serbia, Grant No. 7749560, Exploring ultra-low global warming potential gases for insulation in high-voltage technology: Experiments and modelling EGWIn.

References

- Barakat A., Bianchi P., 2021, SIAM Journal on Optimization. 31 244
- Bishop C. M., Nasrabadi N. M. Pattern recognition and machine learning. New York: Springer, 2006.
- Bressert E., SciPy and NumPy: an overview for developers. Gravenstain Highway North Sebastopol: O'Reilly Media, Inc, 2013
- Casey M. J., Stokes P. W., Cocks D. G., Bošnjaković D., Simonović I., Brunger M. J., Dujko S., Petrović Z. L., Robson R. E., White R. D., 2021, Plasma Sources Sci. Technol. 30, 035017.
- De Urquijo J., Juarez A. M., Rodríguez-Luna J. C., Ramos-Salas J. S., 2007, IEEE transactions on plasma science. 35, 1204.
- Haeffliger P., Franck C. M., 2018, Review of Scientific instruments. 89, 023114.
- Ketkar N., Moolayil J., Ketkar N., Moolayil J., Introduction to pytorch. Deep learning with python: learn best practices of deep learning models with PyTorch. Apress, Berkeley, CA, 2021:27-91



Detailed Program-Book of abstracts



Contents

1	Sunday, 20 th July	3
2	Monday, 21 st July	4
3	Tuesday, 22 nd July	7
4	Wednesday, 23 rd July	10
5	Thursday, 24 th July	13
6	Friday, 25 th July	16
7	Speaker List	17
8	Abstracts of oral presentations	20
9	Program of Poster Session #1	94
10	Program of Poster Session #2	177
11	Program of Poster Session #3	257
12	Program of Poster Session #4	336

Axisymmetric fluid streamer model with curvilinear electrodes in the AMReX environment

I. Simonović¹, D. Bošnjaković¹ and S. Dujko¹

¹ *Institute of Physics Belgrade, University of Belgrade, Pregrevica 118, 11080 Belgrade, Serbia*

We have extended our axisymmetric fluid streamer model, that is implemented in the AMReX library, to include curvilinear electrodes by employing the AMReX inbuilt embedded boundary functionality. We have investigated the dynamics of both positive and negative streamers in the pin-to-plane electrode configuration. The verification of our code is performed by comparing its results to those of the Afivo-streamer open-source code.

Streamers are precursors of lightning leaders and arcs in nature and technology [1]. Streamers are used for purification of polluted gases and liquids, surface processing, and plasma medicine. Further optimization of these applications requires both experimental investigation and theoretical modelling of streamer dynamics.

We have developed an axisymmetric streamer model in the AMReX library [2]. AMReX is an open-source library for massively parallel scientific computing applications with block-structured adaptive mesh refinement [3]. AMReX supports both MPI and OpenMP parallelization on central processing units as well as parallelization on graphic processing units. Although AMReX is implemented in C++ it has both Fortran and Python interfaces.

Our model is based on the first-order fluid model with local field approximation. The time evolution of the number density of electrons is described by the advection-diffusion-reaction equation, while the time evolution of the number densities of positive and negative ions is described by the reaction equations. We employ the finite volume method for the spatial discretization of our model. Time integration is performed by using the second-order Runge-Kutta method.

In this work, we have extended our code to enable for the inclusion of curvilinear electrodes by using the AMReX inbuilt embedded boundary functionality. In this approach, the electrode is included as a curvilinear embedded boundary that conceptually cuts through a rectangular mesh. Thus, various electrode shapes can be generated by combining the basic shapes that are implemented in the classes which already exist in AMReX. For instance, a rod electrode can be generated as a union of a semisphere and a cylinder.

The resulting electric field is determined from the gradient of the resulting electrostatic potential, which

is obtained by solving the Poisson equation. This equation is solved by employing the geometric multi-grid method. We use Dirichlet boundary condition for the electrostatic potential at boundaries that are perpendicular to the applied electric field, and zero Neumann boundary condition at other boundaries.

It is important to note that the AMReX inbuilt linear operator, that is used for solving the Poisson equation and the Helmholtz equation when embedded boundaries are present, is defined only for Cartesian coordinates. For this reason, the coefficients of this linear operator must be explicitly set by the user to be equal to the metric terms for cylindrical coordinates in order to obtain the correct solution of these equations for the axisymmetric model.

Verification of our model is performed by comparing its results with the results of the open-source Afivo-streamer code [1] for both positive and negative streamers in the pin-to-plane electrode configuration.

Acknowledgments: This work is supported by the Science Fund of the Republic of Serbia, Grant No. 7749560, Exploring ultra-low global warming potential gases for insulation in high-voltage technology: Experiments and modelling EGWin.

References

- [1] Teunissen, J. and Ebert, U. Simulating streamer discharges in 3D with the parallel adaptive Afivo framework. *Journal of Physics D: Applied Physics*, **50**, 474001 (2017).
- [2] Simonović, I. *et al.* Axisymmetric fluid streamer model in the AMReX library. *Plasma Sources Sci. Technol.*, **33**, 085012 (2024).
- [3] Zhang, W. *et al.* AMReX: a framework for block-structured adaptive mesh refinement. *Journal of Open Source Software*, **4**, 1370 (2019).